2001

Stress concentration around dowel bars in jointed rigid concrete pavements

Mourad Youssef Riad
West Virginia University

STRESS CONCENTRATION AROUND DOWEL BARS IN JOINTED RIGID CONCRETE PAVEMENTS

Mourad Y. Riad

Thesis Submitted to the
College of Engineering and Mineral Resources
at West Virginia University
In Partial Fulfillment of the Requirements
for the Degree of

Master of Science
in
Civil Engineering

Samir N. Shoukry, Ph.D., Chair
David Martinelli, Ph.D.
Julio Davalos, Ph.D.

Department of Civil and Environmental Engineering

Morgantown, West Virginia
2001

ABSTRACT

STRESS CONCENTRATION AROUND DOWEL BARS IN JOINTED RIGID CONCRETE PAVEMENTS

By
Mourad Y. Riad

Transverse joints in rigid pavements are the locations where most pavement distress appears, leading to detriorating the riding quality and elevating maintenance cost. The state of stresses in the concrete surrounding dowel bars, in dowel jointed concrete pavements, is a major factor that contributes to transverse joint distress. Review of previous studies indicates that many researchers were primarily concerned with identifying the compressive bearing stress on top and bottom of the dowel. Being small compared to the allowable bearing stress of concrete, transverse joint failure is often attributed to unproper construction practice. Most of the previous mechanistic studies on dowel interaction with concrete relied on simplifying assumptions that masked the true stress distribution at dowel-concrete interface.

In this study, the magnitude and state of stresses induced around dowel bars were identified through detailed 3D Finite Element (3DFE) modeling of dowel jointed rigid pavement structures. Both straight and skewed joints were modeled using extremely fine meshing that allows accurate modeling of the friction and separation at dowel concrete interfaces. The model response was examined for the case of joint loading with an equivalent axle load of 18000 lb. It was found that significantly large tensile stresses develop in the concrete on both sides of the loaded dowel. The magnitude of the tensile stress approaches the tensile modulus of rupture of concrete causing tensile cracks to develop on both sides of the dowel bar. The comparison between skewed and straight joints stresses revealed that skewing the joint is an expensive refinement of the joint that does not reduce the magnitude of stresses around dowel bars.

A laboratory apparatus was designed for testing the performance of dowel joints. The setup is capable of testing dowel-jointed specimens under static, dynamic, and fatigue loading conditions. A computer-controlled system of instrumentation was developed to monitor the load-deflection relation in real time. Strain gages bonded to the dowel joint face enabled measurement of the strain around dowel bars. Tests conducted on concrete specimens fitted with epoxy-coated steel dowels indicated excellent matching with the results obtained form the finite element models. The tests also confirmed that visible tensile cracks develop around the dowel upon the application of 3000 to 4000 lb load. Comparison of the measured strains around the dowel bar with those predicted form the 3DFE models indicated excellent agreement. Based on understanding the mechanism of stress development at the dowel concrete interface, a modified dowel bar design was tested. The modified design resulted in reducing the stresses around the dowel by more than 50 percent.

ACKNOWLEDGEMTS

I wish to express my sincere gratitude and appreciation to my research advisor Dr. Samir N. Shoukry for his excellent support, encouragement, perseverance and guidance that was indispensable for the accomplishment of this effort. Thank you for your unlimited help, paternal care, and friendship. I also would like to express my appreciation to Dr. David Martinelli and Dr. Julio Davalos for serving on the examining committee.

I wish to express my deepest and affectionate feelings to my parents for their love, care and support, and for being there when I needed them.

My appreciation is also extended to all my friends and colleges for their encouragement and help through the course of this research work.

The author gratefully acknowledges the financial support for the completion of this research from West Virginia Department of Transportation.

TABLE OF CONTENTS

LIST OF TABLES

LIST OF FIGURES

CHAPTER ONE

INTRODUCTION

1.1 PREFACE

Dowel jointed plane concrete pavements (DJPCP) are in wide use because of their durability, their ability to overcome subgrade weakness, and difficult climate conditions. DJPCP consist of Portland cement concrete slabs supported by one or several foundation layers. When a load is applied to a concrete slab, bending stresses are developed, and the load is transferred and distributed over the foundation layers. Joints are introduced in concrete pavements to control transverse and/or longitudinal cracking that occur due to restrained deformations caused by moisture and temperature variations in the slabs. Three major types of joints have been in use to obtain slab discontinuity; these are contraction joints, expansion joints, and construction joints. Contraction joints are formed by introducing a weakened plane into the concrete by sawing a groove into the concrete while it is in its curing process, and allowing a crack to form at that plane. Expansion joints are created when an intersection is needed between the pavement and other structures, and in many cases within pavements. This is achieved by forming a full depth gap in the concrete slabs. Construction joints are used between paving lanes, or when it is necessary to stop the paving construction. The existence of joints in concrete pavements represents a natural weakness to the global structural system. When joints have no mean to transfer the load across the two slab boundaries (often called dummy joints), each slab edge must bear the full-applied load at a time. This case produces not only high dynamic tensile tresses in the concrete slab, but also large compressive stresses at the foundation layers in addition to increasing the pavement roughness and diminishing the riding quality. To overcome this condition, three means of load transfer mechanisms at the transverse joints have been widely used. These are dowel bars, aggregate interlock, and keyways.

A deep understanding of the mechanical behavior of dowel bars and the induced stresses at their interface with concrete is of high importance for the development of feasible and effective doweled joints. Contact stresses between dowel bars and concrete are of major importance for the improvement of the load transfer efficiency.

1.2 PROBLEM STATEMENT

Rigid pavement joints should transfer loads imposed by moving vehicles whose number exceeds several millions over the course of the pavement's lifetime. This has to be achieved safely, economically, and with an acceptable riding quality to the traveling vehicles. Dowel bars are widely used in rigid pavement expansion and contraction joints as a mechanical device to distribute the wheel loads over slab discontinuities through vertical shear, and/or bending moments. Despite the fact that many studies were conducted to achieve a better understanding of the mechanical behavior of the joints, it appears that transverse joints are one of the most popular spots where pavement distresses could be recorded. Premature distress is often observed around rigid pavement joints (1). The loss in ride quality for many jointed plain concrete pavements (JPCP) is primarily associated with joint related distresses such as faulting and spalling (2). Long-Term Pavement Performance (LTPP) studies indicate that dowel jointed plain concrete pavements (DJPCP) perform better than those without dowels (3). Field surveys showed that spalling is often found at locations along the transverse joints, indicating that spall development is due to a combination of traffic action and daily variations in pavement temperature (4). An expanded review of JPCP distresses could be found in (5). Previous parametric studies related to identifying the variables, which significantly affect the performance of transverse joints, indicated that the dowel concrete interaction takes a major place among those influencing the load transfer efficiency (6).

It is necessary to have a deep understanding of the state of stresses and strains that develop at the dowel-concrete interface and their distributions around loaded dowel bars. These stresses are believed to have a significant contribution in the descent of the dowel/concrete contact modulus, and consequently the deterioration of the load transfer

efficiency at the joint. Stresses as such need to be explored and studied carefully. A great enhancement of the joint performance could then be reached, once these stresses are put to a minimum level, through careful design of the transverse joint and the load transfer mechanism.

1.3 OBJECTIVES OF THE STUDY

The general objective of this research is to identify the magnitude and state of stresses induced at the dowel/concrete interface in rigid pavement joints, subjected to traffic loading. This is accomplished by exploring the locations were high stress concentrations are induced in the concrete socket incasing the loaded dowel bar. Such knowledge would enable redesigning the doweled joint in a manner that eliminates or minimizes the magnitude of such stresses. This would lead to a great saving in the cost of maintaining transverse joints.

1.4 METHODOLOGY

To achieve the previously stated goals, the research is to be conducted along the following steps:

1. Investigation of the published literature on the analysis of joints in jointed concrete pavements addressed to explore the state of stresses induced in the dowel/concrete interface. This serves to define the current state-of-the-art, and help identify the strategies used by other researchers in topics related to load transfer efficiencies in DJPCP.

2. Development of a Three Dimensional Finite Element Models (3DFEM) that simulates the response of multi-layered dowel jointed concrete pavement structures to traffic loading. This includes both straight, and skewed joints. The state and magnitude of the maximum stresses in the concrete surrounding the dowels should be identified.

3. Measurements of laboratory scaled specimens will serve to verify the results obtained from the finite element models, and to explore the main characteristics of the doweled joints.

4. Once the 3DFEM are developed, a close examination of the induced stresses at the dowel/concrete interfaces can be conducted, and a comprehensive study of these stresses and the means to minimize them is to be carried out.

1.5 SCOPE OF RESEARCH

The primary objective of this study is to enhance the performance of the doweled joints in DJPCP. Excessive stresses induced around regular dowel bars and their distribution at the dowel/concrete interface, which are believed to have a major effect on joints distresses, are studied. The study involves also a review of the current knowledge addressed to the formation of stresses at doweled joints. To identify the stresses around dowel bars, 3DFEMs are developed simulating both straight and skewed dowel jointed slabs in a rigid pavement system. The modeling results are used in to compare between the induced stresses in skewed joints with those in straight joints. The study presents an alternative design of the regular dowel bar. The new design is shown to be capable of relieving the stresses at the dowel-concrete interface.

A testing setup is designed and built for testing simulated rigid pavement joints. The setup includes the development of a computer controlled data acquisition system based on “Labview” software. The system is capable of acquiring data from two channels, filtering, storing and plotting the data in real time. Sets of experimental tests, on simulated doweled joints are conducted to experimentally identify the behavior of dowels under selected cases of loading. These tests served also to verify the existence and distribution of the stress concentrations around loaded regular dowel bars. 3DFEMs that simulate the laboratory tests are developed. The results from these models supplemented the results previously obtained and served to verify the full-scale 3DFEMs.

CHAPTER TWO

LITERATURE REVIEW

2.1 INTRODUCTION

The need of load transfer devices to distribute the load across transfer joints and to improve the riding quality was realized when use of transverse joints in rigid pavements were shown essential to the control of transverse cracks resulting from temperature and/or moisture changes. Steel dowel bars, aggregate interlock, and keyways were used as load transfer devices. Field observations, as well as experimental tests, have shown that doweled joints had better performance (7). The first use of smooth round steel dowels for the purpose of transferring the load to the adjoining slab was reported in a pavement constructed near Newports News, Va, between two army camps in 1917-1918 (8). Since then, doweled joints have been used in thousands of miles of rigid concrete pavements. For a long time, the design of dowel bars was mostly based on experience. One rule of thumb was that the diameter of dowel be equal to one-eighth of the slab thickness and dowels being spaced at 30.48 cm (12 in) on centers (9). In this chapter, literature review of the studies addressed to determine the state of stresses induced by dowel bars on surrounding concrete material is presented.

2.2 ANALYTICAL STUDIES

The first attempt to calculate the compressive bearing stress induced by a dowel bar was carried out by Bradbury (1932) (10). Assuming the dowel to be an infinite beam, the concrete to be a Winkler foundation, and using Timoshenko's (11) analysis, Bradbury developed formulas to calculate the dowel length required for allowable shear, bending and bearing stresses. The analysis developed by Timoshenko stated that the general expression for the deflection of the bar gives a wave curve having gradually diminishing amplitude as the distance from the applied load increases. Assuming that the supporting medium is an elastic material, it would follow that the intensity of pressure on the bar at

any point is proportional to the deflection at that point. The bearing stress on concrete (f_c) was given by Bradbury as:

$$f_c = \frac{25P(\ell + 1.5z)}{2\ell^2 d}$$

where: P = the shear on the bar,

l = the total embedded length of the dowel,

z = the maximum width of joint, and

d = the dowel diameter.

The work conducted by Friberg (1940) (12) was the earliest investigation addressed to dowel/concrete contact stresses considering dowel groups. Based also on Timoshenko's analysis, adopted previously by Bradbury, Friberg indicated that the maximum deformation of concrete under the dowel (y_o) could be expressed as:

$$y_o = \frac{P_t(2 + \beta w)}{4\beta^3 E_d I_d}$$

In which: P_t = the shear force on the dowel,

w = the joint width,

E_d = Young's modulus of the dowel,

I_d = the moment of inertia of the dowel bar, and

β = the relative stiffness of a dowel embedded in concrete expressed as:

$$\beta = \sqrt[4]{\frac{Kd}{4E_d I_d}}$$

Where: K= the modulus of dowel support, Tabatabaie (13) reported finding values in the literature ranging from 3 x 10^5 pci to 32 x 10^6 pci .A typical value of 1.5 x 10^6 pci is commonly employed.

d = the diameter of the dowel.

Figure 2.1 illustrates the basic relationship for dowel stresses, developed by Friberg, stating that the induced stresses are relative to the deflection of the dowel with respect to the concrete, which has a maximum magnitude at the face of the joint (y_o). This relation takes the form :

$$\sigma = ky$$

where: σ = the stresses in concrete,

y = the deflection of the dowel.

$$y = \frac{e^{-\beta x}}{2\beta^3 EI}\left[P_t \mathrm{Cos}\beta x - \beta M_o\left(\mathrm{Cos}\beta x - \mathrm{Sin}\beta x\right)\right]$$

M_o= bending moment on dowel at face of concrete = $0.5wP_t$

w = width of joint opening

The computed value for bearing stress should then be compared to the allowable bearing stress of the concrete (f_b) recommended by the American Concrete Institute (ACI) subcommittee 325 where:

$$f_b = \left(\frac{4-d}{3}\right)f_c'$$

In which: f'_c = the ultimate compressive strength of concrete in (psi).

Friberg also found that the maximum negative moment in the slab for both interior and edge loadings occurs at a distance of 1.8l from the load as in Figure 2.2, where l is the radius of relative stiffness defined by:

$$\ell = \sqrt[1/4]{\frac{Eh^3}{12\left(1-\nu^2\right)k}}$$

In which: h = the thickness of the slab,

n = Poisson's ratio, and

k = the modulus of subgrade reaction.

In 1979, Tabatabaie et al. (8) conducted a factorial analysis using two-dimensional finite element (2DFE) program ILLI-SLAB by varying slab thickness, subgrade k-value, load positioning, and joint width opening. In his study, Tabatabaie proposed the following formulation to determine the maximum bearing stress induced in concrete:

$$\sigma_{max} = \Gamma \frac{(800 + 0.068E)}{D^{4/3}} (1 + 0.355J_o) sP$$

In which: P = applied wheel load,

J_o = the width of joint opening,

E = the modulus of elasticity of the dowel bar,

D = the diameter of the dowel bar,

Γ = load location coefficient = 0.0091 for edge loads
= 0.0116 for protected corner loads
= 0.0163for unprotected corner loads

s = dowel spacing.

The critical bearing stress equation established by Friberg (1938) was modified by Ioannides, Lee, and Darter (1990) (14) coupling earlier theoretical investigations, and observations from collected results from finite element studies, as following:

$$\sigma_b = \frac{K(2 + \beta\omega)}{4\beta^3 E_d I_d} \times P_t \times TLE \times f_{dc}$$

Where: TLE = Transferred Load Efficiency = P_T / P_t, typical assumption is 45%

P_T= the total load transferred from the loaded to the unloaded side of the joint along its entire length,

P_t = the total externally applied load,

f_{dc} = the portion of a load carried by the dowel that is subjected to the largest shearing force,

f_{dc} = s/e for edge loading, and

f_{dc} = 2s/(e+s) for corner loading,

e = the effective length (the length along which the dowels are effective to transfer the load) = 1.0 l, and

s = the dowel spacing.

2.3 FINITE ELEMENT ANALYSIS

The fast growth of computer capabilities in the past few decades enabled investigators to make use of their complicated computational techniques into many engineering applications. One of the emerged applications was the development of finite element modeling techniques that proved to be a powerful tool for the analysis of complicated structures that imposed a quite prohibitive task if attempt by conventional analytical methods. The finite element method was first employed to model the response of rigid pavements in the early 1970's (15). Despite the fact that many finite element codes and models have been developed for the study of doweled concrete joints, very little studies were addressed to investigate the induced stresses around dowel bars.

In 1978, Tabatabaie et al. (16) developed a two-dimensional finite element (2DFE) program named ILLI-SLAB written in Fortran IV, and based on the classical theory of a medium-thick plate on a Winkler foundation. The Winkler foundation was applied for the subgrade, while dowel bars were modeled using two nodded bar element with two degrees of freedom per node. The relative deformation of the dowel bar and the surrounding concrete was represented as the stiffness of a vertical two-nodes spring element with one degree of freedom per node. The spring element extended between the dowel bar and the surrounding concrete. The results obtained from the program, and presented by the authors indicate that the dowel bar reduces the edge stress from 5.25 to 2.76 Mpa, which is a stress reduction of 48 percent. While Experimental data from a series of full-scale static load tests conducted in eight U.S. Air Force bases in 1959 showed that the actual average stress reduction was only 28 percent (17). The same results were also obtained from small-scale model tests (18). This disagreement is related to the adopted hypothesis by the authors that the dowel bar is extremely effective, neglecting the deformation of the surrounding concrete.

In 1983, S. Tayabji and B. Cooley (19) developed the computer program JSLAB, for the analysis of jointed concrete pavement consisting of nine slabs. The program employed 2DFE code to model concrete pavement slabs with dowels, aggregate interlock, or keyed joints. Additionally, the program included consideration of curling behavior due to linear temperature variation in the slab. The primary objective for developing the program was to evaluate the behavior of joints and load transfer devices. Tayabji used finite element plate bending model, to analyze the concrete pavement. He selected a twelve-degrees of freedom rectangular plate element. The dowels at the joints were presented by a thick two nodded beam element, which had two degrees of freedom per node. The joint response to load was analyzed using JSLAB for edge loading and corner loading. For the cases of uniformly spaced doweled joint, a non-uniformly spaced dowel joint, and for the case of no load transfer across the joint. The results of JSLAB were in contrast with the results obtained using previously developed analytical models, which gave the following relationship: (20).

$$\sigma = \sigma_o \left[\frac{1}{1 + JE} \right]$$

Where: σ = the maximum edge stress along a doweled joint,

σ_o = the maximum stress along a free joint, and

JE = the ratio between the deflection of the unloaded slab and the deflection of the loaded slab.

Also, JSLAB could not give the localized stress induced at the concrete slab around dowel bars. A number of errors due to neglection of equilibrium condition of the dowel bar stiffness matrix were discovered, and discussed by Guo and Dong in 1992 (21). After modifying the program, a new version JSLAB-92 produced the same results as the program ILLI-SLAB.

In 1995, Guo et al. (22) developed a two-dimensional component dowel bar model that could be integrated into a finite element program to predict the responses of the load transfer system, including distribution of bending moments, shear forces, and

bearing stresses of each dowel. The model was tested for the case of a 80.1 KN (18 kip) single axle load located at the transverse joint and one tire is at the longitudinal edge of a 25.4 cm (10 in) slab. Bending moments and shear forces of the dowel bar were plotted. Although the results obtained from the finite element model were in reasonable agreement with experimentally measured results, the model was still dependant on the input value of the coefficient of dowel-concrete interaction.

In 1985, Ozbeki et al. (6) conducted a parametric study using JSLAB to determine which parameters have the most significant effect on the performance of transverse joints. It was concluded from the study that the variables that appreciably affect pavement response are the modulus of subgrade reaction (k), and the modulus of dowel-concrete interaction (G). A sensitive analysis of those two parameters indicated that a pavement is considered to have a good support condition when K is greater than 54.29 MPA/m (200 pci), and that the response of the pavement changes appreciably for values of G less than 54290 MPA/m (200,000 pci).

In 1994, Chatti et al. (23) introduced the effect of truck dynamics into the study of rigid pavement responses. A linear dynamic finite element model named DYNA-SLAB was developed, and was essentially an extension of the program ILLI-SLAB. Also in 1994, Zaghloul et al. introduced the use of commercially available three-dimensional finite element programs in pavement studies (24) by using ABAQUS to determine the load equivalence factors. The slab and subgrade were modeled using 3D brick elements, and dowels were modeled using bar elements. The use of bar elements in this case does not accurately simulate the behavior of the dowel bar; since bar elements behave as keys to transfer shear forces, due to their aspect dimensional ratio, neglecting bending. Another study using ABAQUS was developed by Uddin et al. (25) in 1996 who examined the effect of pavement discontinuities on surface deflections of a pavement subjected to falling weight deflectometer (FWD) load. In this study, the slab, cement treated base, and subgrade were modeled using 3D elastic brick elements, pavement cracks were modeled using gap elements, and dowels at the transverse joint were modeled using beam elements.

The first study found in the literature that explored the nature of developed stresses at the dowel/concrete interface was presented by Channakeshava et al. in 1993 (26). The study focused on developing a 3D finite element model that would have an adequate simulation of plain concrete pavements with doweled joints, overcoming the limitations of 2D models. The concrete slab material was modeled using a plastic constitutive model augmented by a smeared cracking model, progressive softening of dowel load transfer was considered. Dowel bars were modeled using discrete bending elements, with three discrete nonlinear springs connecting each end of the dowel to the slab, to account for looseness. The use of nonlinear springs at the end of the dowels, allowed the effects of local stress concentrations to occur. Among the findings of this study, it was observed that dowel-concrete interface stiffness is reduced due to high stress concentrations near the dowel. To capture the effect of local stress concentrations, a localized joint response analysis was performed, in which a typical joint region was cut out of the pavement and supported rigidly, and loaded through the dowel. Channakeshava observed in this study the development of tensile stress component in the elements above the dowel, along with large compressive stresses in the elements below the dowel. However, the exact location and the magnitude of the tensile stresses were not identified.

In 1998, Shoukry and William (27) examined the effect of dowel bar looseness on the load transfer efficiency (LTE) across the joint. This was achieved through 3D finite element modeling of two dowel-jointed concrete slabs subjected to FWD load. The study revealed the distribution of the maximum principal stresses developed around the dowel bar, indicating the formation of high stress intensity in the concrete material reaching 3.31 MPa (480 psi) when a looseness of 0.02032 cm (0.008 in) is applied.

2.4 EXPERIMENTAL STUDIES

In 1938, Friberg (28) presented a study of the characteristics of failure and the rate of deflection of transversely loaded single dowels encased in concrete. The modulus of dowel reaction was established by conducting a set of laboratory tests, in which a load

was applied on dowels extending through 20.32 cm (8 in) wide and 22.86 cm (9 in) long concrete blocks. The depth of concrete below the dowel varied from 6.35 to 21.59 cm (2.5 to 8.5 in) and dowel diameters were 1.905, 2.54, and 3.175 cm (¾, 1, and 1.25 in). Tests were conducted by applying the load at a point 1.27 cm (0.5 in) from the face of the concrete, and observations were made of the deflection of the dowel at the face of the concrete, as well as slope readings of the dowel, simultaneously as the load increased till failure. An interesting finding of Friberg was the failure characteristics of the concrete emphasized as a formation of horizontal crack, extending from the dowel toward each side, merging into a fane-shaped failure, and complete failure was accompanied by a vertical crack extending from top to bottom of the specimen. The modulus of dowel reaction for 1.905 and 2.54 cm (¾ and 1 in) greased dowels in 15.24 and 17.78 cm (6 and 7in) concrete is deduced from these tests to be 300 times the unit crushing strength of cylinders of the concrete.

In 1947, the University of Illinois published an investigation report (29), which presented the experiences in Illinois pertaining the use of joints in concrete pavements, during the period from 1928 to 1940. The report is entirely based on experimental laboratory tests and field investigations on joints, mounted with various types of load transmission devices. The principal purpose of the laboratory tests was to determine whether a joint or load transmission device possessed defects, which might make it undesirable. Among several types of tests, load transmission tests were conducted on plain dowels consisting of 1.905 cm (¾ in) in diameter, and 60.96 cm (24 in) in length round steel bars. Concrete specimens consisting of three concrete blocks 17.78 cm (7 in) thick, 30.48 cm (1 ft) wide and 96.52cm (38 in) long were connected by two expansion joints. Deflections at the joint were measured as the load was applied till failure of the specimen, and the load deflection relations as well as the permanent set curves were plotted. The characteristics of the joints were predicted from the shape and slope of the curves. Also by treating the data analytically, mathematical relations were derived to predict the amount of load transfer to be expected under certain assumed conditions. The amount of load to be transferred (R_2) by a device under given conditions was found to be:

$$R_2 = \frac{P(d - L)}{2d + sP}$$

In which: P= the numerical value of the wheel load,

d= the deflection of a free slab calculated by Westergaard to be

$$d = \frac{0.433P}{k\ell^2},$$

L = the lost motion,

s = the deflection per load determined from the load deflection curve,

k = the modulus of subgrade reaction, and

l = is the radius of relative stiffness of the slab.

One of the major conclusions from the laboratory tests was that it emphasized the importance of increasing the bearing area between the load transmission device and the concrete.

In 1956, Keeton (30) conducted an experimental study on the load transfer characteristics of dowels in airfield pavements expansion joints. The tests were carried out using a B-45C tire and wheel mounted to a specially designed cart to apply the load of 222.411 KN (50000 lb) on a jointed slab mounted with instrumented dowel bars. A moment strain factor was determined for the dowel in prior of installation, and was used to plot the shear and moment diagram along the dowel bar, as the load is applied on one edge of the joint.

In 1958, Teller and Cashell (31) presented an experimental laboratory study of the effects of several variables influencing the structural performance of dowel bars subjected to a load applied alternately on either side of a joint, for a desired number of cycles. For this purpose, a new testing machine was built providing a testing condition approaching closely those found when a heavy wheel load crosses a transverse joint of a pavement in service. Tests were performed on concrete slabs 121.92 cm (4 ft) wide by 304.8 cm (10 ft) long divided transversely at mid-length by a joint in which four dowel bars were installed. Collected data consisting of the difference in strains and the

difference in deflections measured on the loaded and unloaded sides of the joint opening were used to plot an exponential relation between dowel diameter and load transfer capacity. It was also found that an appreciable increase in the percentage of load transferred is obtained by increasing the diameter of the dowel. It was indicated that for round steel dowels at a spacing of 30.48 cm (12 in), the dowel diameter in eighths of an inch should equal the slab depth in inches. Regarding the dowel length, it was indicated that with a 1.905 cm (3/4 in) dowel diameter, maximum load transfer requires an embedment length of about 8 dowel diameters. With larger dowels, full load transfer is obtained with an embedment length of about 6 diameters. Among the experimental investigations, high intensity and localized effect of the pressure exerted by the dowels were recorded by strain gage measurement on the joint face over the installed dowel bar. It was emphasized that the high bearing pressures between the dowel and the concrete, particularly in the region above and below the dowel near the face of the joint, tend to brake down or wear the concrete during repetitive loading and thus increase whatever looseness may have existed initially.

In 1979, Ciolko et al. (32) studied the relative ability of dowels to transfer load across joints. Load, and deflection relations were studied by applying a set of incremental static load between repetitive loading after 5,000, 20,000, 100,000, 300,000, 600,000, and 1750,000 cycles for a load reaching 44.6 KN (10,000 lb) on slab specimens. The specimens consisted of four 0.9 m (3 ft) wide slabs with transverse joints containing three 3.2 cm (1.125 in) diameter dowels. The test results verified many of Teller's findings. It was indicated that an increase in joint width, load magnitude, and repetitions increased dowel looseness, and consequently decreased the load transfer efficiency of the dowels. The results indicated that the dowel specimens lost (4-9) % of their initial capacity as a result of the application of the repeated loads.

In 1994, Sargand and Hazen (33) presented a study to examine the load transfer mechanism under traffic loading. Field monitoring of instrumented sites provided strain data that enabled to calculate the induced stresses in concrete, deflection at joints,

moments and shear forces in dowels. Based on the results from the field study, one of the conclusions was that larger diameter and stiffer bars transfer more loads across the joint.

In 1997, Hammons (34) conducted a laboratory scale experimental study on five jointed rigid pavement models as a part the work presented for the purpose of developing a 3D finite element model of rigid pavements. Each rigid pavement model consisted of two Portland cement concrete slabs, 91.5 cm (36 in) by 122.0 cm (48 in) by 5.1 cm (2 in) thick separated by a joint, and supported by rubber block simulating the subgrade. The joint was mounted with smooth steel bars 0.6 cm (0.25 in) in diameter, 43.4 cm (15.5 in) long, and spaced at 10.2 cm (4 in) center to center. The testing was conducted by applying the load on one side of the joint through a displacement controlled hydraulic actuator acting on a circular rubber pad at a rate of 0.25 mm/min (0.01 in/min). Collected data consisted of surface strains, and displacements on the top of the slabs. Load-deflection curves and load-strain traces were plotted for each test. A composite plot of deflection load transfer efficiencies versus load was carried out. The presented plots indicated that the maximum load transfer efficiencies occurred at low loads. As the load was increased, it was noticed that localized crushing of the slabs develops at dowel/concrete contacts. The experiments confirmed the observations and predictions that the effectiveness of the load transfer mechanism decreases with localized damage in the immediate vicinity of the joint.

In 2000, Sargand (1) presented an experimental study to evaluate the dowel response under environmental conditions, by monitoring the strains induced in dowel bars during concrete curing, and under applied dynamic loads. The collected data indicated that the stiffness of dowel bars resisted slab curling inducing high amounts of bending moments in the dowels. It was also indicated that the bearing stresses next to the dowel bars due to temperature and moisture changes exceeded the allowable bearing capacity of concrete, which would lead to expect some progressive concrete deterioration at the dowel interface and a reduction in load transfer efficiency over time. Analyzing the dynamic bending moments in the dowel bars due to traffic loading represented by FWD tests showed them to be minor to those induced due to environmental changes.

2.5 STRAIGHT JOINTS VERSUS SKEWED JOINTS IN RIGID PAVEMENTS

Transverse joints may be oriented either at a right angle with the pavement centerline (perpendicular joints), or at an angle to the centerline (skewed joints). The skewing angle usually offset the joint about 0.6 m (2 ft) per 3.66 m (12 ft) (35). Opinions about skewing the joint and its effect on concrete pavement are quite diverse. While some consider it an advantage, others argue that it is an unnecessary and costly refinement since adequate dowels can effectively eliminate faulting (3).

The AASHTO pavement design guide (1993) advises that skewing the joints will improve the performance of the plain and reinforced concrete pavement with or without dowels. The guide also states that skewed joints have the following advantages: (1) reduce deflections and stresses at joints, thereby increase the load-carrying capacity of the slab and extend the pavement life; (2) reduce the impact reaction in vehicles as they cross the joints, hence a smoother ride is achieved if joints have some excessive amount of roughness. Results from Field tests and Long Term Pavement Performance (LTPP) data indicate that the use of skewed joints is a mean of enhancing load transfer with non-doweled joints (3). It was also shown that skewed joints perform better than perpendicular joints primarily in terms of faulting and spalling particularly for non-doweled joints, however they are also more susceptible to corner breaks (37). It is believed that skewing from a counterclockwise rotation of transverse joint compel the impact of the wheel crossing the joint to fall on the obtuse angle at the outside edge of the pavement (38).

While AASHTO design guide (1993) considers skewing the doweled joints will enhance the pavement performance, others take the position that doweled jointed will not benefit much from being skewed. Long-term studies on the performance of doweled and non-doweled skewed joints showed that progressive deterioration in terms of faulting was observed with non-doweled joints (39). Also measurements obtained from test sites in Illinois revealed that doweled load-transfer system is more effective than aggregate interlock in reducing deflections at pavement corners and aggregate-interlock becomes

ineffective in transferring the load across the joint when joint opening exceed 0.9 to 1.0 mm (40).

From the practical point of view, skewed joints have numerous problems such as they are more difficult to construct, they can be more susceptible to errors in terms of angles and how to sawcuts line up. Skewed basket makers would have problems getting the correct skew angle because they would have to retool their equipment to make them skewed. Moreover, patching the skewed joint is one of the most difficult procedures, and most importantly, skewed joints are remarkably less economic due to the limited competitive pricing. During the course of this study (Feb. 2000), PennDOT decided to change its practice of using skewed joints after reviewing the results of (LTPP) program analysis project (41).

2.6 CONCLUSIONS

The presented review indicates that the research conducted to study the pavement joints and particularly the induced stresses around dowel bars were mainly addressed to the identification of compressive bearing stresses above and under the dowels. The state of stresses around dowels is not fully identified in the literature. There is a lack of sound approach to identify with any degree of accuracy the modulus of dowel support (k), which makes it difficult to rely on the analytically developed formulas that are sensitive to its value. It is also noticed from the review that the looseness of the dowels was believed to be mainly a result of initial misfit and is gradually developed by crushing of concrete particles in the compression zones around the dowels, disregarding the contribution of the tensile stresses at the dowel/concrete contact. It is also noticed that 2DFE was unable to capture the full state of stresses around dowel bars. It is believed that the state of stresses at the dowel/concrete interface needs to be closely explored. Such a study could reveal important facts about the formation of different types of stresses that could have a significant effect on the behavior of rigid pavement joints along with compressive bearing stresses. The above review also reveals that skewing the transverse joint is still an issue among pavement designers. Although the performance of some

pavements with skewed joints was satisfactory, it is unlikely that the same design would give the same results with the progressive number of trucks and axle loads. This requires integration between field and analytical studies, which would provide a better understanding for the observed pavement performance and consequently leads to the development of the current design procedures.

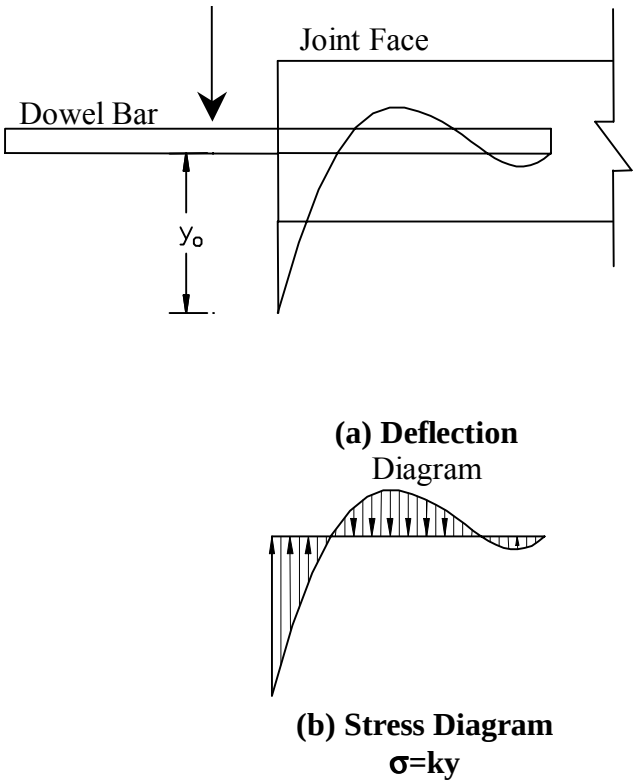

FIGURE 2.1 Friberg's analysis of dowel bar support

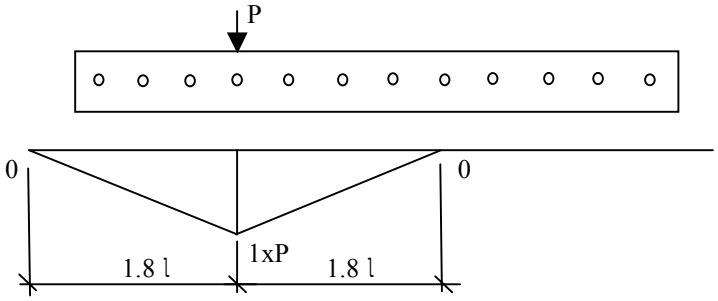

FIGURE 2.2 Distribution of transferred load through a group of dowels by Friberg

CHAPTER THREE

MODELING OF CRITICAL STRESSES AROUND DOWEL BARS

3.1 INTRODUCTION

The finite element method proved to be a powerful tool for solving complicated problems that are difficult to solve by analytical approaches. A brief review of the explicit finite element method is presented in Appendix I. In this study, explicit finite element method was applied to identify the state of stresses at the dowel/concrete interface. For this purpose, two finite element models (FEM) were developed. The first model is for a multi layered rigid pavement structure. It consists of two plain concrete pavement slabs supported by a base, and subgrade. The two slabs are connected through a doweled straight expansion joint. The second model represents a rigid pavement structure with doweled skewed expansion joints. Both models were developed using the same mesh and material properties. The states and magnitudes of stresses at the dowel-concrete contacts were examined in each model.

3.2 FINITE ELEMENT MODELS

3.2.1 Mesh details

The concrete rigid pavement structures were modeled as a multi-layered system consisting of two dowel jointed concrete slabs, supported by a base, and a subgrade. Although the region under investigation is localized at the vicinity of the joint, full slabs were modeled to eliminate undesired influence of boundary conditions on the results. A full lane width of 3.66 m (12 ft) was considered, and the slab length was taken to be 4.57 m (15 ft). A small gap of width 9.5 mm (⅜ in) was constructed between the two slabs to allow for the expansion and contraction of concrete; consequently, dowel bars are the only means of load transfer. All layers were meshed using hexahedron solid brick elements with 24 degrees of freedom per element. Realizing the fact that transverse joints

are critical stress zones that can initiate pavement failure, an extremely refined mesh was developed at this region, to accurately capture the flow of stresses around the dowel bars. Figure 3.1 illustrates the FEM simulating the straight joint structure, and Figure 3.2 illustrates the FEM simulating the skewed joint structure. Dowel bars of diameter 3.175 cm (1.25 in.) and length 45.72 cm (18 in.) were modeled using extremely fine mesh of solid brick elements as shown in Figure 3.3. This mesh was designed to reveal the localized deformations and the development of contact stresses that take place at the interfaces between dowels and the surrounding concrete.

3.2.2 Boundary conditions

The boundary conditions for the finite element models were selected to match those found in a real pavement structures. The depth to bedrock was assumed to be typical of what can be found in West Virginia, i.e. from 1.50-5.0 m (42). In this study, it was taken as 1.80 m. Non-reflective boundaries, which simulate the semi-infinite extension of layers were applied at the bottom and sides of the subgrade as well as all edges of the base as indicated in Figures 3.1 and 3.2. The use of non-reflecting boundaries prevents the reflection of stress waves within the loading time duration under investigation; thus simulates the continuity of the layers.

3.2.3 Interfaces

The interface type and frictional characteristics between the model components were carefully selected. A sliding interface was introduced between each dowel bar and the surrounding concrete material, where the coefficient of sliding friction was taken to be 0.05 (no experimental data could be found in the literature). The dowel/concrete interface allows for non-uniform and partial contact along the interface as a result of dowel bar bending and its localized deformation at the points or lines of contact. A sliding interface with a coefficient of friction of 1.4 with the possibility of separation was applied between the concrete slab and the base layer. This value was selected based on the AASHTO pavement design guide recommendation (43). The solution of the contact problem is based on satisfying two conditions; the first one is that surfaces may coalesce

or separate during the motion of the two bodies, the second is the impenetrability of the two bodies. To satisfy the last condition: a) the contacting points move with the same displacement and velocity in the direction normal to the contact surface, b) the momentum is balanced on the contact surface, c) no tensile traction forces can occur on the contact surface. No interface was assumed between the base course and the subgrade, since these two granular layers can not deform as rigid bodies.

3.2.4 Material models

3.2.4.1 Concrete Material Model

An anisotropic brittle damage model, developed by Govindjee et al. (44), was used to simulate the behavior of the concrete material in slabs. The models allow progressive degradation of both tensile and shear strengths across smeared cracks that are initiated under tensile stresses. Failure of the material is assumed to initiate when the maximum principal stress exceeds a threshold value (concrete modulus of rupture, f_n). Once this stress has been reached at a point within the body, a smeared crack is initiated there normal to the first principal direction. The restriction on the normal traction is given by:

$$\phi_t = (\mathbf{n} \otimes \mathbf{n}) : \boldsymbol{\sigma} - f_n + (1-\varepsilon) f_n (1 - e^{-H\alpha}) \leq 0$$

Where: $n_{(3x1)}$ = a unit vector normal to the smeared crack,

ε = a constant of small value, nearly zero (for computational stability)

H = the softening modulus, set automatically by the program based on element and crack geometries

α = an internal variable to measure the intensity of the crack.

$\sigma_{(3x3)}$ = the actual stress tensor of the element

" $\otimes$ " is the dyad product resulting a (3x3) vector

" : " is the double dot product resulting a scalar value

The shear traction is limited to be less than or equal to ϕ_s, where

$$\phi_s = f_s(1-\beta)(1-e^{-H\alpha})$$

Where: f_s = the initial shear traction that may be transmitted across a smeared crack plane, and

β= the shear retention factor.

Once initiated, the crack is fixed at this location and will reposition with the motion of the body. Across this smeared crack, the tensile and shear tractions are limited by some critical value that decreases exponentially with the increase in deformation. The degradation is implement by reducing the material's modulus normal to the smeared crack plane according to a maximum dissipation law that incorporate exponential softening. As the damage progresses the shear tractions allowed across the smeared crack plane asymptote to the product βf_s. It is important to notice that the shear degradation is coupled to the tensile degradation across the smeared crack so that they reach their asymptotic values simultaneously. Compressive failure is governed by a check using a simplistic J_2 yield function given by:

$$J_2 = \mathbf{s} : \mathbf{s} \cdot \sqrt{\frac{2}{3}}\sigma_y \leq 0$$

Where: s = the deviator stress tensor, and

σ_y = the concrete compressive strength.

If J_2 violated the above condition, a J_2 return mapping is executed. In this case, the stresses in the element diminish in an exponential decay, indicating failure in compression, and stresses are redistributed on the surrounding elements.

3.2.4.2 Steel, base and subgrade material models

Linear elastic material models were implemented for the steel dowel bars as well as for the base course and subgrade. The choice of using linear elastic material model for these items was based on the past experience with modeling rigid pavements subjected to FWD loading. Obtained results from previously developed 3D finite element rigid pavement models indicated that the stresses induced in the base and subgrade layers are very small, which validates the assumption of applying a linear elastic behavior to its material (45). In Ohio, field measurements of strains induced by traffic loads in rigid

pavements collected by Sargand et al. (46) were found within the elastic range of the used materials. The material constants used for each material model are listed in table 3.1

TABLE 3.1 Constants used for material models

Item	Material model	parameter	value
Concrete	Anisotropic brittle damage	Young's Modulus *(psi)*	3.00E+6
		Poisson's ratio	0.18
		Density *(lb/in3)*	2.24e-4
		Tension limit *(psi)*	375
		Shear limit *(psi)*	1250
		Fracture toughness *(lbs/in)*	0.8
		Shear retention factor	0.03
		Viscosity *(psi/sec)*	104
Base course	Linear elastic	Young's Modulus *(psi)*	45.00e+03
		Poisson's ratio	0.30
		Density *(lb/in3)*	2.210e-4
subgrade	Linear elastic	Young's Modulus *(psi)*	4.00e+03
		Poisson's ratio	0.40
		Density *(lb/in3)*	1.950e-04
Dowel bars	Linear elastic	Young's Modulus *(psi)*	29.00e+06
		Poisson's ratio	0.30
		Density *(lb/in3)*	7.324e-04

3.2.5 Loading

The extremely fine mesh used in these models to capture the growth of stresses around the dowel bars [element size is 0.4 cm (0.157 in) around dowel bars], makes it uneconomical to study the whole model responses subjected to the travel of a moving load along the two concrete slabs under consideration. Thus both models were subjected to falling weight deflectometer (FWD) impact load over two equivalent plates

representing a single axle load traveling over the joint. Previous studies (Brown, 1973 and CROW, 1998) (47) established a relation between rolling-wheel load and the pulse characteristics (shape and duration) of the FWD load expressed as:

$$\log(t_b)=0.20+0.5h_1-0.94 \log (V_{RW})$$

where t_b = Block time pulse duration, sec

h_1 = Thickness of surface layer, m

V_{RW} = Speed of Transient wheel (km/h).

The applied FWD load simulates a traveling axle load over the joint with a speed of 112 km/h (70 mph). The equivalent loading plates are 30.48 cm (12 in) in diameter, and 182.88 cm (72 in) spaced center to center. The load was applied symmetrically along the longitudinal centerline of the model. For the case of the straight joint model, both loading plates were located at one side on the joint, representing an edge loading condition. For the case of the skewed joint model, each loading plate was located at one side of the joint. Figure 3.4 shows the position of the loading plate as well as the studied dowel hole. Figure 3.5 illustrates the load-time history applied on each loading plate.

3.3 MODEL VERIFICATION

The model was verified by comparing the FEM strain results versus strain gage measurements of the compressive and tensile stresses induced around dowel bars. For this purpose, a reduced model was developed, consisting of a cut out segment from the concrete slab, containing one dowel bar, and subjected to a shear load amounting 9000 lbs over a contact area (20x13.8cm)(7.89x5.43 in). Experimentally measured data (reported in chapter 4) were obtained from a test carried out in the laboratory on a full-scale specimen representing the concrete slab segment, and subjected to the same loading conditions of the reduced model. A good agreement could be obtained between the experimentally measured, and the collected finite element strains from the reduced model. This verification will be discussed in details in chapter 5.

3.4 MODELS RESULTS

3.4.1 Location of maximum stresses around dowel bars

Modeling the concrete slab and the embedded dowel bars as three-dimensional solid elements allows the study of the various types of stresses induced at any spot inside the pavement structure. This was not available when using two-dimensional modeling techniques, or when using beam and spring elements to represent the dowel bars as previously adopted in earlier studies. As the main purpose for developing the 3D finite element model was to catch the stress concentration at the dowel/concrete interface, it was important to localize the regions where maximum stresses take place. Intuitively, the nearest dowel to the applied load will carry the largest portion of the load transferred to the unloaded slab. Friberg (1940) stated that dowel shear decreases linearly to zero at a distance of 1.8l from the point of loading where l is the radius of relative stiffness. Furthermore, Tabatabaie (1978) confirmed Friberg's approach, but concluded from his study that the distance from the load where the dowels are effective was only 1.0 l. Realizing this fact, stresses were investigated around the closest dowel to the FWD loading plate, and where the largest amounts of stresses are anticipated. In search of the location where the maximum stresses are induced in the concrete material around the selected dowel, it was concluded from Friberg's study that this would be expected at the joint face, where the maximum deflection of the dowel bar takes place.

3.4.2 Model response

Figure 3.6 illustrates the deformation of the skewed joint model due to the application of the FWD load. Figure 3.7 and Figure 3.8 illustrate a section through the straight joint slab at the position of the dowel hole under investigation, showing the maximum principal stress and the vertical stress respectively. Figure 3.9 shows the deformation of the dowel bar in the skewed joint model due to the application of the FWD load. The deformation of the dowel bar tends to have a V shape rather than an S shape previously assumed by many researchers. Figure 3.10 shows the vertical stress along the dowel bar under study from the straight joint FEM, the skewed joint FEM, in comparison with Friberg's formulation:

$$\sigma = ky$$

where: σ = the stresses in concrete,

K= the modulus of dowel support =1,500,000 pci.

y = the deflection of the dowel.

$$y = \frac{e^{-\beta x}}{2\beta^3 EI}\left[P_t Cos\beta x - \beta M_o\left(Cos\beta x - Sin\beta x\right)\right]$$

P_t = Load carried by the dowel = 1012.46 lb

M_o= bending moment on dowel at face of concrete = $0.5wP_t$

w = width of joint opening= ⅜ in

$$\beta = \sqrt[4]{\frac{Kd}{4E_d I_d}}$$

d = the diameter of the dowel = 1.25 in.

E_d = Young's modulus of the dowel = 29e+06 psi.

It is noticed that the FEM results indicate that the high compressive stresses occur at the face of the joint, and diminish sharply at about one inch inside the concrete. On the other hand, Friberg's solution gives a longer distance for the dissipation of the stress magnitudes, which measures about four inches from the joint face. The reason for this lies in the assumption made by Friberg, of a uniform modulus of dowel concrete support all along the dowel bar to satisfy the wave shape assumed for its deformation. Figure 3.11 to Figure 3.13 illustrate the distribution of vertical stresses, maximum principal stresses, and shear stresses respectively along the dowel/concrete contact interface at the face of the joint, for both loaded and unloaded slabs. Also, Figure 3.14 to Figure 3.17 show examples of the fringes for the stresses around the dowel bar holes.

3.5 DISCUSSION OF RESULTS

Figures 3.11 to 3.13 reveal important facts about the formation of compressive and tensile stresses around the dowel bar holes. Figure 3.11 shows that the maximum compressive bearing stress of 7.46 Mpa (1081.98 psi) occur at the loaded slab. According to ACI, the compressive bearing stresses of concrete (f_b) has the form:

$$f_b = \left(\frac{4-d}{3}\right) f_c'$$

Where: d = the dowel diameter, and

f_c' = the concrete compressive strength (psi).

f'_c is related to the concrete's modulus of elasticity by the equation :

$$E_c = \left(40{,}000\sqrt{f_c'} + 1{,}000{,}000\right)\left(\frac{w_c}{145}\right)^{1.5} \qquad (48), \text{ and } (49)$$

where: w_c= unit weight of hardened concrete= 145 pcf for normal weight conc.

To obtain the corresponding concrete compressive strength of the assumed concrete material, values of E_c= 3e+06, and d=1.25 in were substituted in the above equation. The computed f_c' was found to be 2500 psi. The allowable bearing stress was then calculated to be 15.8 Mpa (2291.7 psi). Obviously, the maximum compressive tress at the concrete-dowel interface is found less than the allowable bearing stress. Consequently, it is concluded that crushing of concrete particles in compression zones has not occurred yet. Figure 3.11 indicates the development of two tensile stress components positioned at 90 and 270 degrees with respect to the vertical axis. The magnitude of the tensile stress reaches 2.5 Mpa (362.6 psi) on both the loaded and unloaded slabs.

The allowable tensile strength of the concrete material is given by:

$$f_r = 7.5\sqrt{f_c'} \qquad (50)$$

where: f_r = the modulus of rupture of concrete (psi), and

f_c' = the concrete compressive strength (psi).

For f'_c = 2500 psi, the modulus of rupture would be 2.58 Mpa (375 psi). This indicates that a tensile crack has occurred in the concrete material on the sides of the dowel bar. The small difference of 12.4 psi between the magnitude of the tensile stress concentration, and the modulus of rupture is due to the fact that the FEM stresses are calculated at the element center, which is 0.2 in from the edge of the dowel.

The tensile stresses at the dowel-concrete interface result in the development of tensile cracks, before any crushing of concrete particles due to excessive compressive bearing stresses. Taking into consideration the effect of environmental changes, and fatigue loading induced by moving axle loads across the joints, it is believed that the tensile cracks would propagate, causing the entire failure of the joint.

Figure 3.13 indicates that the bearing stress induced in the dowel/concrete interface is accompanied by high magnitudes of shear stresses, which increase the possibility of provoking concrete failure around the dowel bar.

3.5.1 Effect of skewing slab joints on the development of stress concentrations at the dowel/concrete interface.

The plots in Figure 3.11 to Figure 3.13 indicate that both straight and skewed joints experience similar stress magnitudes. The reason for this similarity is due to the localized effect of the wheel load. The fact that the vehicle axle load passes the skewed joint with one wheel at a time does not prevent the development of excessive stresses at the dowel/concrete interface. Special attention should be directed to the shear stresses induced in concrete around dowel bars and found to be higher in magnitude in the case of loaded skewed joints than it's magnitude in the case of perpendicular joints as shown in Figure 3.13. This indicates that the distribution of the wheel load over the effective dowels could be more severe in the case of skewed joints.

3.6 CONCLUSIONS

The state of stresses induced at the interface between loaded regular dowel bars and the surrounding concrete material indicates the occurrence of two opposite modes of stresses that take place close to each other. One is the formation of compressive bearing

stresses on the top and the bottom of the dowel bar socket, and the second is the formation of tensile stresses in the concrete material on both sides of the dowel bar. These two modes of stresses are believed to be critical to the development of distresses at the transverse joints in rigid pavements. Upon the application of standard single wheel axle load, the tensile stress at the concrete/dowel interface initiate horizontal cracks on both sides of the dowel bar. Those cracks propagate, and increase the susceptibility of concrete failure, in addition to the reduction of the load transfer efficiency. The tensile cracks explain the development of initial looseness of dowels. Once the tensile crack sets, redistribution of stresses around the dowel bar occurs, and excessive compressive bearing stresses causes failure of concrete particles by crushing those elements on top and bottom of the dowel bar. This creates minute gaps between the dowel bar and the surrounding concrete, which expand and increase the amount of looseness around the dowel bar. The existence of gaps and/or cracks around the dowel bar at the joint face decreases the load transfer efficiency through the joint, which decreases the riding quality of the rigid pavement. Also the formation of cracks increases the potential of dowel corrosion by exposing the dowel bar to moisture attacks. Plots of stress distribution along the dowel length indicate that the region of high stresses is limited to be around one inch from the joint face. This suggests that some means of strengthening the concrete material surrounding the dowel bar may lead to longer lasting transverse joints. The FEM results reveal that skewing the joint was not beneficial to the performance of concrete at its interface with dowel bars. It could be concluded that the extra cost for skewing the joint was not benefitial in any reduction of stress concentrations around the dowel bars in concrete pavement joints.

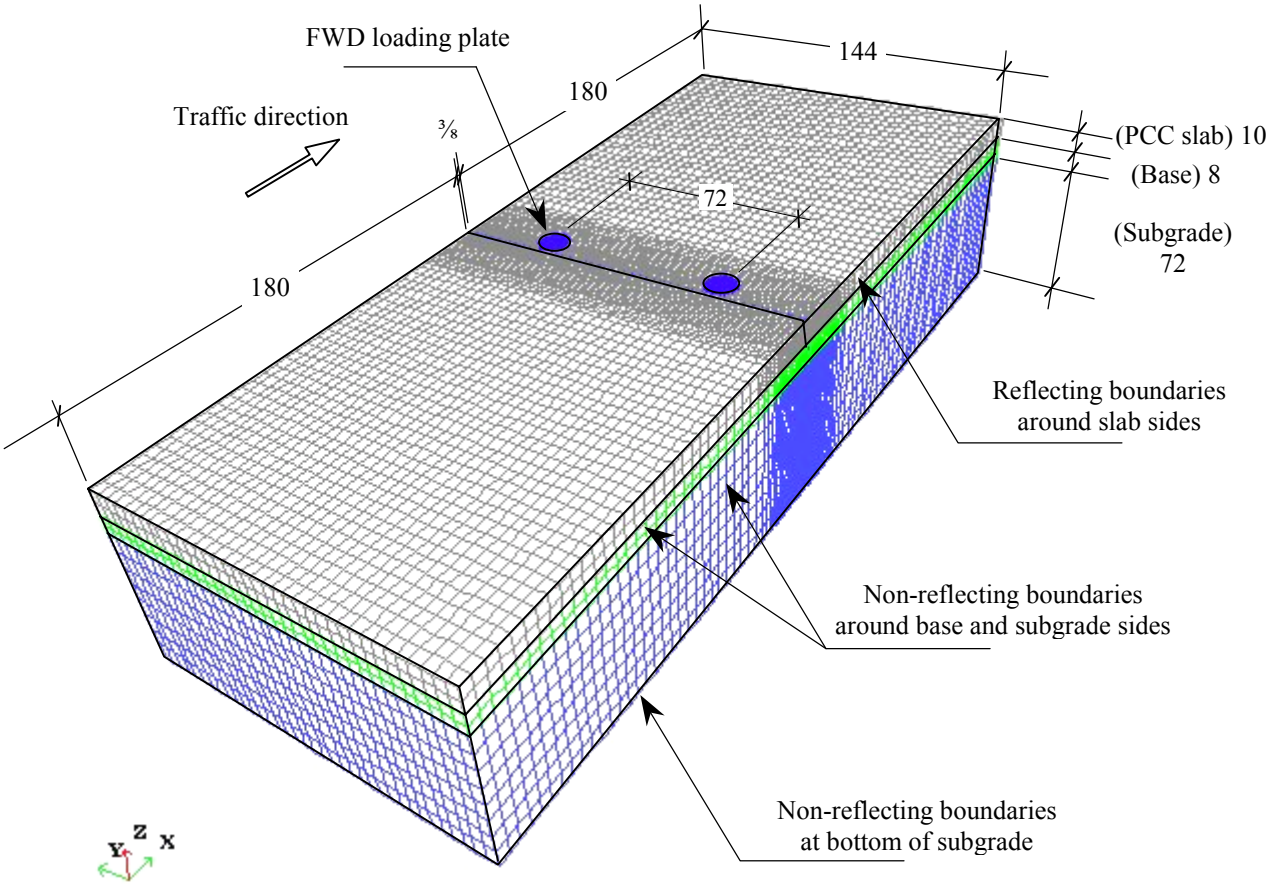

(Dimensions in inches)

FIGURE 3.1 Finite element model of pavement structure with straight joints

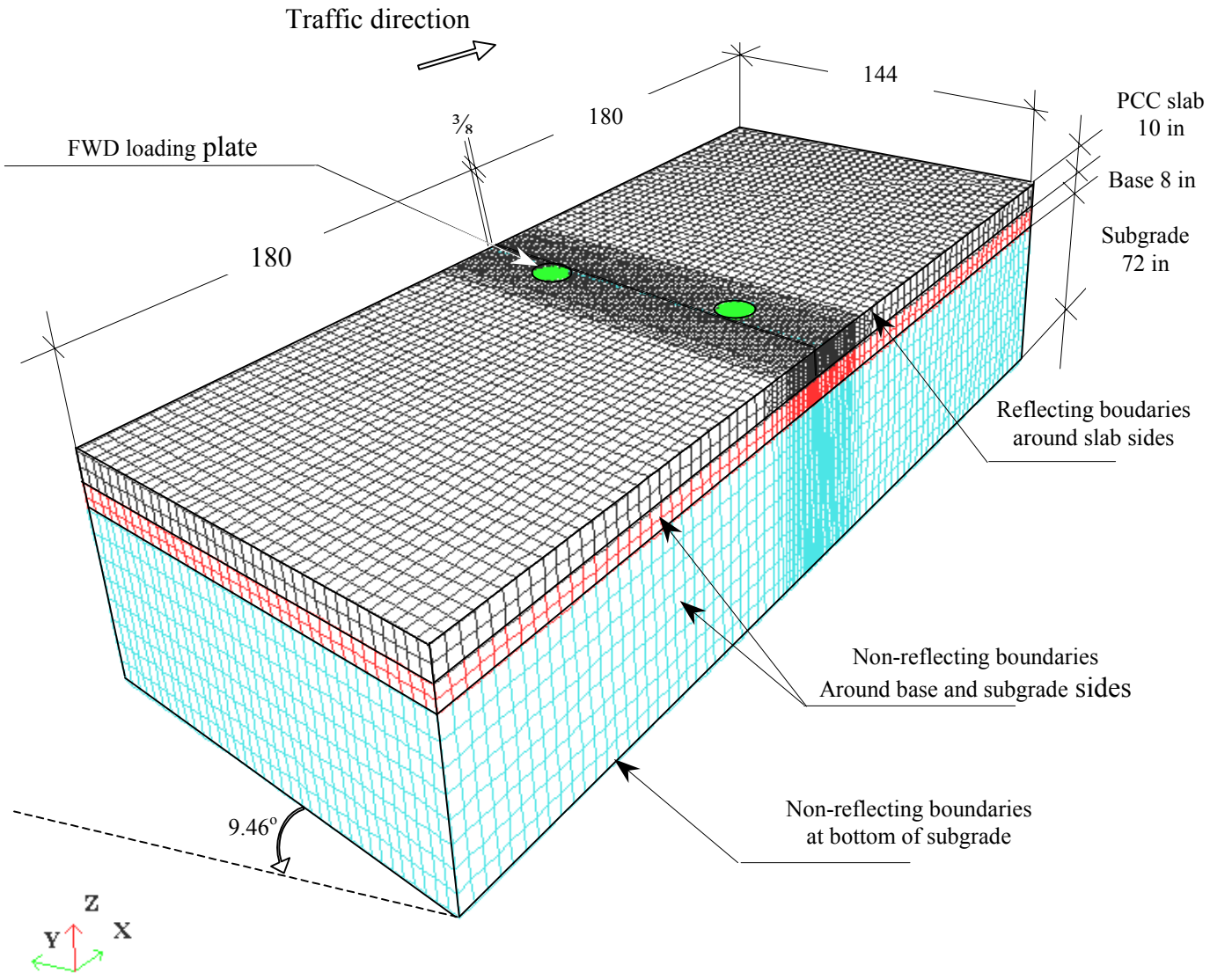

(Dimensions in inches)

FIGURE 3.2 Finite element model of pavement structure with skewed joints

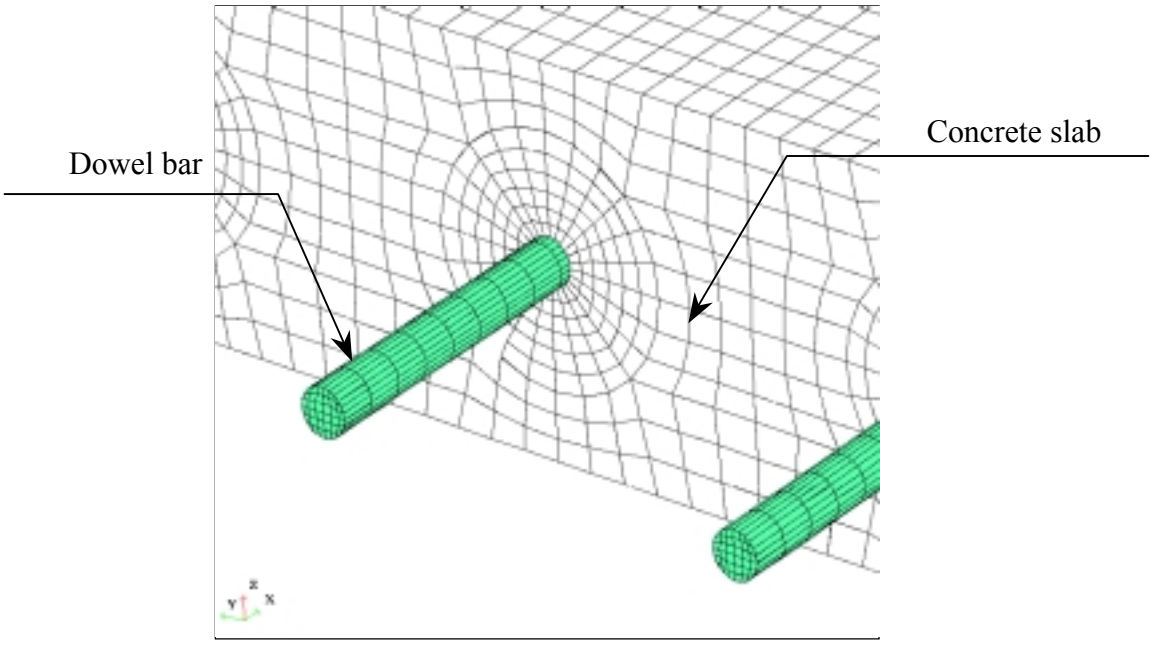

FIGURE 3.3 Finite element mesh at joint

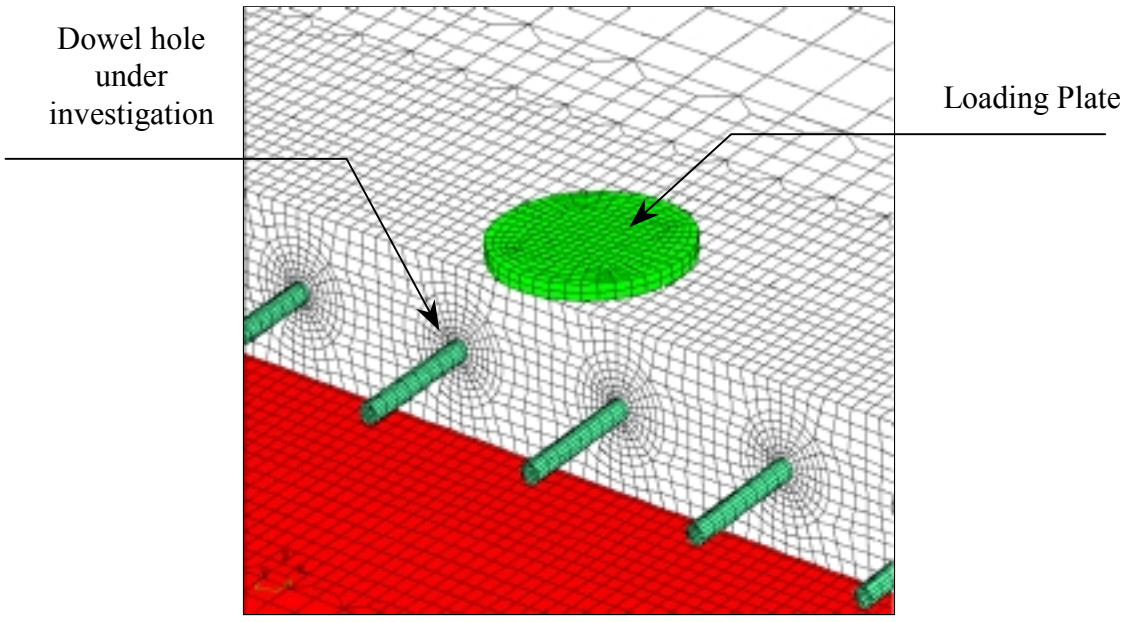

FIGURE 3.4 Position of dowel hole under investigation

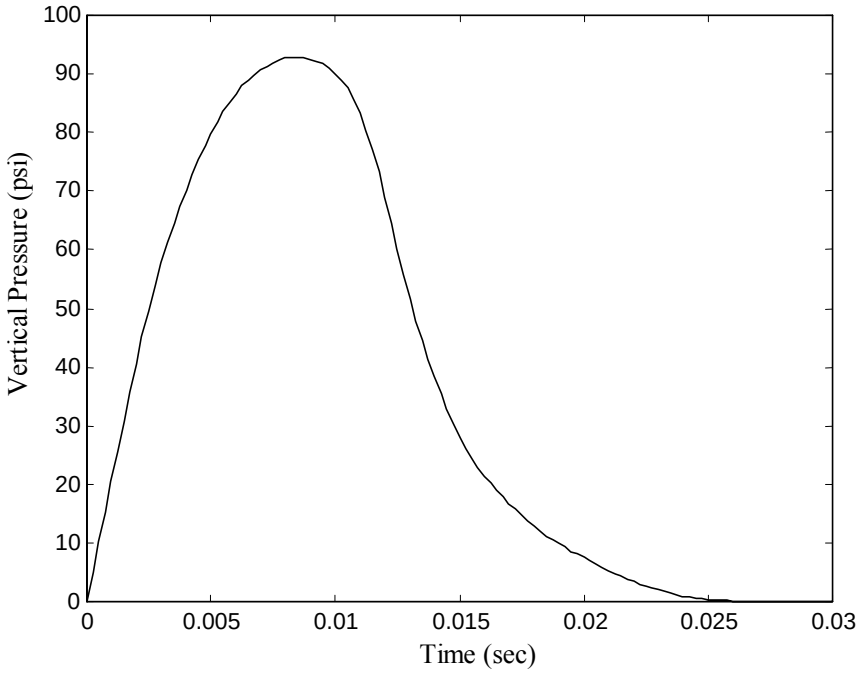

FIGURE 3.5 Impact FWD load

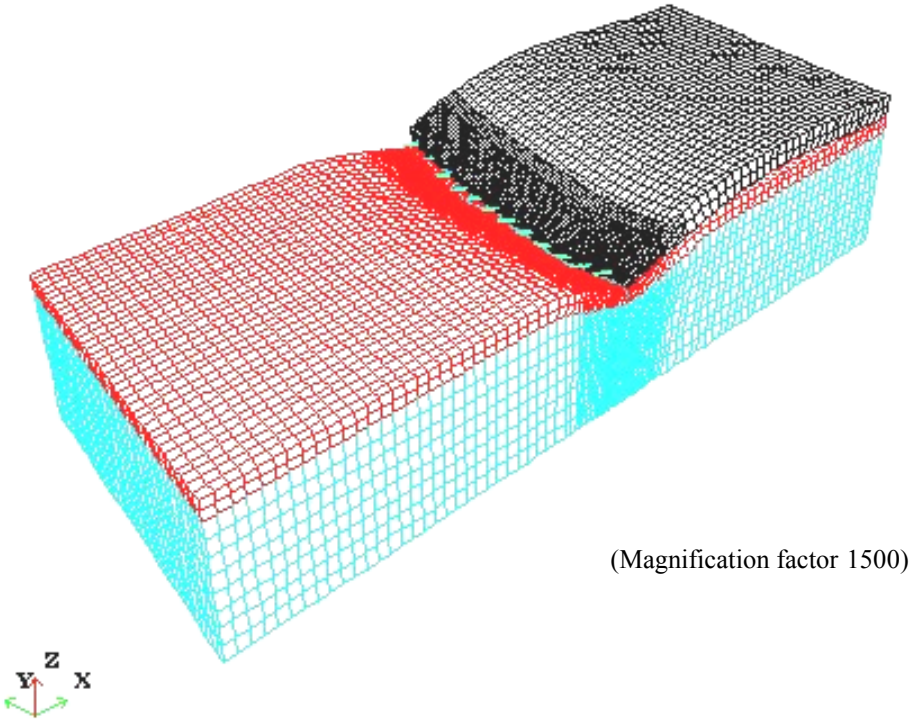

FIGURE 3.6 Deformation of skewed joint pavement, one slab removed, due to FWD load

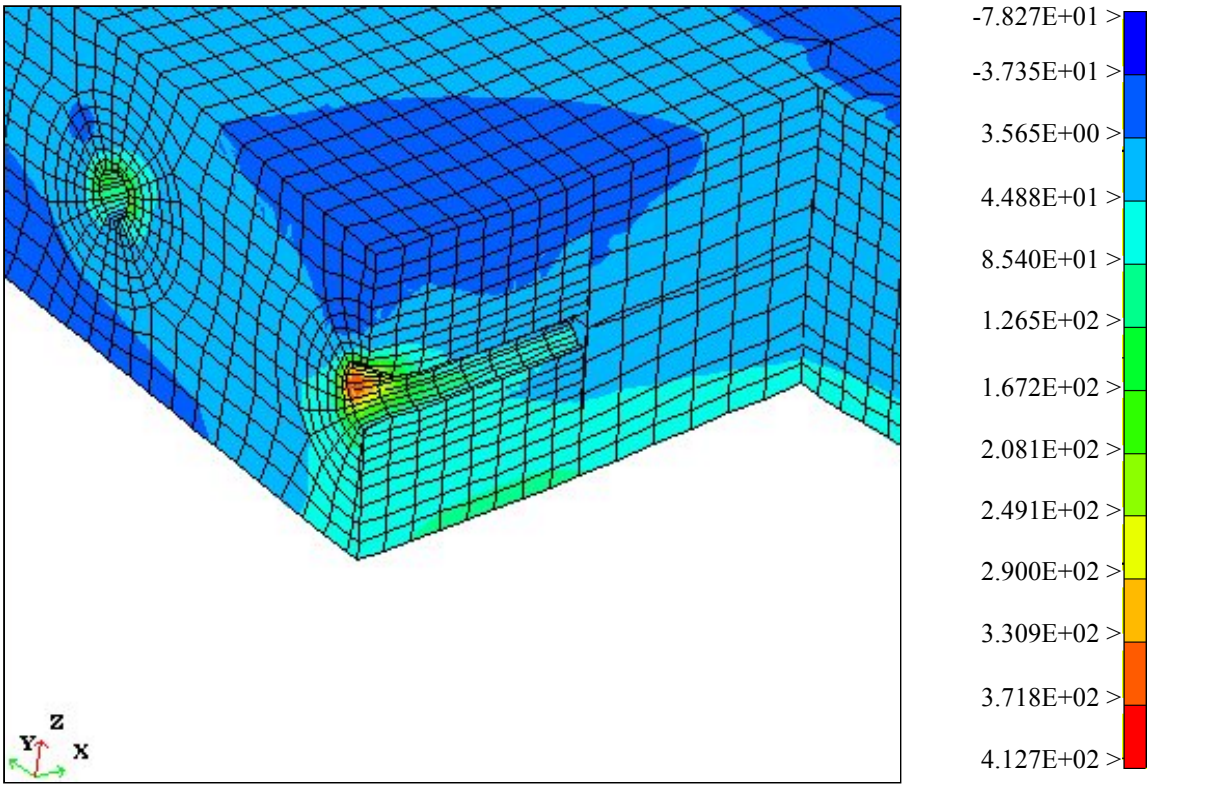

FIGURE 3.7 Section in straight joint slab showing maximum principal stresses in deformed dowel hole

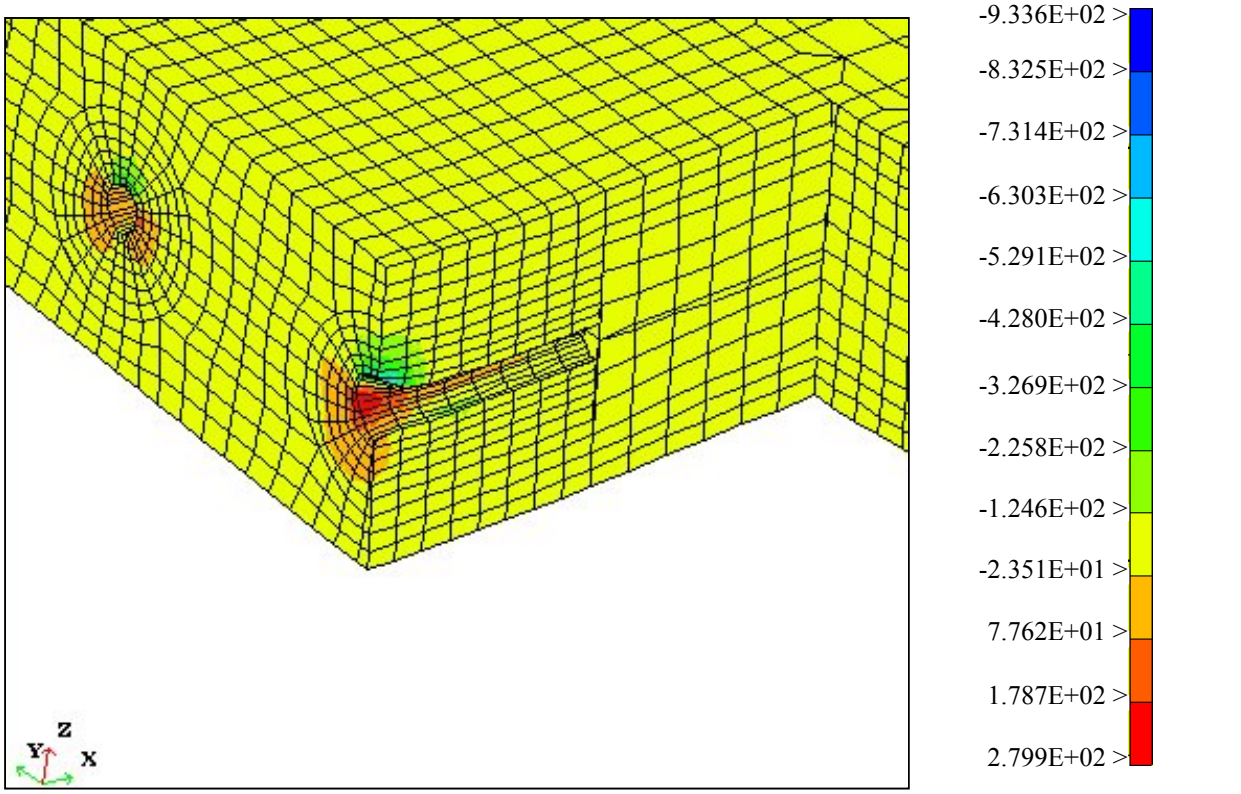

FIGURE 3.8 Section in straight joint slab showing vertical stresses in deformed dowel hole

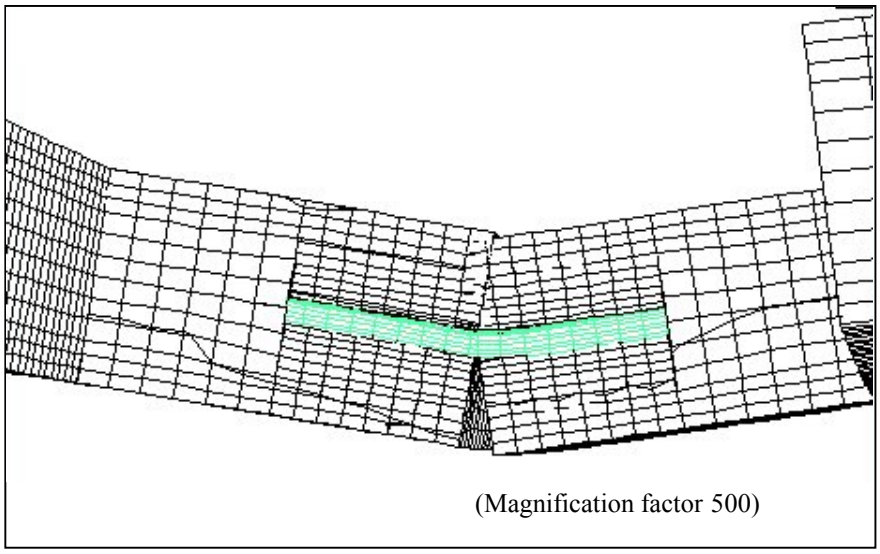

FIGURE 3.9 Deformation of dowel bar

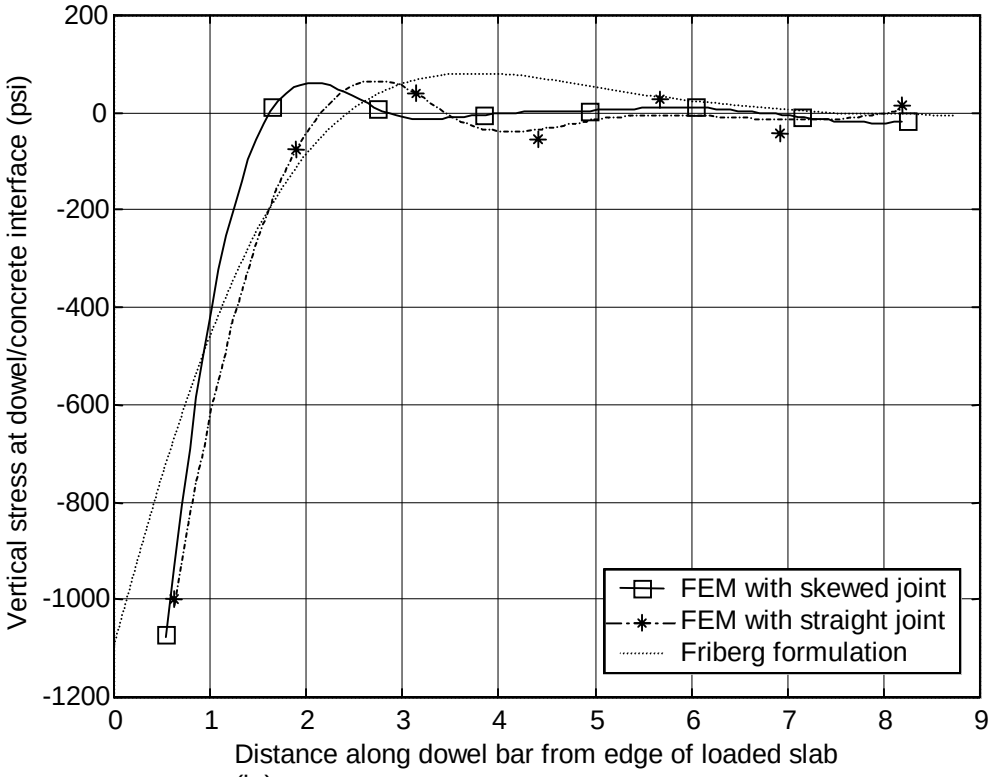

FIGURE 3.10 Vertical stress along dowel bar

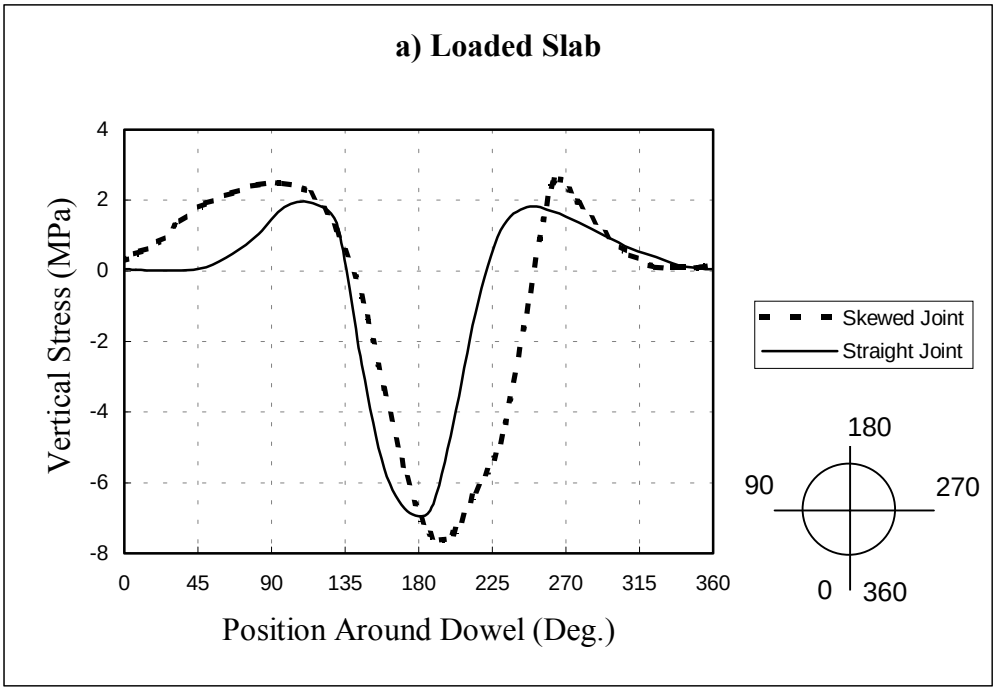

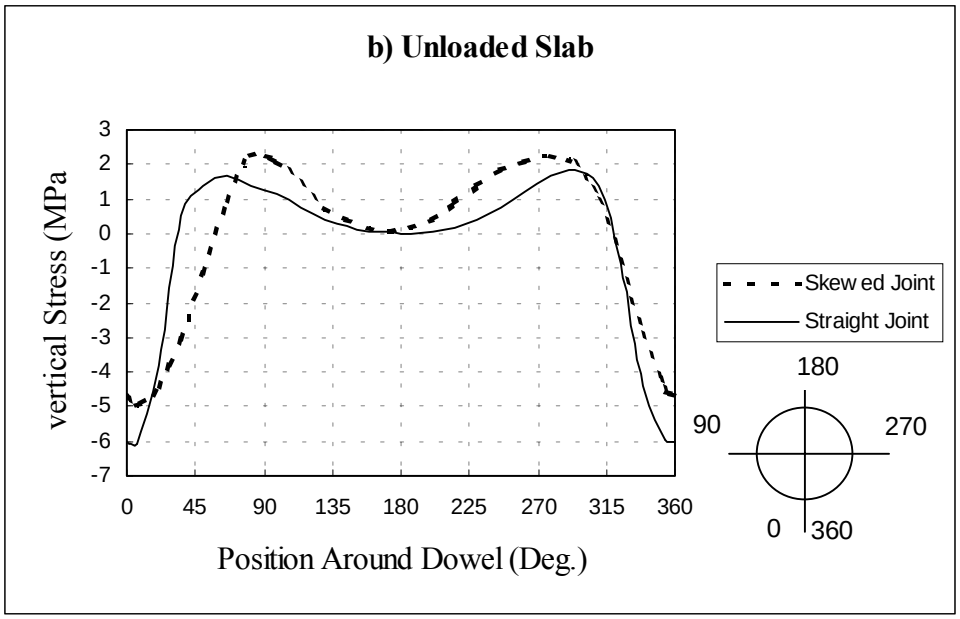

FIGURE 3.11 Vertical stress at dowel/concrete interface

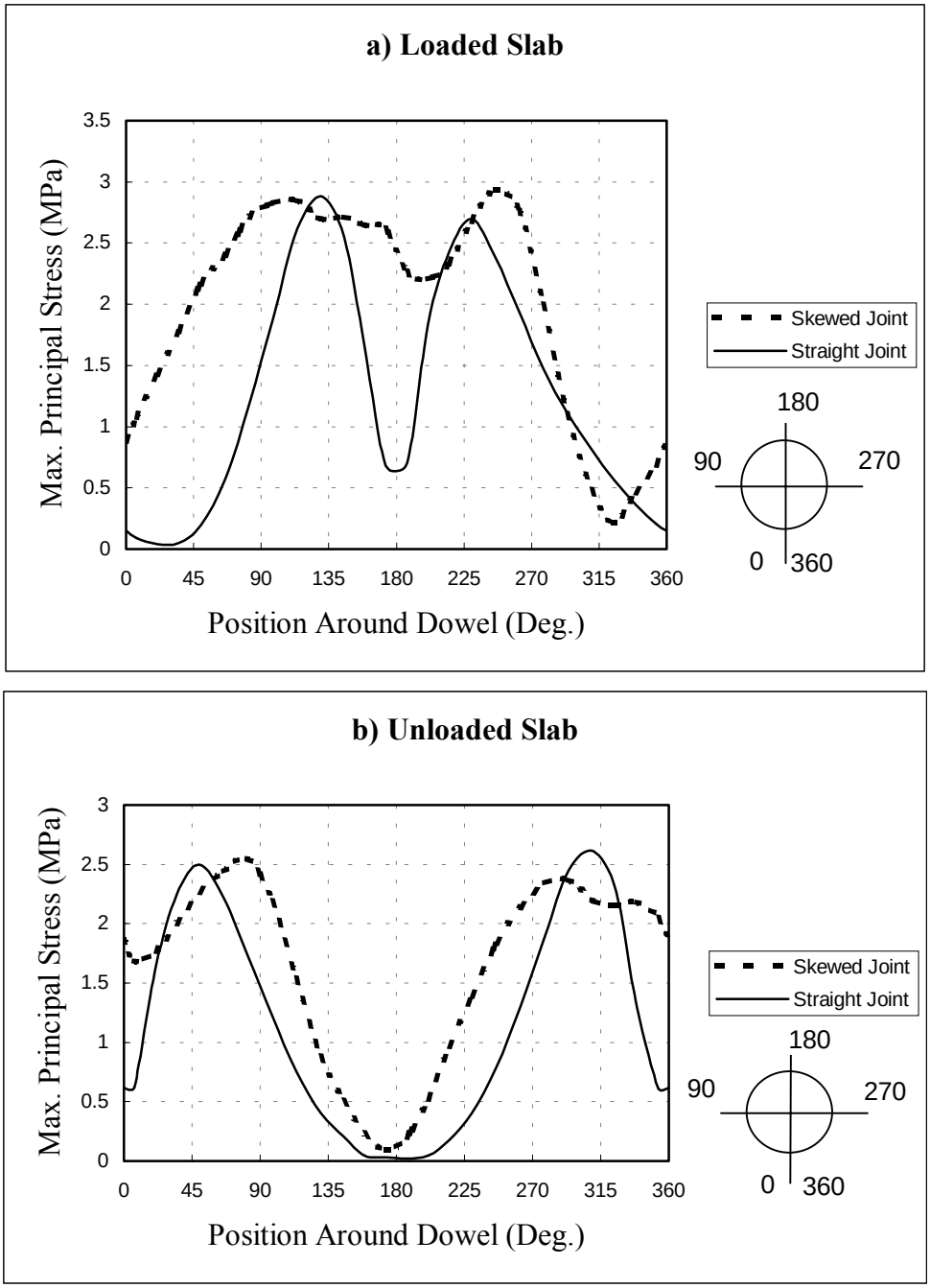

FIGURE 3.12 Maximum principal stresses at dowel/concrete interface

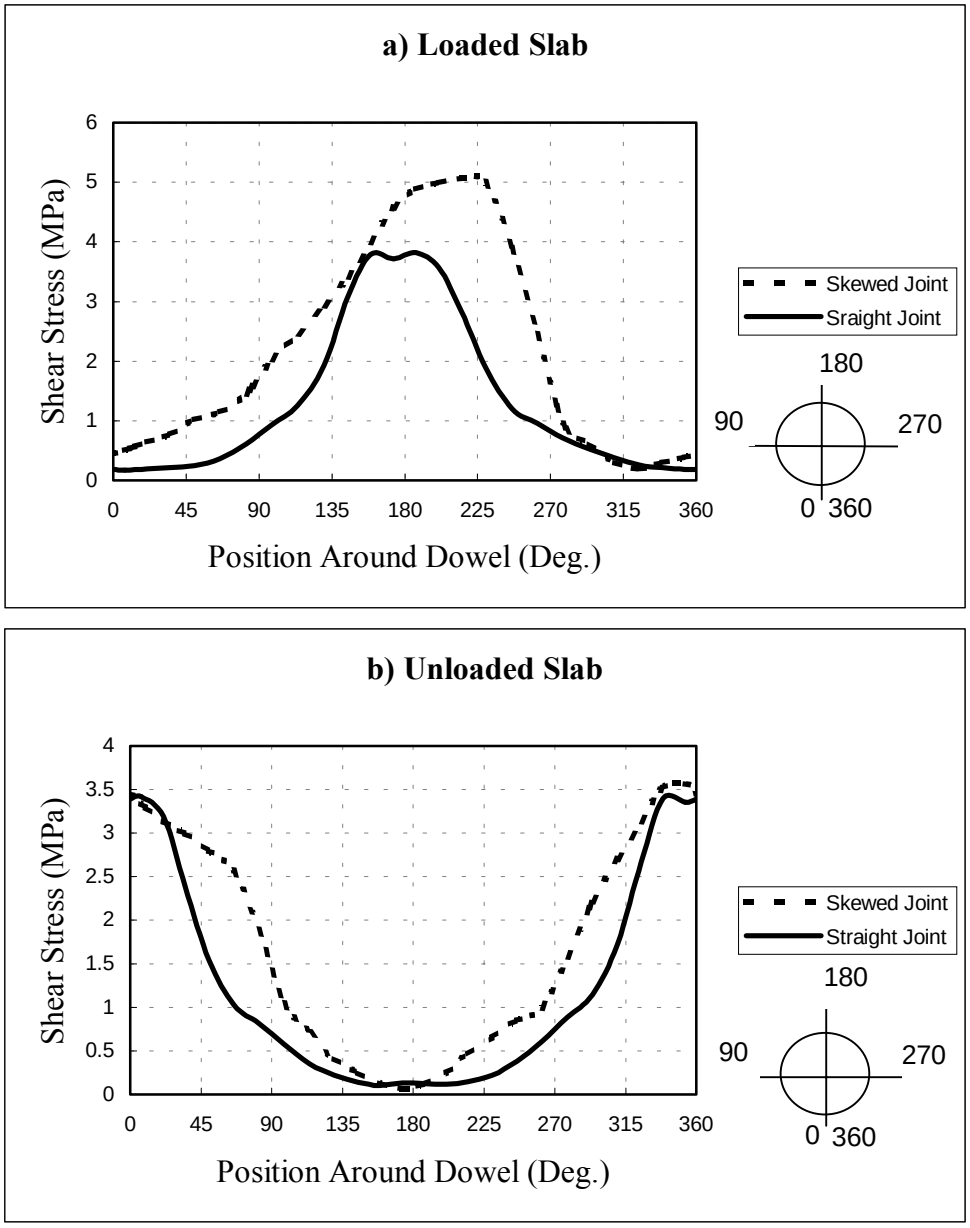

FIGURE 3.13 Shear stresses at dowel/concrete interface

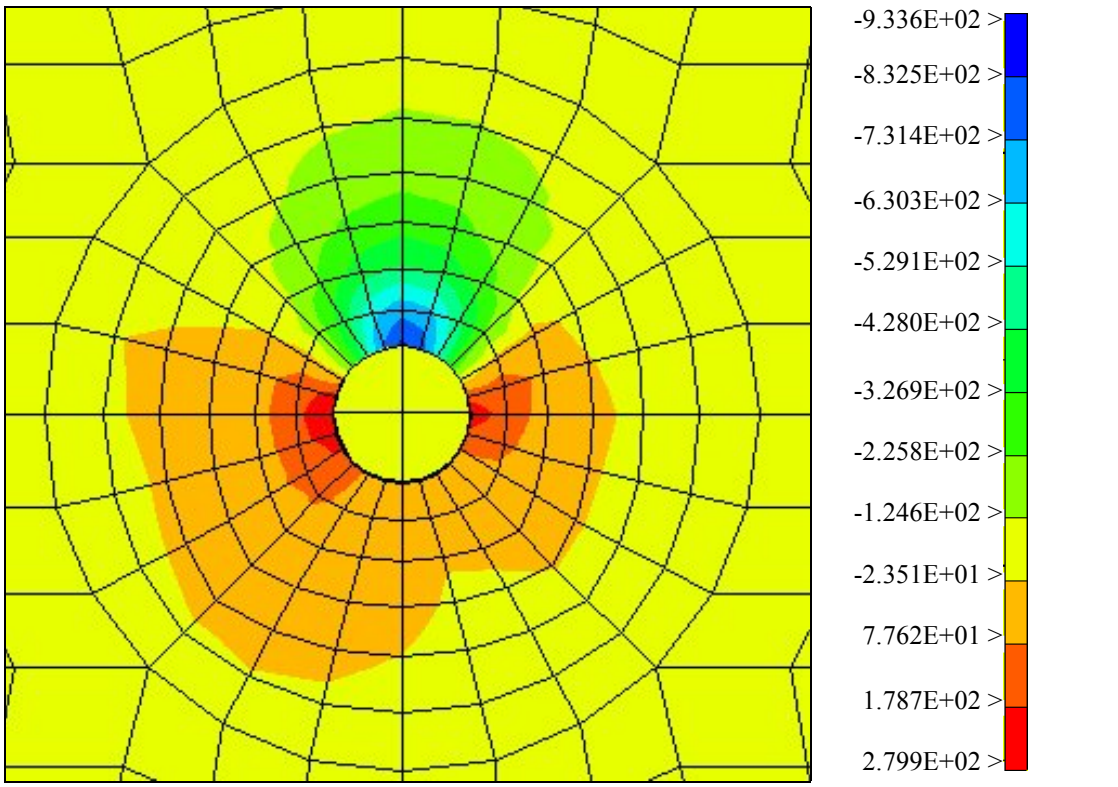

FIGURE 3.14 Fringes of vertical stresses around loaded dowel in straight joint model

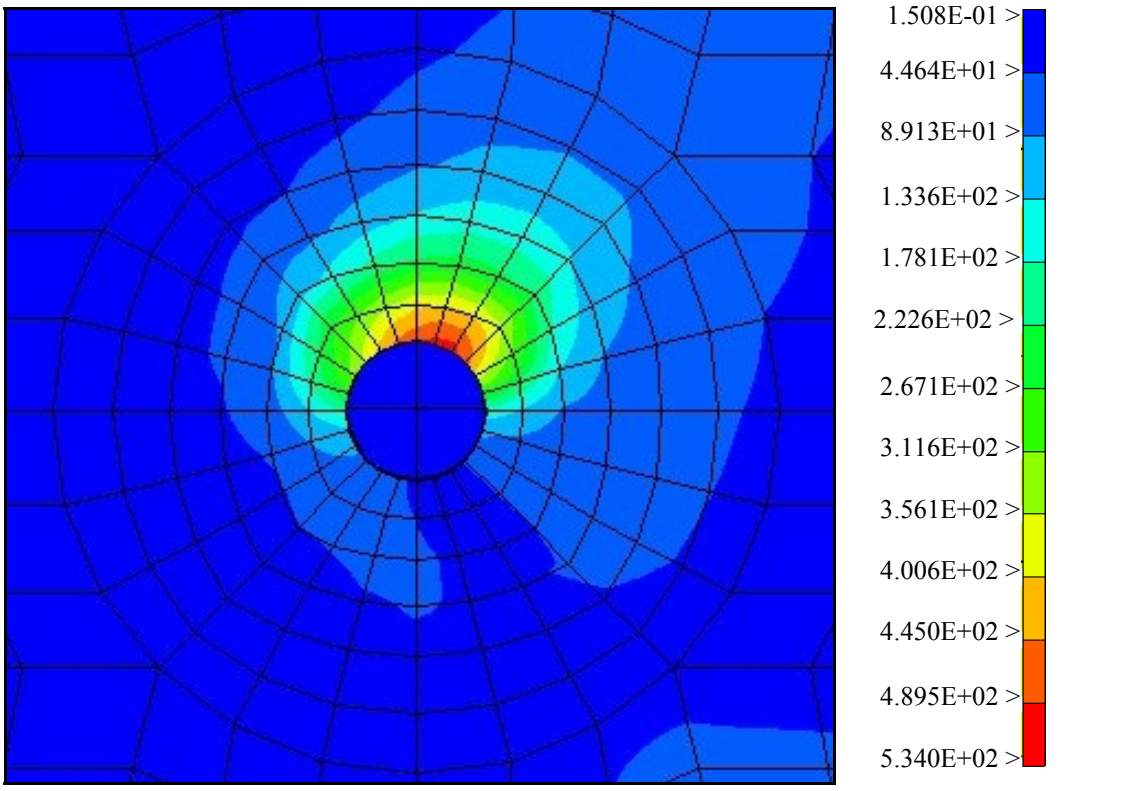

FIGURE 3.15 Fringes of shear stresses around loaded dowel in straight joint model

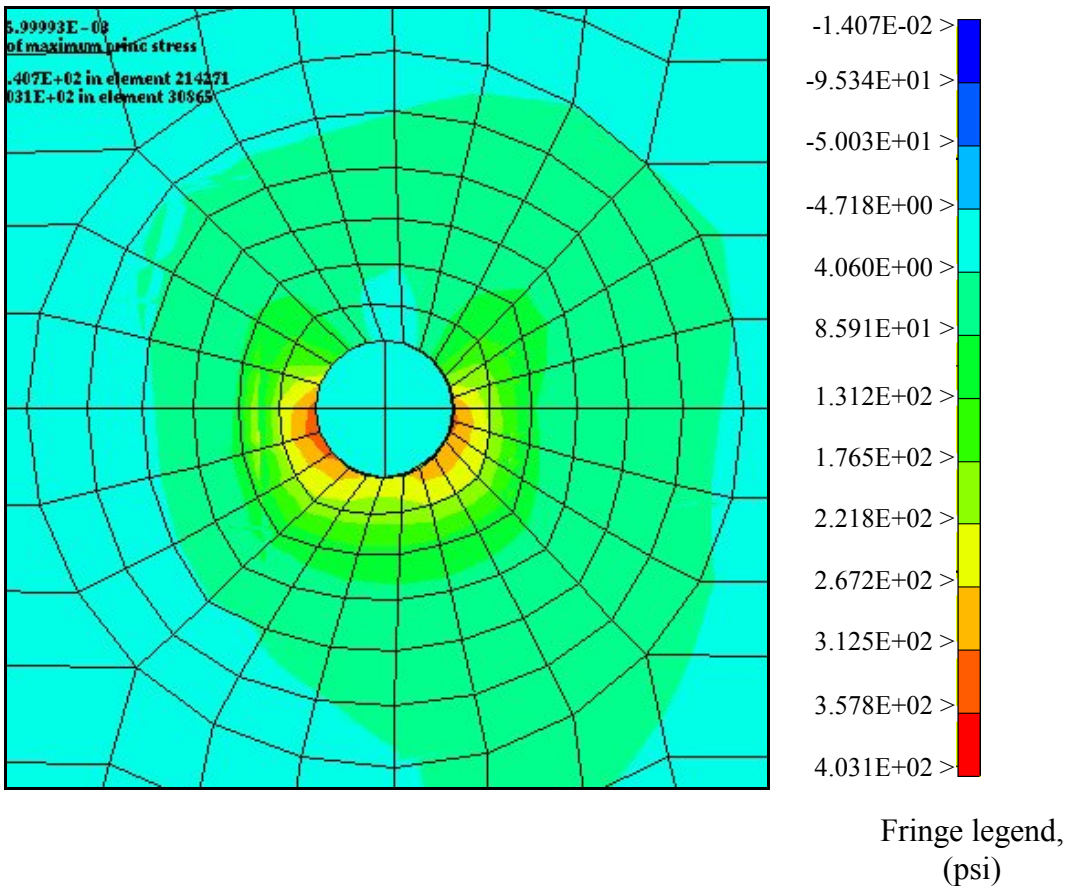

FIGURE 3.16 Fringes of max. princ. stresses around unloaded dowel hole in skewed joint model

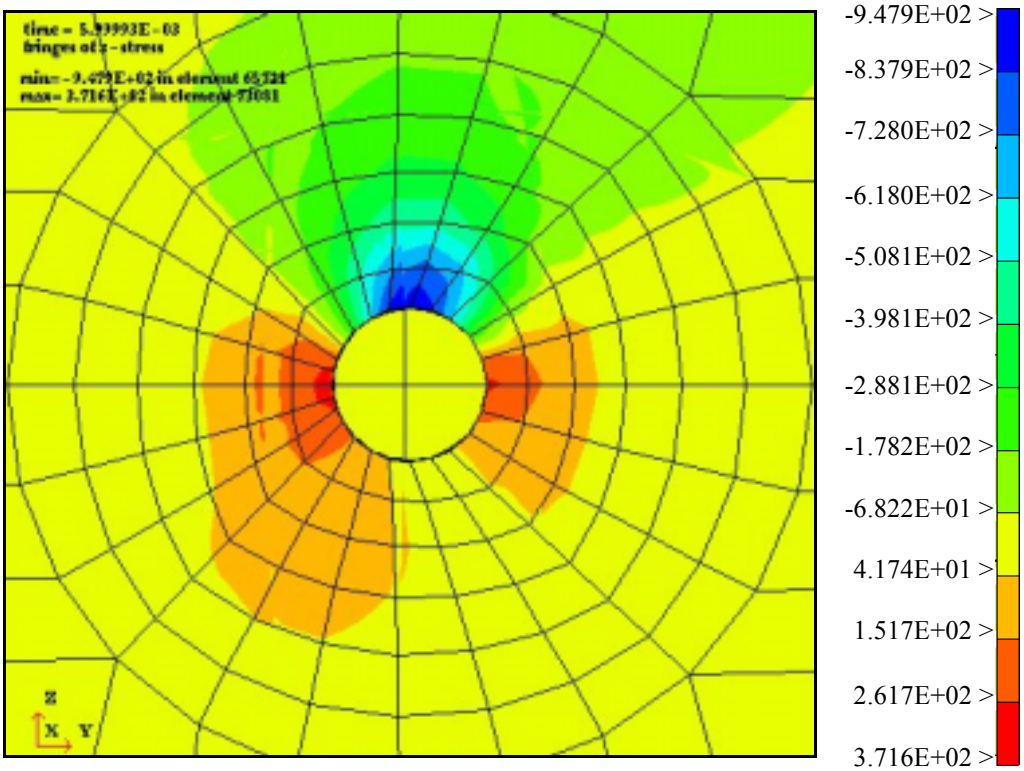

Fringe legend, (psi)

FIGURE 3.17 Fringes of vertical stresses around loaded dowel hole in skewed joint model

CHAPTER FOUR

LABORATORY STUDY

4.1. INTRODUCTION

In this chapter, a laboratory experimental study on simulated doweled joints is presented. The objectives of the experimental tests are to validate the findings from the finite element study, and to study the characteristics of the loaded doweled joints. The current chapter includes the description of the test rig, the associated instrumentation, the preparation of the specimens, and the tests results. The test rig was designed to conduct a set of load transmission tests on simulated doweled joints. The reason for conducting the study in the laboratory is to exercise maximum control on the specimens, the loading equipments, and the measuring sensors. This approach served to conduct all tests in absence of thermal effects, and moisture variations, which would be very expensive to isolate, in field-testing.

4.2. TEST RIG STRUCTURE

The test setup shown in Figure 4.1 consists of a loading frame where concrete specimens could be mounted, and tested. The supporting system is carefully set to be highly rigid. The testing setup is designed for testing two types of specimens. The first type consists of specimens with embedded dowels at their ends, while the second is specimens that simulate simulating complete joints. The loading, and data retrieval systems are computer controlled, which eliminates human interference in loading and data collection, thus minimizing human errors.

Figure 4.2 schematically illustrates the testing setup used in testing the first type of specimens. It consists of a hydraulic actuator manufactured by MTS [3] that reacts against a structural steel frame [7]. The actuator is capable of applying static as well as dynamic loads of known magnitudes to a capacity of 88.96 KN (20,000 lbs). The

hydraulic actuator is driven by a hydraulic pump [18]. The pump is controlled by a programmable controller unit [8] that is connected to a computer [10]. The computer-control-software automates the application of the load. The program was set to apply loads of desired magnitude, with selected rates of loading-unloading, as well as cyclic loading of desired frequencies. The load is transmitted to the specimens through a ram fitted with a spherical joint that ensures axial loading of the specimen. The load is applied on a steel plate, resting on 20x13.8 cm (7.89x5.43 in) rubber pad [14]. The pad dimensions ratio were selected according to the rectangular contact tire print dimensions ratio of 1:1.45 (width:length) (9). The rubber pad provides a uniform pressure distribution on the specimen over an area equivalent to a single truck tire contact. The magnitude of the applied load is measured using a load cell [4]. The specimens supporting system consists of a structural I beam [11], resting on the load floor [17]. A very thin plaster layer [21] was cast at the floor-beam interface to ensure the stability of the supporting system under loading conditions. The concrete specimen [1] rests at its rear end on a steel support [12] while the dowel bar [2] at its front end rests on a V-block [13]. The V-block is placed close to the face of the concrete specimen (0.3 in) in order to establish a case of pure shear loading. Vertical displacements data are measured using a linear voltage displacement transducer (LVDT) [5], mounted using a magnetic block [22]. The magnetic block rests on a steel support [16], which also carries the V-block [13]. The displacement of the face of the concrete specimen is measured in reference to a rigid steel strip [15] bonded to the top of the concrete specimen. The measure data including the load magnitudes, vertical displacements, and strains [6] are fed to two data acquisition systems [23] and [9].

The data acquisition system [23] is an in-house built system that consists of a switch box [20], to which the signals are fed from the load cell [4] and the LVDT [5]. The box is connected to a 16bit analogue to digital converter connected to a personal computer. This system was manually programmed to acquire, filter and display the plot of the load deflection relation in real time. The computer program will be described in details later in this chapter. The load and displacement signals are also monitored in real time through an oscilloscope [26]. The oscilloscope monitoring of signals is important to

ensure that the signals received from the measuring transducers are not corrupted by electronic noise. The second data acquisition system [9] is basically a Micro Measurement System 6000 that is designed for the measurement and recording of strain gage data as well as loads and displacements. This system is driven by a computer [10] that also controls the MTS hydraulic pump. The computer software that controls the system 6000 is supplied by Micro Measurements and is capable of real time storage and plotting of signals received from 20 sensors simultaneously. Figure 4.3 shows the employed instrumentation.

Figure 4.4 is a schematic drawing of the setup used for testing the second type of specimens that simulate full joints. Figure 4.5 illustrates the mounting of the full joint specimens. In this case the specimen ends were fully fixed to the supporting system via eight threaded rods at each end [24]. Two roller supports [25] are placed under the mid length of each concrete block forming the joint. Two LVDTs [5] and [5'] are used to collect vertical displacement data from both the loaded and the unloaded side of the simulated joint

4.3. TEST SPECIMENS

The experimental program included two types of specimens. In total, nine concrete specimens were prepared. The first type is half joint (HJ) specimens. Each contained a partially embedded dowel at each of its ends as illustrated in Figure 4.6. The width of the specimens [30.48 cm (12 in)] was selected to be the commonly used spacing between centers of dowel bars placed in rigid pavement joints. The length of the specimens [182.88 cm (72 in)] was selected to provide a sufficient span that would satisfy the pure shear loading condition, once the specimen is simply supported, and loaded in the vicinity of the support. This condition allows neglecting the effect of bending stresses in the specimen. Dowel bars were embedded, one at each end of the specimen, so that each end could be tested at a time. For this type, five specimens (HJ31) were fitted with dowel bars of 3.17 cm (1.25 in) in diameter. Those specimens provided ten dowel joints, from number HJ31-1 to HJ31-10. Two specimens (HJ38) were fitted

with dowel bars of 3.81 cm (1.5 in) in diameter. Those specimens provided four dowel joints, from number HJ38-1 to HJ38-4. Care was taken in order to obtain a smooth face at the specimen's ends that allows bonding of strain gages and facilitates visual observation of crack developments around the dowel bar.

The second type of specimens consists of two full joints. Two full joint (FJ) specimens were prepared. In this case, dowel bars [3.17 cm (1.25 in)] are totally embedded in plain concrete blocks as shown in Figure 4.7. The purpose of this arrangement is to study the performance of doweled joints under simulated loss of support conditions. The construction of these specimens was performed in two stages. The first stage consisted of casting half the specimen forming a plain concrete block [30.48 cm (12 in) wide, 91.4 cm (36 in) long, and 25.4 cm (10 in) thick], with half the dowel bar embedded. The half specimens were set to cure for 14 days, after which strain gages were bonded to the designated locations around the dowel bar as shown in Figure 4.8. The strain gages were then insulated against moisture penetration and tested to be functional under wet conditions. A sheet of carton, approximately 4 mm (0.16 in) thick was placed to cover the strain gages in order to protect them against any abrasion that may occur during the casting of the second part of the joint as shown in Figure 4.9. The second stage was to cast the remaining part of the joint, covering the exposed part of the dowel bar.

4.4. MATERIAL PROPERTIES

4.4.1. Concrete materials

All specimens were cast using Portland cement concrete with 1.25 cm (1/2 in) nominal maximum size aggregate. The concrete mix was proportioned to obtain a target compressive strength ranging from 27.6 Mpa (4000 psi) to 41.4 MPa (6000 psi), and a slump average of 8.9 cm (3.5 in). For each cast, eight standard concrete cylinders 15.2 cm (6 in) by 30.5 cm (12 in) were prepared to test the compressive strength of the concrete mix. The concrete mix proportions, with a listing of the used materials sources are listed in Table 4.1. Appendix II contains the concrete composition provided by the concrete

mix supplier. All specimens were allowed to cure for twenty-eight days, covered with wet burlap and plastic sheets. Testing of concrete cylinders indicated a mean compressive strength of 37.9 Mpa (5500 psi) after 28 days for HJ specimens, and 27.57 Mpa (4000 psi) for FJ specimens.

TABLE 4.1 Concrete Mix Proportions

Constituent	**Item**	**Supplier**	**Wt.** ***(lb)***	**Abs. Vol.** ***(cu. ft.)***
Cementitious Materials ASTM C 150 & C 618	Type 1	Armstrong Cement	564	2.87
Aggregates ASTM C 33 & ASTM C 330	Greer 57 Limestone Stocker Sand Greer 67 Limestone	Greer Stocker & Gravel Greer	950 1147 950	5.64 6.99 5.64
Percent Air			6%	1.62
Water			265	4.25
		TOTAL	3876	27
Air-Entraining Agent ASTM C 260	MB AE 90	Master Builders		2.82 oz/yd
Other Admixtures ASTM C 494	Polyheed 997	Master Builders		39.48 oz/yd

4.4.2. Dowels

All dowels were 45.72 cm (18 in) long, epoxy coated dowel bars, round in cross section, with a diameter of 31.75 mm (1.25 in) and 38.1 mm (1.5 in). Table 4.2 contains a listing the dowel material properties. Appendix II contains the steel properties certificate provided by the dowel bar supplier.

TABLE 4.2 Physical properties of steel dowel

DESCRIPTION	Yield *PSI*	Tensile *PSI*	Elongation *% In 8"*
Kankakee, IL steel Division Diam. 1¼ in (ASTM A706-96b)	63,400 (437 Mpa)	98,000 (676 Mpa)	14.0
Kankakee, IL steel Division Diam. 1½ in (ASTM A706-95b)	80,800 (557 Mpa)	115,800 (798 Mpa)	12.0

4.5. INSTRUMENTATION AND DATA ACQUISITION

4.5.1. Instrumentation

Instrumentations for the laboratory experiments were selected to provide data for the magnitude of the applied load, vertical displacements of the top surface of the joint, and strains at the joint's face around the dowel bars.

The applied load was measured using MTS strain gage load cell, and monitored through the MTS controller unit, which also provides an additional DC output signal. Figure 4.10 illustrates the calibration curve for the load cell. The calibration report from MTS could be found in Appendix III.

Deflections were measured using LVDTs that translate linear displacement into alternating current (AC). The AC current is fed into a signal conditioner module that produces a direct current (DC) voltage proportional to the input displacement. Two types of LVDTs were used in this study. The first is model (060-A797-05) manufactured by Sensotec with a range of ± 0.5 in. The second is model (060-3590-06) manufactured also by Sensotec with a range of ± 0.2 in. Figure 4.11 and Figure 4.12 illustrate the calibration

charts for both LVDTs respectively. The Sensotec Calibration certificates of the LVDTs are given in Appendix IV.

Surface strains were measured using foil resistance strain gages. Two types were selected to capture the vertical strains around the dowel bars. The typical properties of each type are listed in table 4.3.

TABLE 4.3 Strain gages properties

Strain Gage type	Resistance Ω	Gage length *(in)*	Gage factor	Strain level *με*	Fatigue life *Cycles*
CEA-06-500UW-120	120	0.5	2.065	±1500	100,000
WK-06-10CBE-350	350	1.0	2.05	±2200	1,000,000

4.5.2. Data acquisition

Two data acquisition systems were employed for the collection and storage of the test results. The first was used during several pilot tests, where the aim was to test the accuracy of the measuring equipments, and to monitor the stability and behavior of the specimen. During this stage, only the applied load, and the displacement of the joints edge were measured. For efficient real-time monitoring and plotting of the load-displacement relation, a data acquisition system was built. The system software was developed in 'Labview" programming language. The software performs the following functions:

1. Drive the analog to digital (A/D) board to sample the signals from two channels at a specified sampling rate; one carries the loading signal, and the other carries the displacement signal.
2. Store the samples over a specified period of time. The time period selected was chosen to be five times the sampling rate, which was set at 0.1 sec. for static loading-unloading tests.
3. Employ a median filter to filter out the electronic noise.

4. Display a real time plot of the load-displacement relation on the computer monitor.
5. Store both the filtered and unfiltered data in an ASCI file.
6. For monitoring of load-displacement relation during fatigue testing, the program is provided with a counter that counts the number of loading cycles.

Figure 4.13 illustrates the block diagram for the developed virtual instrument, which is actually the real executable code. The program consists of a set of functions, sub-virtual instruments (VI) nodes, control and indicator terminals sustained in a loop that controls the program flow as long as the stop controller is not used to stop the execution of the loop. Once the program is set to run, it starts by reading one immediate scan from the specified input analog channels. The output of this subVI is a one-dimensional array that contains scaled analog input data for each measured channel. The collected data is then split to two scalars representing the output voltage from the load cell, and the current displacement reading. The actual load is obtained by multiplying the output voltage from the load cell by the specified calibration factor, and the actual displacement is obtained through zero offsets. The offsets are carried out by subtracting the current displacement reading from an initial reading indicated at the beginning of the test when the displacement is zero. A new array is then rebuilt, transposed, and transformed into a text string, which is written and appended into a specified file. This file could be easily accessed later, and opened by most spreadsheet programs. Another subVI is then used to open the built text file, read and convert it into two-dimensional single precision array of numbers, and close it afterwards. The array is once again split into displacements and load magnitudes, and conveyed into different fields. The load array passes through a threshold peak detector that analyses the input sequence for a valid peak, and keeps a count for the number of peaks encountered. The displacements array is introduced into a median filter that filters the input sequence for a given rank. The median of a data sequence is the midpoint value in the sorted version of that sequence. The filtered data are then rebuilt into a new array, and another sbVI is used to plot it into an XY graph, illustrating the displacement versus the load. Once the whole operation is finished, another loop takes place after a specified number of milliseconds indicated by a time

resolution controller. When the test is finished, an optional feature to store the final filtered array into a text file is provided. An example of the program output is shown in Figure 4.14.

The second data acquisition system is System 6000 manufactured by Micro Measurements Group, and operated by the Strain Smart software. This system was selected for acquiring strain data. System 6000 is capable of measuring and recording dynamic strains during high frequency fatigue testing. Strains can be measured independently through an expandable number of channels at the required frequency. The system contains also modules capable of acquiring data from load cells and LVDTs.

4.6. LOADING

Loading was applied to the concrete specimens in a manner that creates direct shear of the loaded dowel. Specimens HJ31-1 to HJ31-5 were tested to study the static load-displacements characteristics, failure load magnitudes, failure modes, and the repeatability of the test results. The loading configurations consisted of applying five sequences of loading-unloading cycles. The first sequence (LH7000) starts from zero, to 1000 lbs, then back to zero. Then loading-unloading cycles were applied in the same fashion with a 1000 lbs increment in the maximum load for every cycle till the maximum load reached 31.14 KN (7000 lbs) as illustrated in Figure 4.15. The second sequence (LH9000) follows the same procedure, up to 40.03 KN (9000 lbs). The third (LH12000), fourth (LH15000) and fifth (LH19000) sequences were performed for peeks of 53.38 KN (12000 lbs), 66.72 KN (15000 lbs), and 84.52 KN (19000 lbs) respectively. The loading and unloading rates were fixed at 1.112 KN/sec (250 lbs/sec). Following each loading sequence, the repeatability of the measured data was checked by performing an additional set of three loading-unloading cycles having the same peak loading magnitude of that sequence, and with the same loading rate.

Two dowel support conditions were used for testing half joint specimens:

1. The exposed part of the dowel bar is allowed to bend freely as illustrated in Figure 4.16.
2. The exposed part is fully restrained for bending as shown in Figure 4.17.

Figure 4.18 and Figure 4.19 show the two supporting arrangements respectively.

Since both the above dowel support conditions are not fully representative of the type of dowel support experienced in rigid pavement transverse joints, it was decided to conduct tests on full joints where the dowel bar is fully embedded in concrete. A ramp load (R9000) that increases in magnitude at a constant rate of 0.111 KN/sec (25 lbs/sec) up to 40.03 KN (9000 lbs) was used for testing full joint (FJ) specimens. The maximum load magnitude of 9000 lbs corresponds to the standard wheel load used in pavement design. Figure 4.20 illustrates the method of load application on FJ specimens. The R9000 loading configuration was also applied on specimens HJ31-6 to HJ31-10 and HJ38-1 to HJ38-4 for collection of strain data around the dowel bars. Table 4.4 shows a list of the specimens and the applied loading configurations.

Table 4.4 Loading of different specimens

`

Specimens		Load					
Type of spec.	**Spec. No.**	**LH7000**	**LH9000**	**LH12000**	**LH15000**	**LH19000**	**R9000**
Half joints	HJ31-1	✓	✓	✓	✓	✓	
	HJ31-2	✓	✓	✓	✓	✓	
	HJ31-3	✓	✓	✓	✓	✓	
	HJ31-4	✓	✓	✓	✓	✓	
	HJ31-5	✓	✓	✓	✓	✓	
	HJ31-6						✓
	HJ31-7						✓
	HJ31-8						✓
	HJ31-9						✓
	HJ31-10						✓
	HJ38-1						✓
	HJ38-2						✓
	HJ38-3						✓
	HJ38-4						--
Full joints	FJ-1						✓
	FJ-2						✓

4.7. HALF JOINT TESTS

4.7.1. Load-displacement

Figure 4.21 to Figure 4.31 illustrate typical examples of the load-displacement relations obtained from HJ specimens. This set of results was obtained from the tests conducted on specimens HJ31-1 to HJ31-5. Specimens HJ31-1 and HJ31-2 were tested with unconstrained dowel bars; while specimens HJ31-3 to HJ31-5 were tested with constrained dowel bars. Figure 4.21 illustrates the results from specimen HJ31-1 subjected to load LH7000. The plot indicates the development of permanent residual displacement after each loading-unloading cycle. The magnitude of the residual displacement increases as the load increases. Figure 4.22 illustrates the failure of specimen HJ31-1 while subjected to load LH19000 at a load of 15,400 lbs. As the load

magnitude increases after 14,000 lbs, a highly nonlinear zone appears, indicating the start of the specimen failure. Figure 4.23 shows the results obtained from specimen HJ31-2 subjected to load LH7000. The same observations concerning residual displacements and slopes in Figure 4.21 are applicable. Figure 4.24 shows the failure curves for specimen HJ31-2 at 17,500 lbs. Figure 4.25 illustrates the load-displacement relation of specimen HJ31-3 subjected to load LH7000. It is noticed that due to the effect of constraining the exposed part of the dowel bar, the maximum and residual displacements in this case are relatively smaller than those obtained from the previous specimens. Although the curvature in this plot is found opposite to the curvature of the unconstrained specimens, the slope break point occurred at about 3,900 lbs, close to what was previously noticed for the first two tests. Figure 4.26 shows the load-deflection relation of specimen HJ31-3 subjected to load LH19000. The maximum applied load was set not to exceed 19,000 lbs, which is 1,000 lbs below the maximum capacity of the hydraulic actuator for safety purposes. The effect of constraining the exposed part of the dowel is mostly recognized at the first cycles of loading till a load of about 5,000 lbs where the curvature of the load-displacement relation is opposite to that obtained in the first two specimens. Beyond this load, the behavior of the specimens is qualitatively similar, with a higher load capacity for the case of constrained dowel bar. Figure 4.27 and Figure 4.29 show the load-displacement relation for specimen HJ31-4 and specimen HJ31-5 respectively at the sequence of loading LH9000. Figure 4.28 and Figure 30 illustrate an example of repeated three cycles of loading-unloading on specimen HJ31-4 and specimen HJ31-5 respectively for a maximum load of 9000 lbs following the application of the sequence LH9000. The overlapping of the three plots corresponding to the three cycles of loading within each individual specimen demonstrates the level of accuracy that the results provide. Figure 4.31 shows the load-displacement relation of specimen HJ31-5 subjected to load LH19000. No failure was reached at this stage for specimens HJ31-3, HJ31-4, and HJ31-5. The various test results indicate that the test rig, and the supporting arrangement did not have any influence on the repeatability of the load-displacement relations. The results of similar supporting arrangements are fairly close to each other. The maximum vertical displacements, as well as the residual displacements after each sequence of loading are listed in Table 4.5. The recorded magnitudes of displacements corresponding to the

maximum load at each cycle tends to form two slopes deviating at a load ranging from 3000 lbs to 4000 lbs. This is shown in Figure 4.32 where a relation between the measured maximum displacements after every cycle is plotted versus loading magnitude. At a load ranging from 3000 lbs to 4000 lbs, a deviation in the specimen behavior occurs, due to stress hardening for the case of unconstrained dowels, while softening in the case of constrained dowels.

As failure was not reached for the case of constrained specimens, fatigue testing was applied on specimen HJ31-4 and HJ31-5. For specimen HJ31-4, fatigue loading from 1,000 lbs to 9,000 lbs was applied and failure of the specimen occurred after 850,000 cycles. Fatigue testing applied on specimen HJ31-5 with amplitudes ranging from 1,000 lbs to 19,000 lbs resulted in failure of specimen after 282,400 cycles. The applied cyclic loading had a Sine wave shape, with a frequency of 10 Hz.

Table 4.5 Maximum and residual vertical displacements at the joint's face

Peek load / Specimen	7,000 *(lbs)*		9,000 *(lbs)*		12,000 *(lbs)*		15,000 *(lbs)*		Failure load *(lbs)*
	Max. displ. *(in)*	Residual disp. *(in)*	Max. displ. *(in)*	Residual disp. *(in)*	Max. displ. *(in)*	Residual disp. *(in)*	Max. displ. *(in)*	Residual disp. *(in)*	
HJ31-1	0.0103	0.0022	0.0128	0.0032	0.0162	0.004	0.0202	0.0055	15,400
HJ31-2	0.0102	0.002	0.0125	0.003	0.0165	0.0042	0.0205	0.0055	17,500
HJ31-3	0.0088	0.001	0.0115	0.0012	0.0145	0.002	0.017	0.0028	__
HJ31-4	0.011	0.001	0.0135	0.0015	0.014	0.0021	0.0172	0.0025	__
HJ31-5	0.010	0.0009	0.0132	0.001	0.0174	0.0018	0.0204	0.0023	__

4.7.2. Discussion of load-displacement results

4.7.2.1. Residual displacements

The results indicate that residual permanent displacements are developed following each cycle of loading. The amount of the permanent displacement is directly

proportional to the magnitude of the maximum applied load. Figure 4.33 Illustrates a plot showing the relation between the developed residual displacements and the applied load at load LH7000. It is believed that this phenomenon is mainly a result of two possible components. The first is due to the ductility of the steel dowel and the supports. The second is due to the development of tensile hair cracks and crushing of concrete particles by compressive bearing stresses. The development of the permanent residual displacement gives an indication of the effectiveness of the used dowel bar in transferring the load across the joint. The smaller the magnitude of the residual displacement, the better the joint performs. Considering the effect of fatigue loading due to the passage of millions of traveling axle loads, the developed residual displacement may be translated into faulting.

4.7.2.2. Failure mode.

The first failure mode observed in this study through all specimens is the formation of horizontal tensile cracks in the concrete material initiated at both sides of the dowel bar as illustrated in Figure 4.34. These cracks propagate towards the sides of the specimens as the load increases, accompanied by spalling in the compression zone on top of the dowel bar. Full failure occurs by splitting of the concrete material as shown in Figure 4.35, accompanied by a sudden vertical fracture from the top of the dowel bar, and extends to the top of the specimen as shown in Figure 4.36. The same mode of failure was observed by Friberg (28). The initiation of visible horizontal cracks indicates the development of high tensile stresses on both sides of the dowel bar. This confirms the finite element model results reported in chapter 3.

4.7.2.3. Effect of dowel fixation

Comparison between the load-displacement relations of the constrained specimens (HJ31-1 and HJ31-2) and unconstrained specimens (HJ31-3 to HJ31-5) indicates that the dowel support arrangement has a major effect on residual displacements, stiffness, and load magnitude at failure. It is noticed that unconstrained dowel bar against flexural deformations introduce bending stresses at the dowel-concrete interface, which accelerates the joint failure. This is evident as both tests performed on

unconstrained dowels resulted in failure loads of 15,400 lbs 17,500 lbs. On the other hand, no failure load could be reached through the three tests conducted on constrained dowel specimens. Moreover, the permanent residual displacement following each sequence of loading cycles, are smaller in the cases where the dowels were constrained. The stiffness of the constrained specimens is relatively higher than that of the unconstrained ones. This is evident from the slope of the load-displacement relations in both cases, where it is found higher for the case of constrained dowels. The reason for the superior performance of the specimens with constrained dowels is that the bending of the dowel bar causes excessive vertical displacements in the vicinity of the joint, which causes the concrete incasing the dowel bar to split under tensile stresses along the center of the specimen. This case of loading is much more severe than what happens in rigid pavement joints, however it is more close to reality than the case where the dowel is constrained.

4.7.3. Load-strain results

Half joint specimens HJ31-6 to HJ31-10 as well as HJ38-1 to HJ38-4 were subjected to load R9000. Strain data on the side and top of the dowel bar were collected during the test procedure, and plotted against the corresponding load. Figure 4.37 to Figure 4.39 illustrate the load-strain relationship for specimen HJ38-1 to specimen HJ38-3 respectively. The positive strain values correspond to tensile strains at the sides of the dowel, while the negative strains correspond to compressive strains at the top of the dowel bar. Data for specimen HJ38-4 were not available due to the damage of the specimen's face during construction, hence preventing adequate application of strain gages. Also entrapped air was found on the sides of the dowel bar in specimen HJ38-3. For this particular specimen, the tensile strains shown in Figure 4.39 were collected at a distance from the side of the dowel measuring 0.5 in. Figure 4.37 and Figure 4.38 indicate that high tensile strains are developed at the sides of the dowel bar, as predicted, in addition to high compressive strains on the top of the dowel. The magnitude of tensile strains shown in Figure 4.39 is relatively small compared to what was measured in the previous two tests, as a result of measuring the strains at a distance from the dowel bar. The compressive strains at the top of the dowel bar are found fairly close to each other

(from 1200 με to 1500 με). Residual permanent strains are observed at the end of the test, varying in magnitude from one specimen to the other. This variation is related to the nature of the concrete mix, which does not provide exactly similar compositions of aggregates, paste, and entrained air at similar regions in different specimens. These variations are more likely to be noticed in small strain magnitudes rather than in large ones, at which the effect of the concrete composition is less considerable.

Figure 4.40 to Figure 4.44 illustrate the load-strain relations for half joint specimens HJ31-6 to HJ31-10 respectively. The maximum vertical tensile strains on the sides of the dowel bars are found to be around 2000 με, while the compressive strains on top of the dowel bars, are found measuring around 1500 με. The compressive strains at the top of the dowel for specimen HJ31-8 were not collected as a crack in the concrete material was observed at this location prior to testing.

4.8. TESTS ON FULL JOINT SPECIMENS

4.8.1. Load-displacement results

Figure 4.45 illustrates the load-deflection relations for the full joint specimen FJ1. Vertical displacements were measured at the face of the loaded and the unloaded sides of the joint. The specimen failed at 6000 lbs due to flexural tensile stresses at the top of the concrete block over the roller support. Flexural stresses initiated a tensile crack, which propagated downward towards the specimen's support. The variation between the loaded and unloaded sides of the joint gives an indication of the effectiveness of the joint to transfer the load. The load transfer efficiency based on deflections measured at maximum load was found to be 74%. It is noticed that the slope of the load-displacement relationship for both loaded and unloaded sides of the joint diverge at a load of about 3000 lbs, confirming the previous observations for the half joint specimens. Figure 4.46 illustrates the load-deflection relations corresponding to the full joint specimens FJ2. In this specimen, the ramp load was stopped at a load of 4000 lbs. The load transfer efficiency for this specimen is calculated to be 75% at maximum load.

4.8.2. Load-strain results

Figure 4.47 illustrates the load-strain relation for the full joint specimen FJ1, and Figure 4.48 illustrates the load-strain relation for specimen FJ2. Strains were measured on the unloaded side of the specimen; consequently the compressive strains correspond to the compressive zone at the bottom of the dowel bar. While the compression strains in specimens FJ1 and FJ2 are similar in magnitude, the tensile strains differ. The tensile strains recorded for specimen FJ1 is approximately four times higher than that in specimen FJ2. At this stage, it is obviously difficult to identify which is more correct, however comparison between the measured and FE strains will clarify this issue, in Chapter 5.

FIGURE 4.1 Test rig

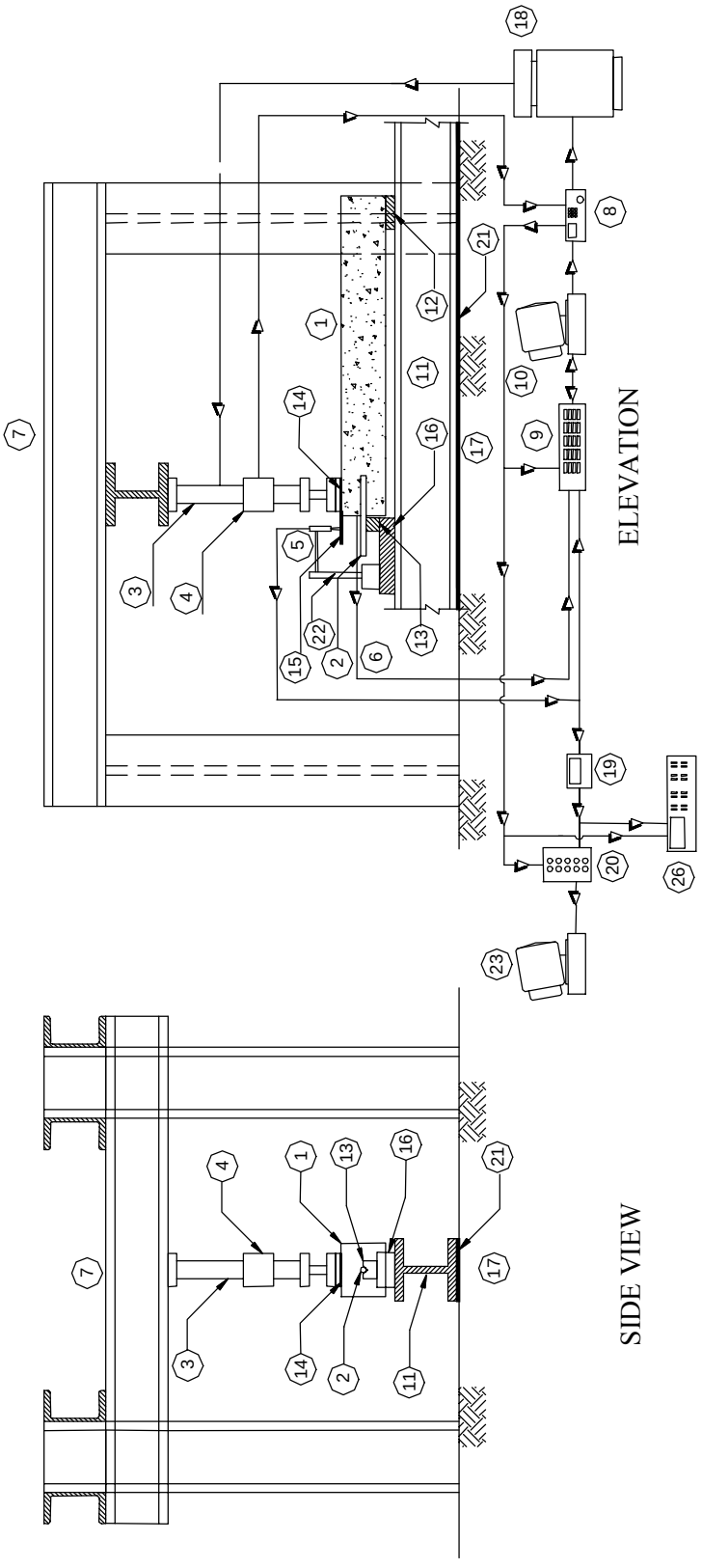

FIGURE 4.2 Schematic drawing for test rig mounted with half joint specimen

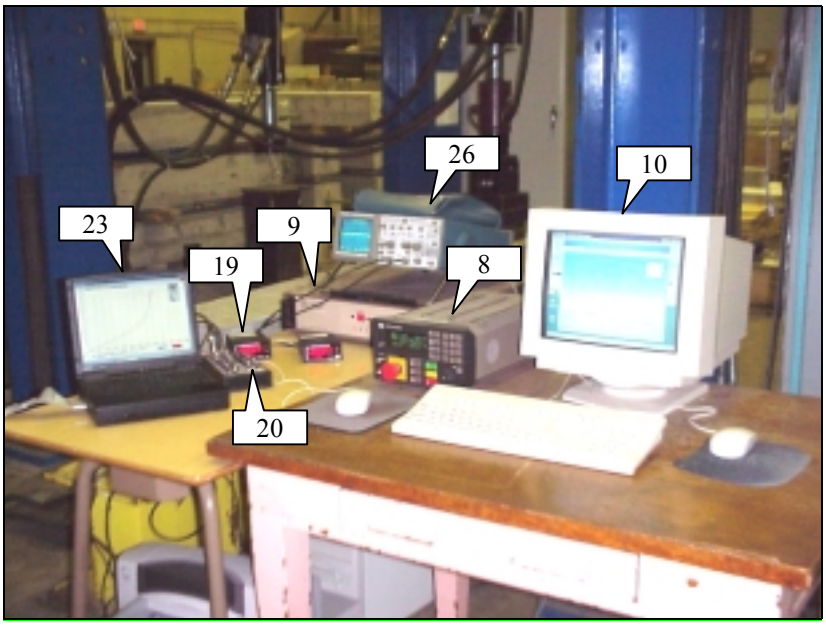

FIGURE 4.3 Instrumentation

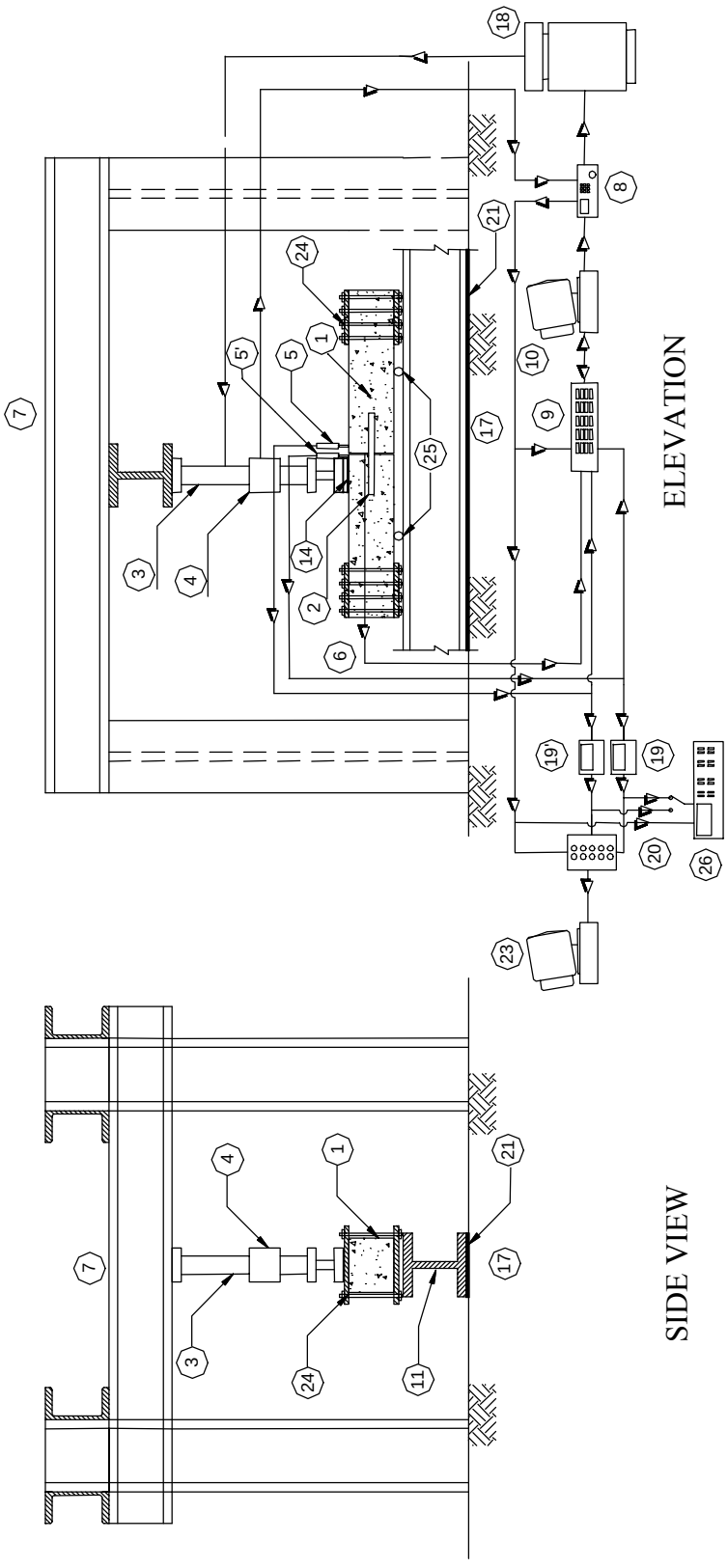

FIGURE 4.4 Schematic drawing for test rig mounted with full joint specimen

FIGURE 4.5 Test rig mounting full joint specimen

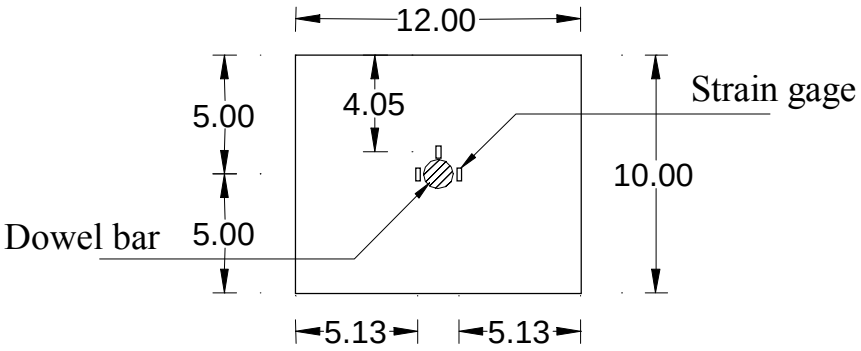

(a) Face of half joint specimen showing locations of strain gages

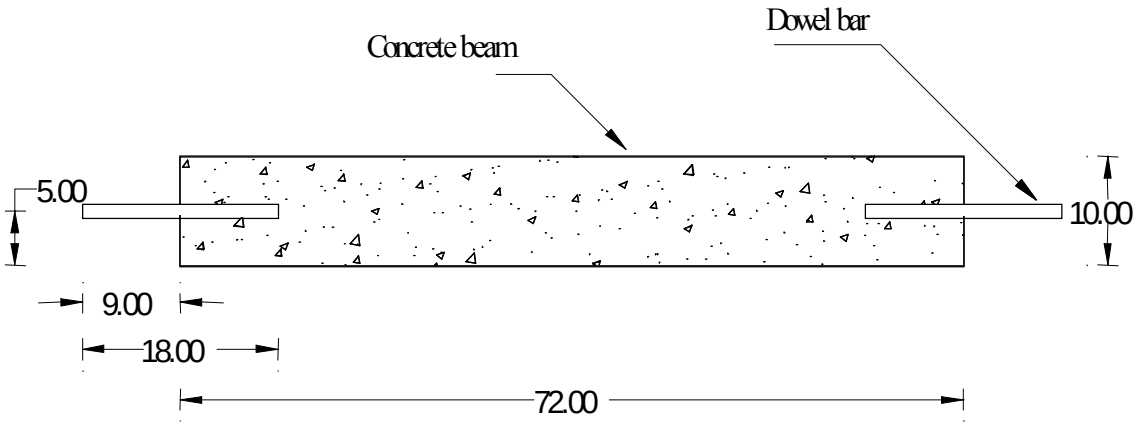

(b) Longitudinal view of half joint specimen

FIGURE 4.6 Details of half joint specimens

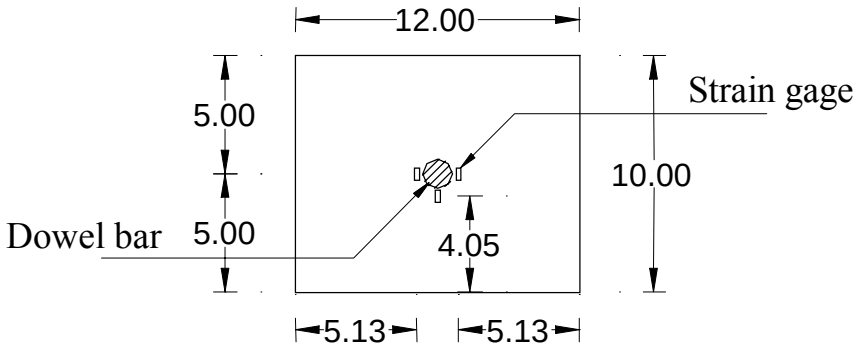

(a) Interior face of full joint specimen showing locations of strain gages

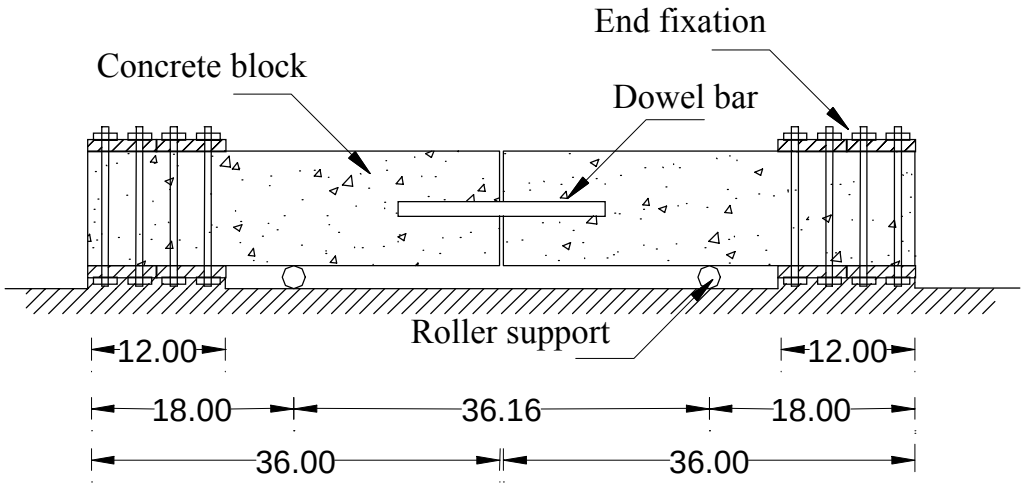

(b) Longitudinal view of Full joint specimens

FIGURE 4.7 Details of full joint specimens

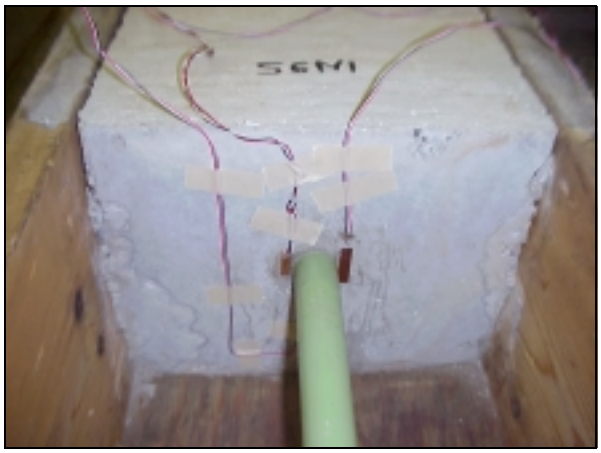

(a) Installation of strain gages at sides of dowel bar

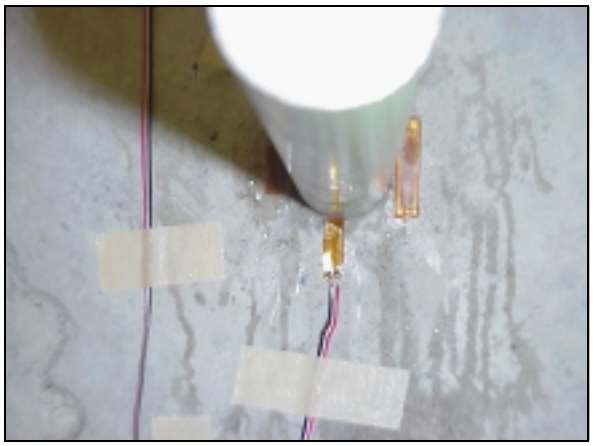

(b) Installation of strain gage at bottom of dowel bar

FIGURE 4.8 Installation of strain gages at joint face in full joint specimens

FIGURE 4.9 Full joint specimen ready for second stage of construction

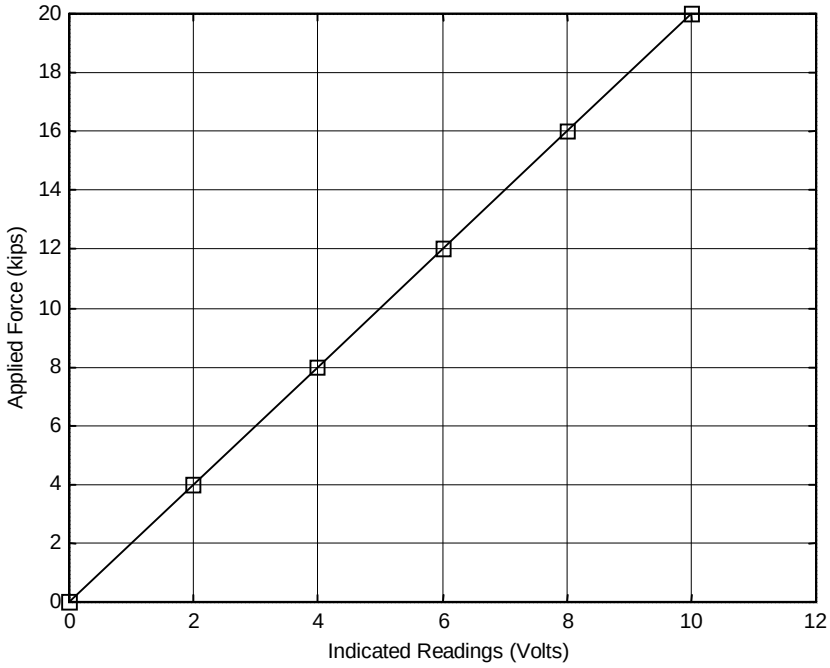

FIGURE 4.10 Calibration chart for MTS load cell

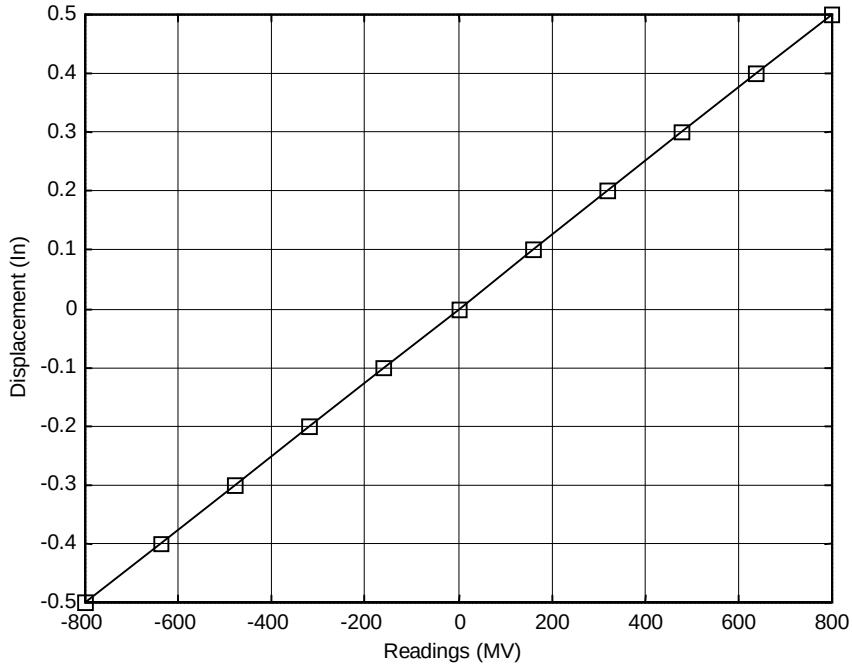

FIGURE 4.11 Calibration chart for LVDT model (060-A797-05)

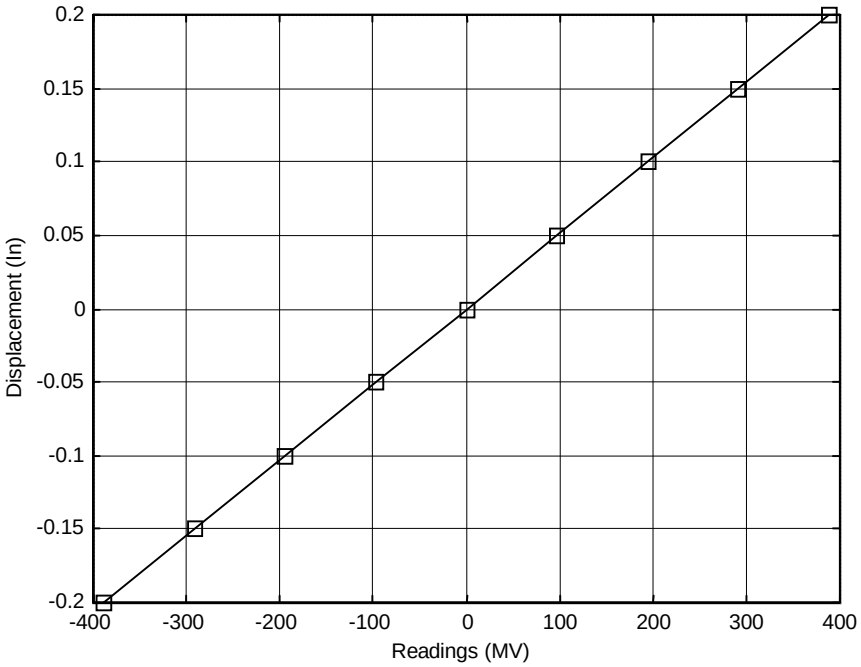

FIGURE 4.12 Calibration chart for LVDT model (060-3590-06)

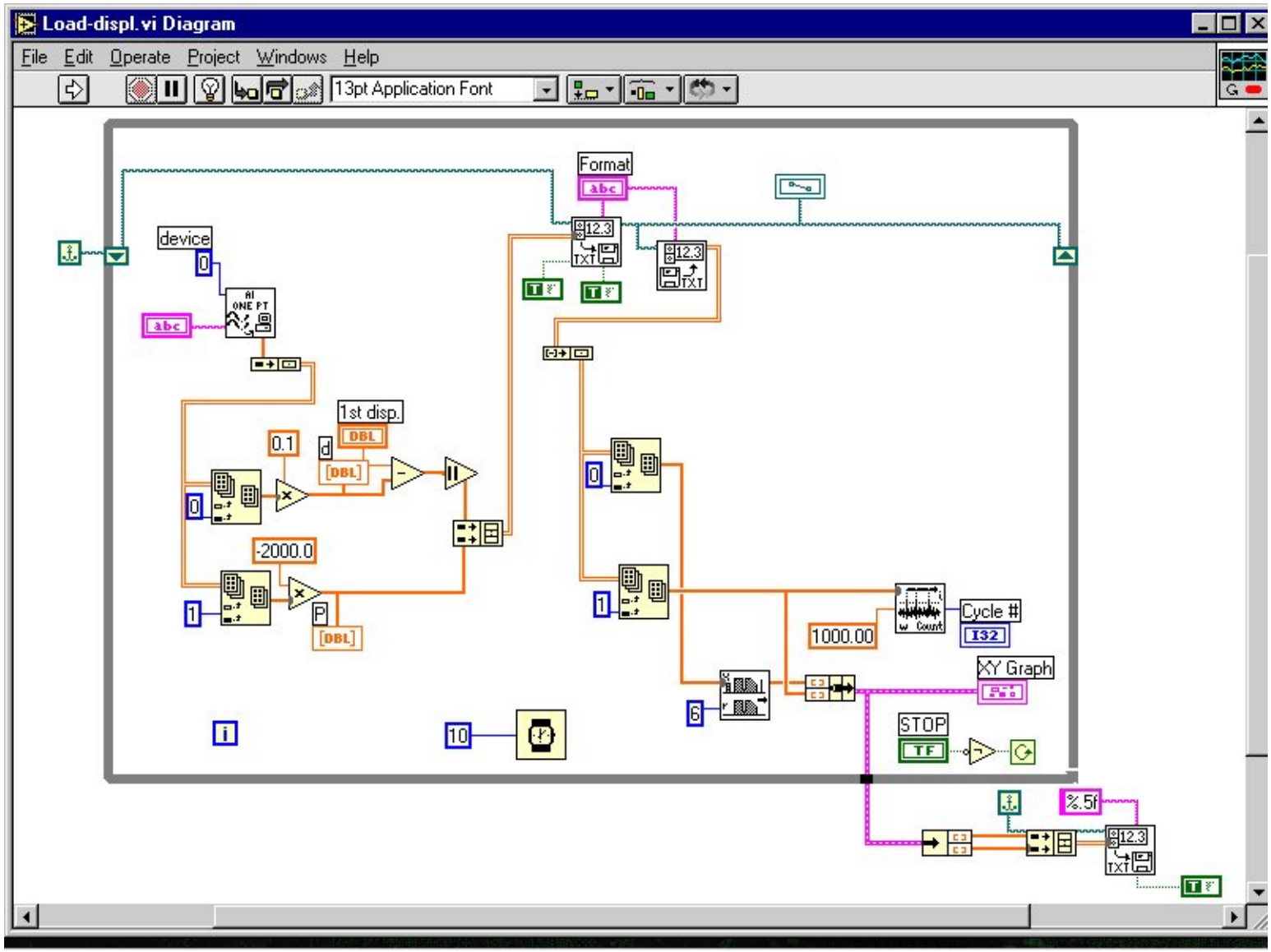

FIGURE 4.13 Block diagram of Labview data acquisition program

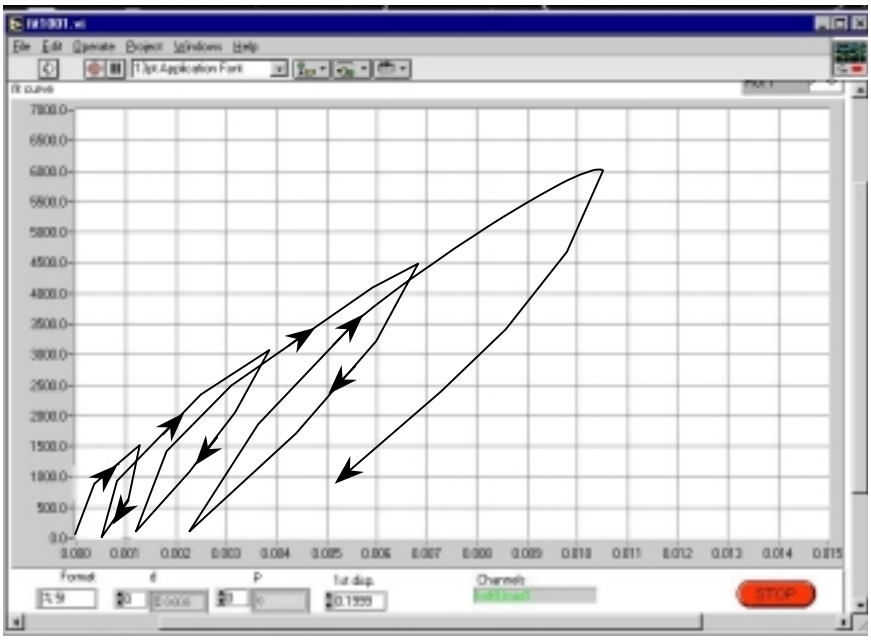

FIGURE 4.14 Example of the Labview data acquisition program output

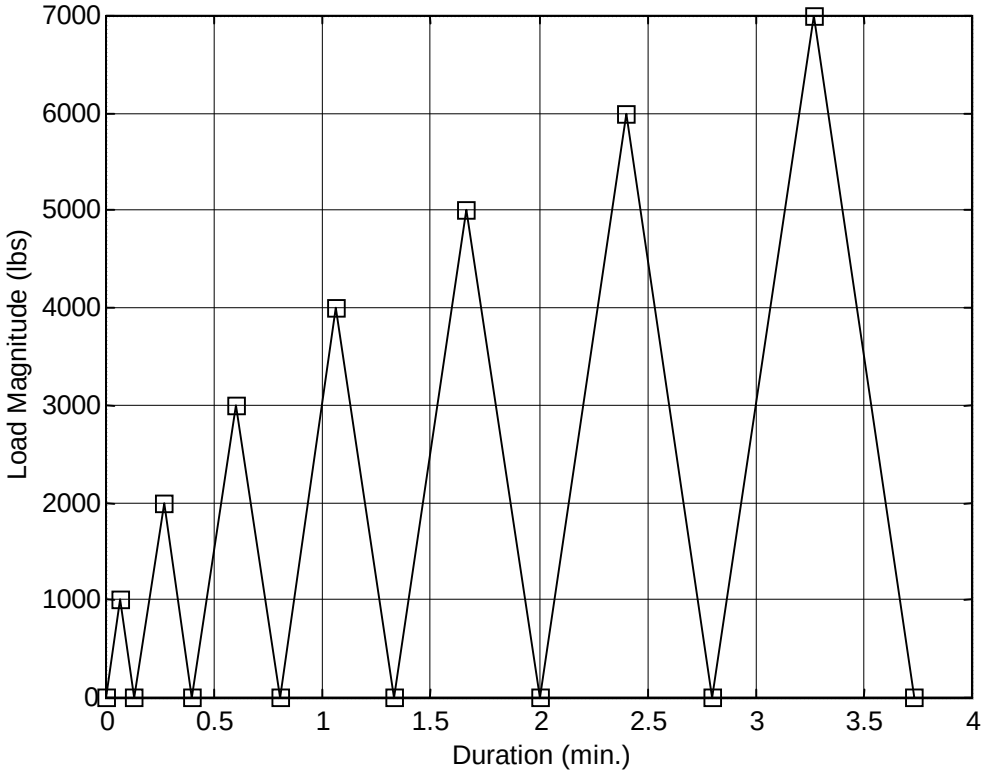

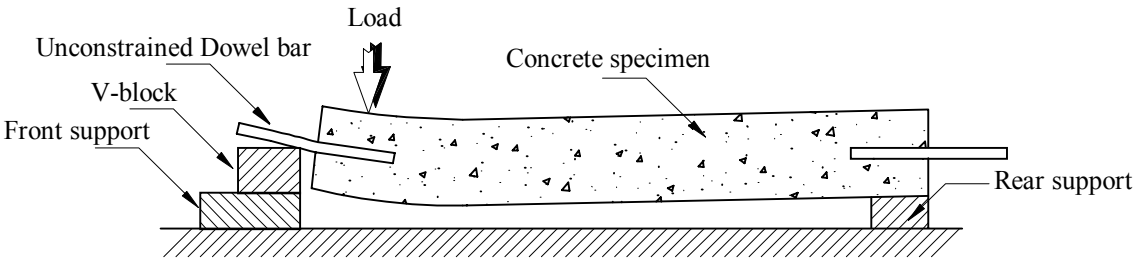

FIGURE 4.16 Loading of half joint with unconstrained dowel bar against flexural bending

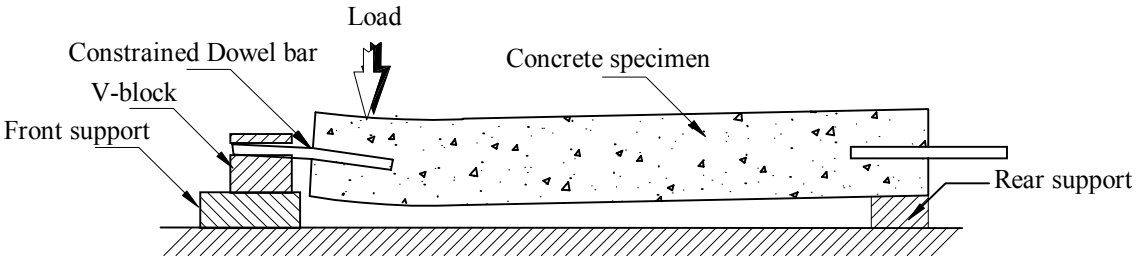

FIGURE 4.17 Loading of half joint with Constrained dowel bar against flexural bending

FIGURE 4.18 Exposed part of Dowel unconstrained aginst bending for half joint specimens

FIGURE 4.19 Exposed part of Dowel constrained aginst bending for half joint specimens

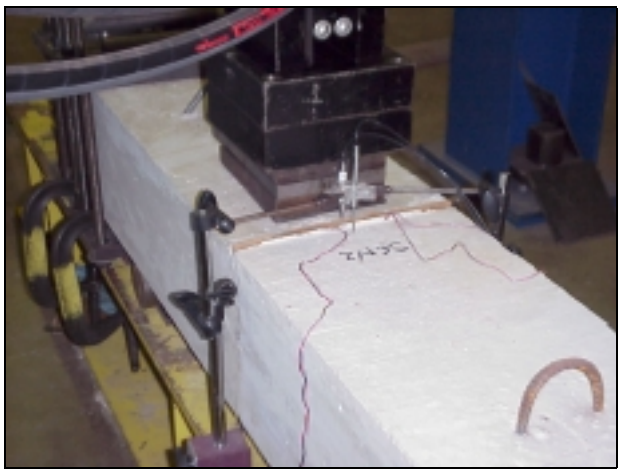

FIGURE 4.20 Loading for full joint specimens

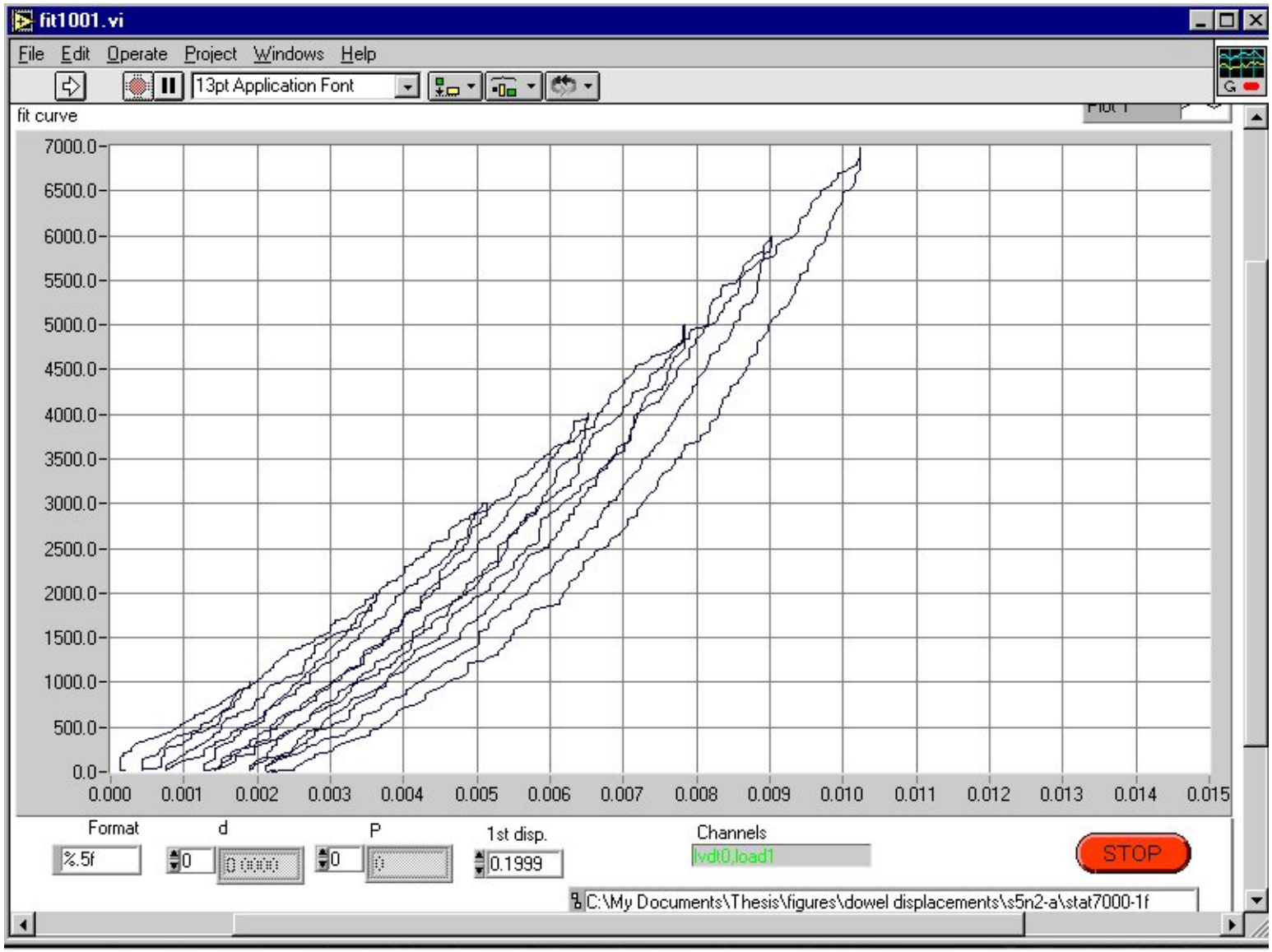

FIGURE 4.21 Load-displacement relationship for specimen HJ31-1

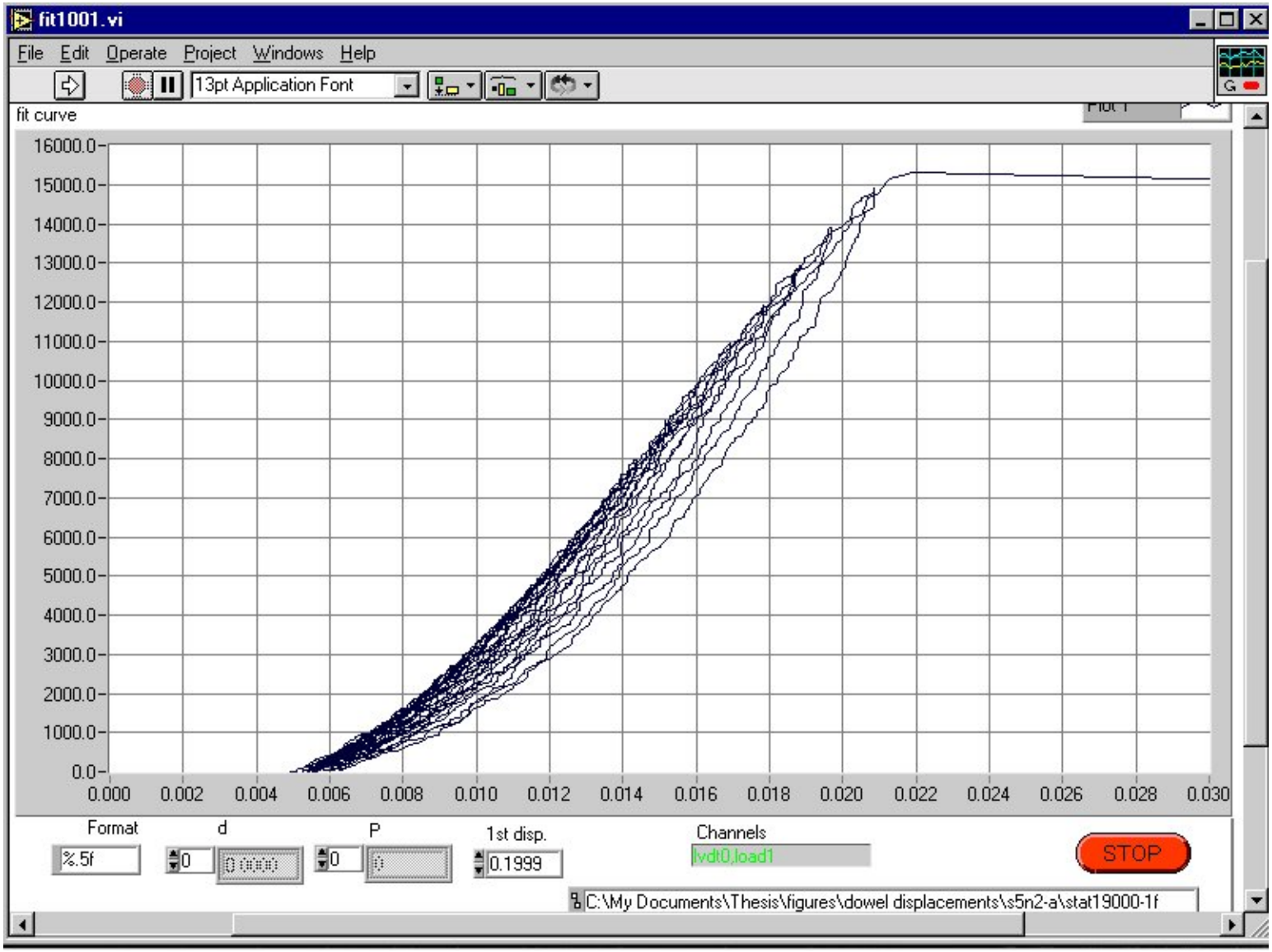

FIGURE 4.22 Failure load for specimen HJ31-1

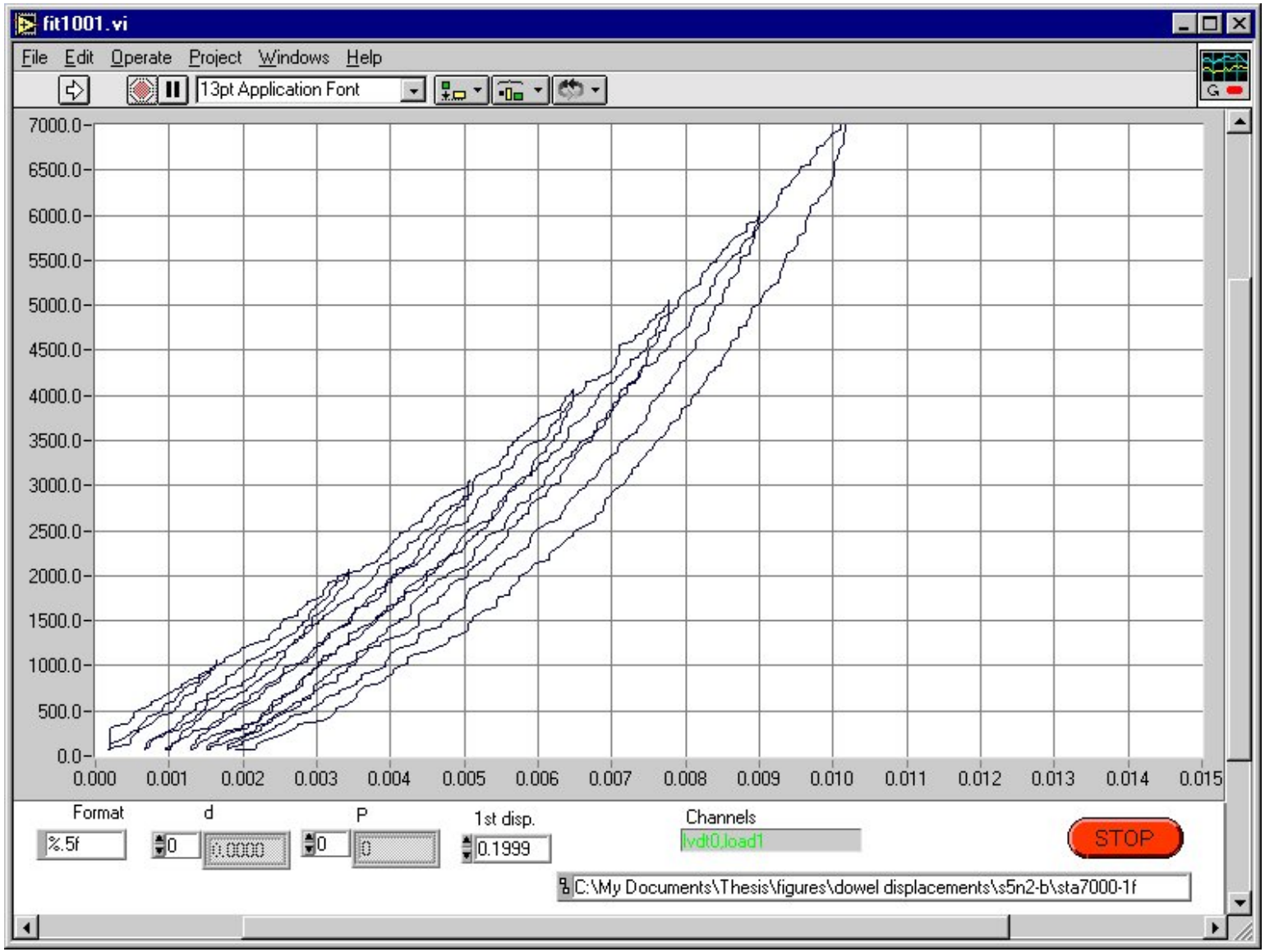

FIGURE 4.23 Load-displacement relationship for specimen HJ31-2

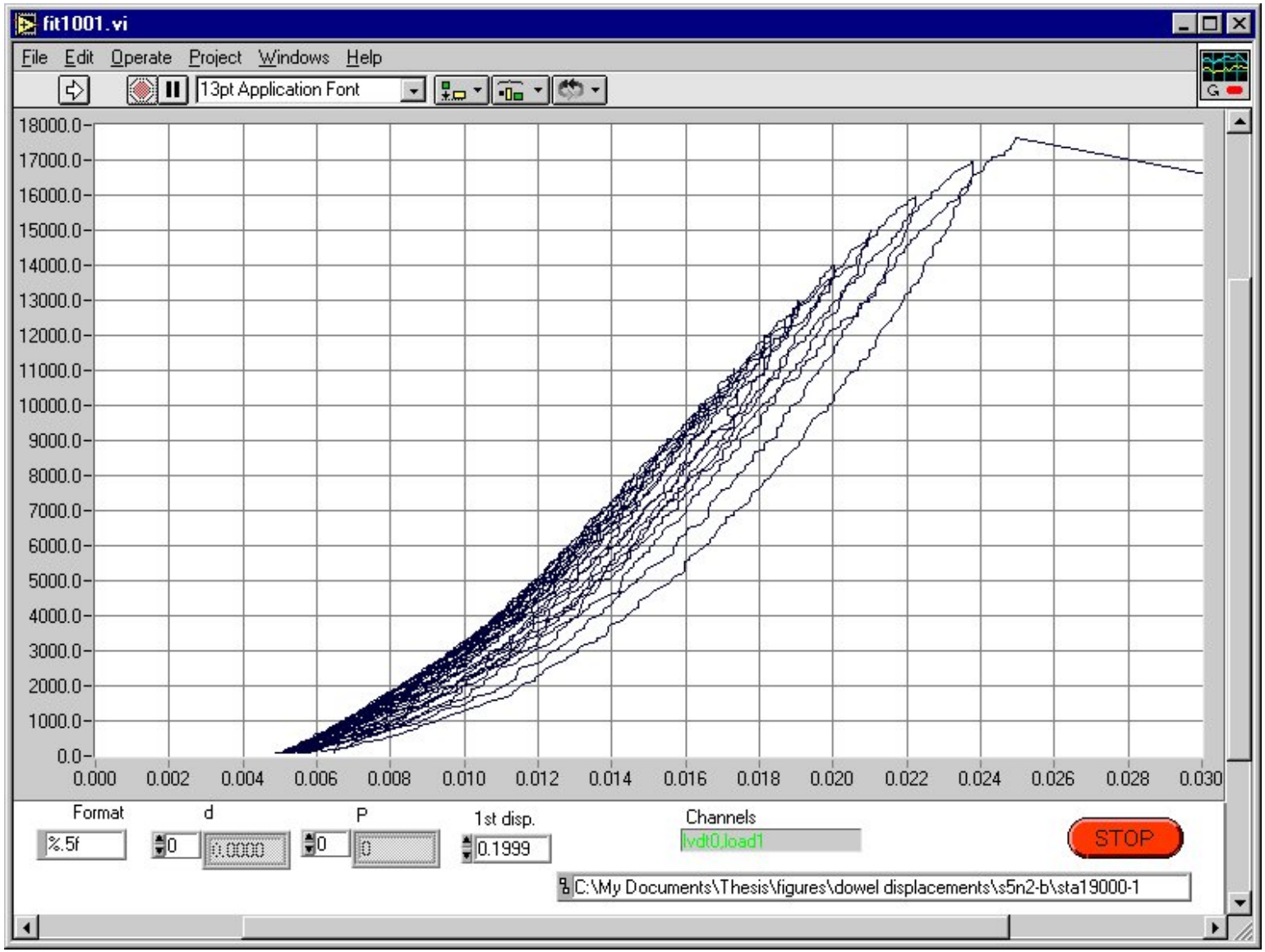

FIGURE 4.24 Failure load for specimen HJ31-2

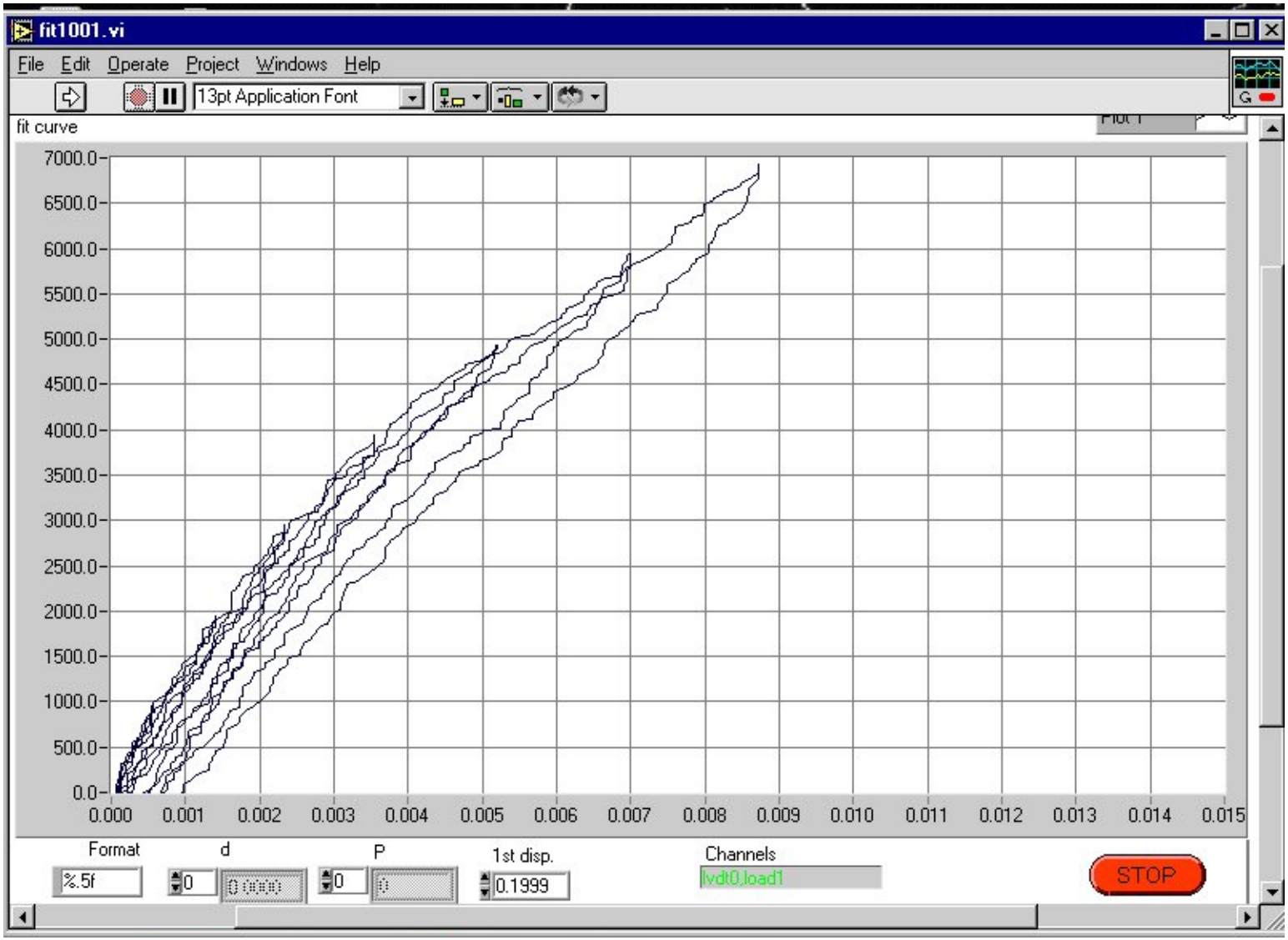

FIGURE 4.25 Load-displacement relationship for specimen HJ31-3

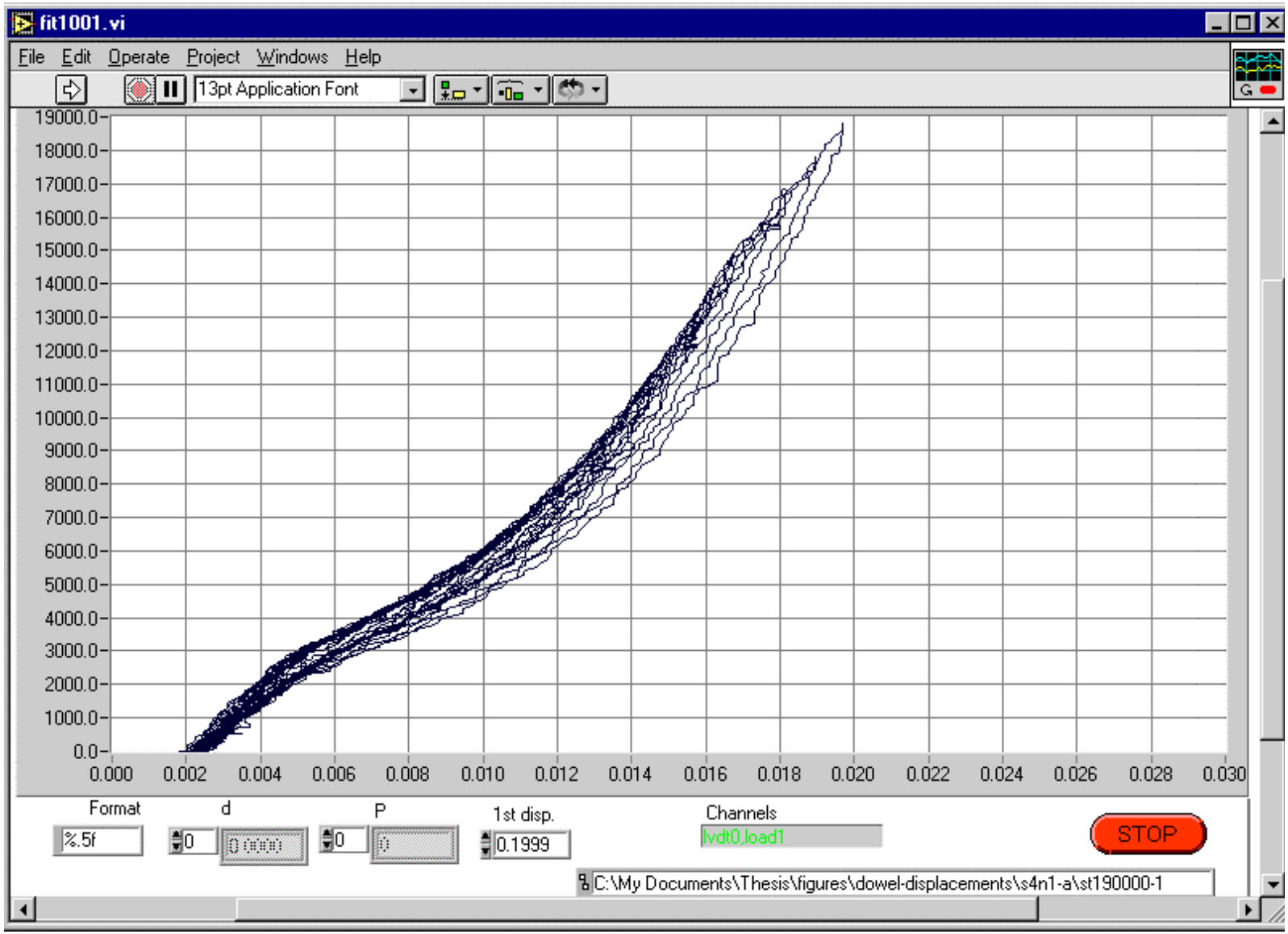

FIGURE 4.26 Load-displacement relationship for specimen HJ31-3 (LH19000)

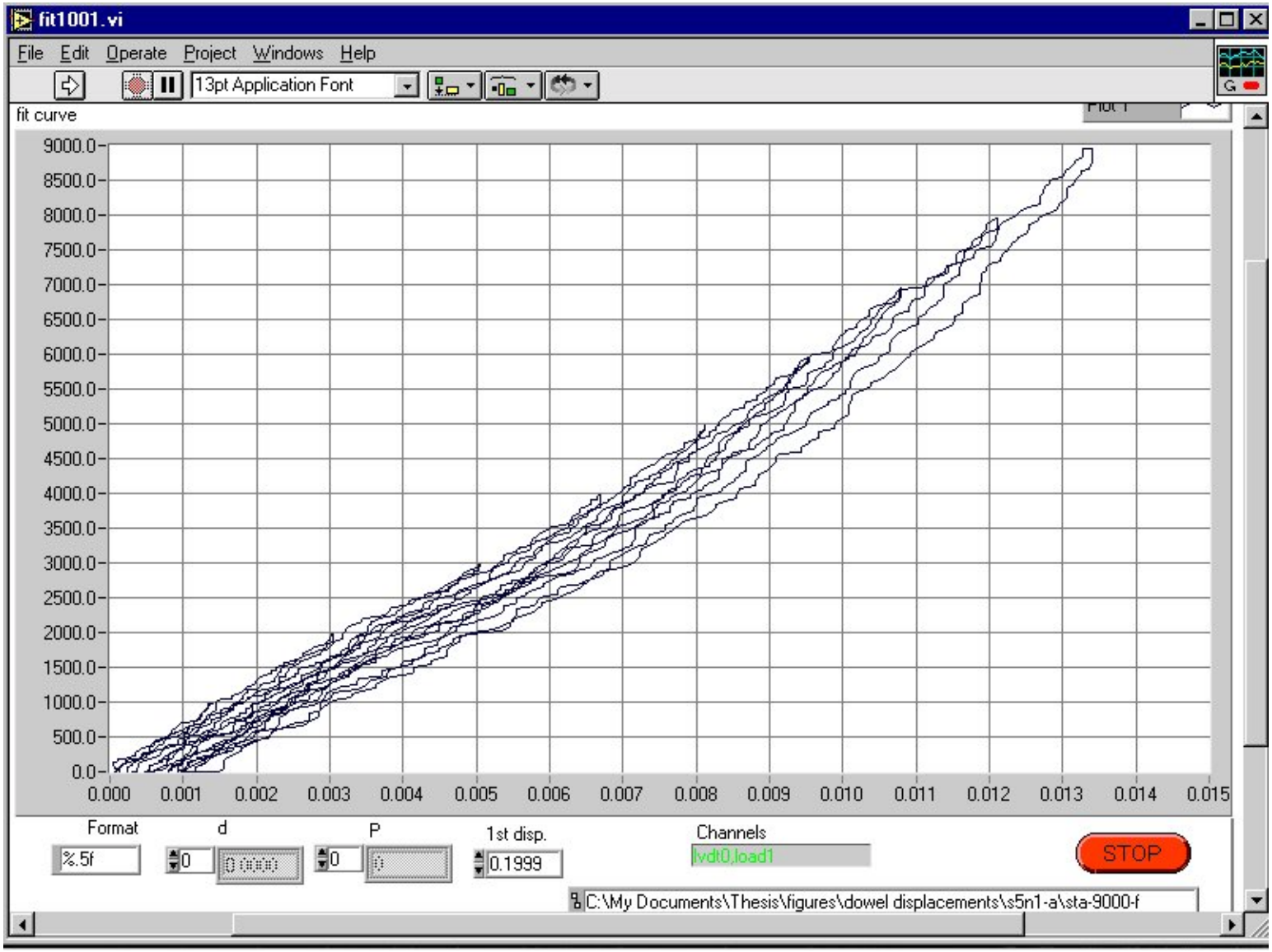

FIGURE 4.27 Load-displacement relationship for specimen HJ31-4

FIGURE 4.28 Repeatability in results for specimen HJ31-4

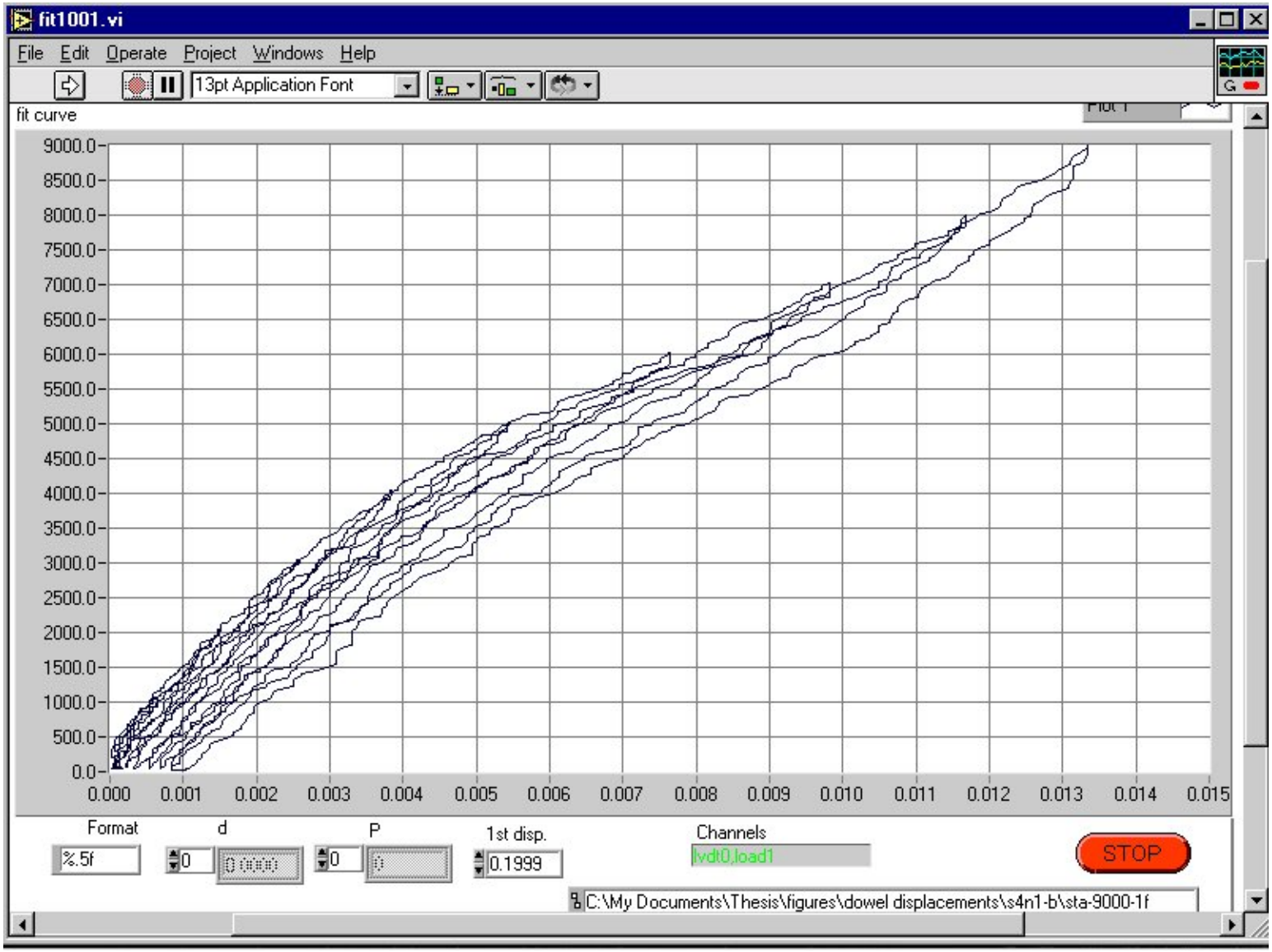

FIGURE 4.29 Load-displacement relationship for specimen HJ31-5

FIGURE 4.30 Repeatability of results for specimen HJ31-5

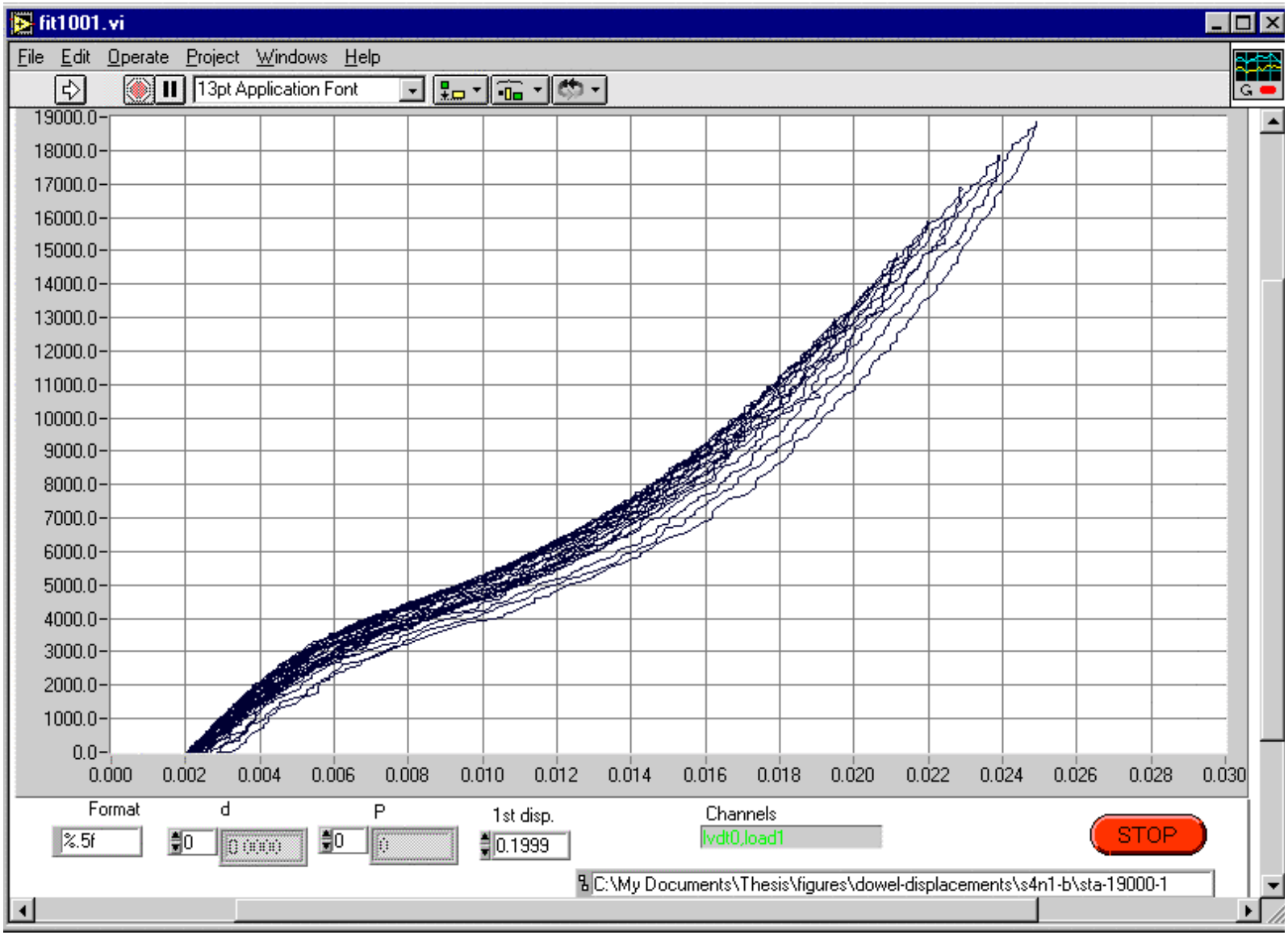

FIGURE 4.31 Load-displacement relationship for specimen HJ31-5 (LH19000)

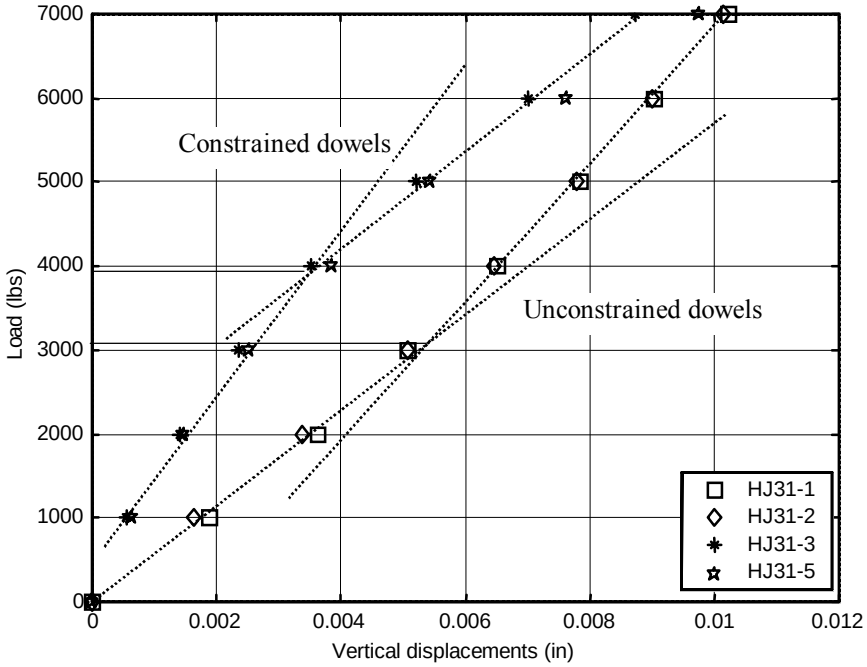

FIGURE 4.32 Vertical displacements vs load for LH7000

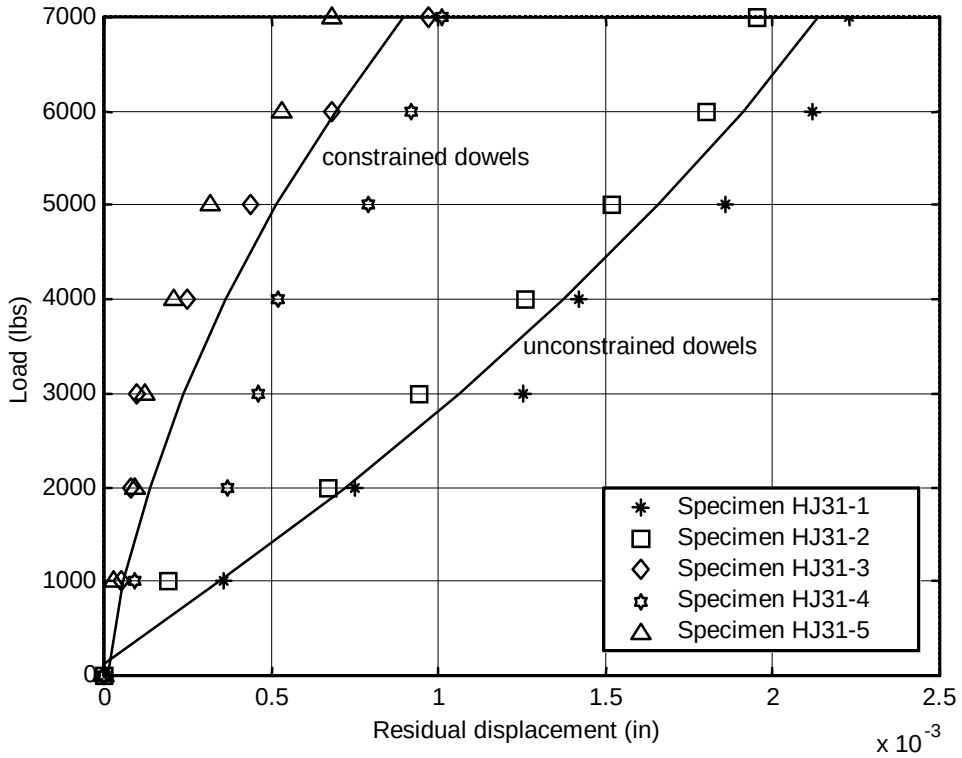

FIGURE 4.33 Residual displacements vs Loads at first sequence of loading

FIGURE 4.34 Initiation of horizontal crack at both sides of loaded dowel bar

FIGURE 4.35 Propagation of horizontal crack at the sides of loaded dowel bar

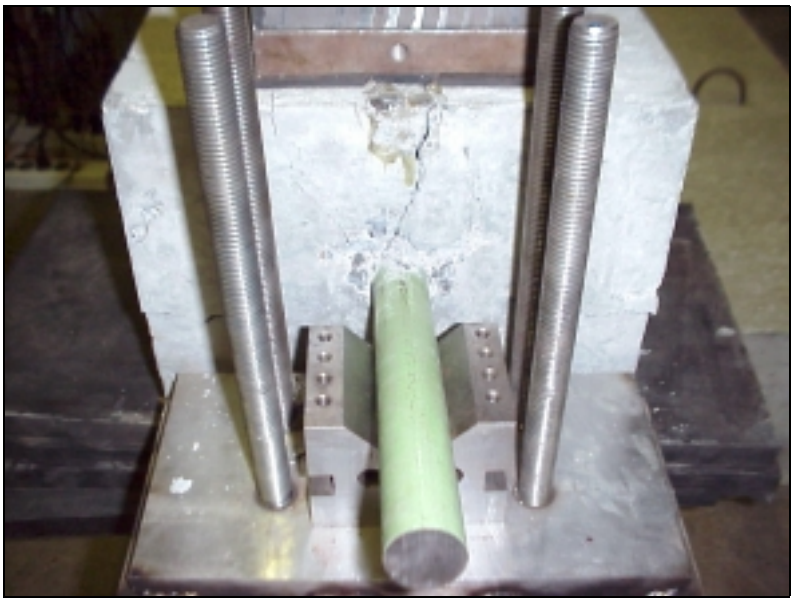

FIGURE 4.36 Fan shaped cracks at failure of half joint specimens

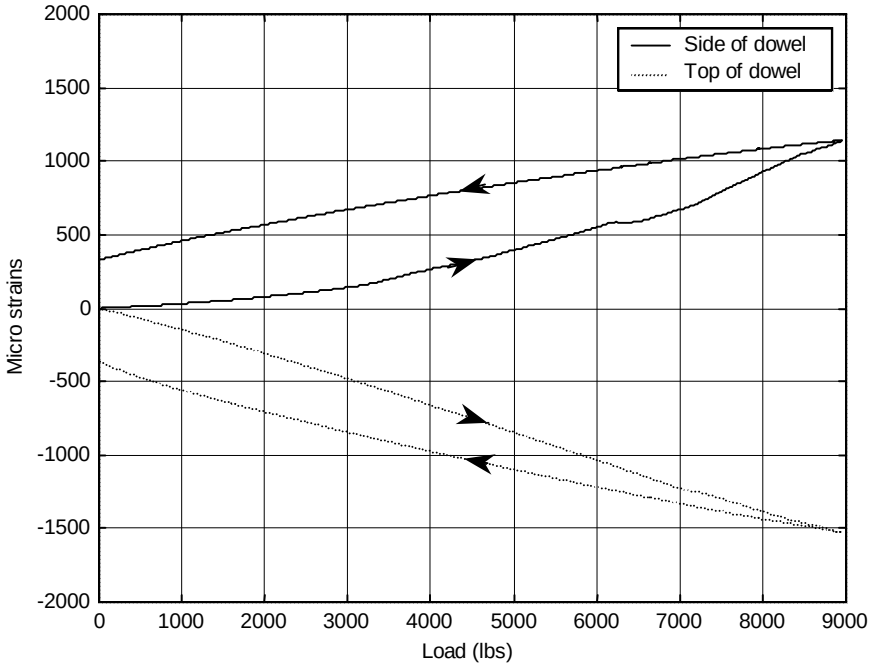

FIGURE 4.37 Load-strain relationship for specimen HJ38-1

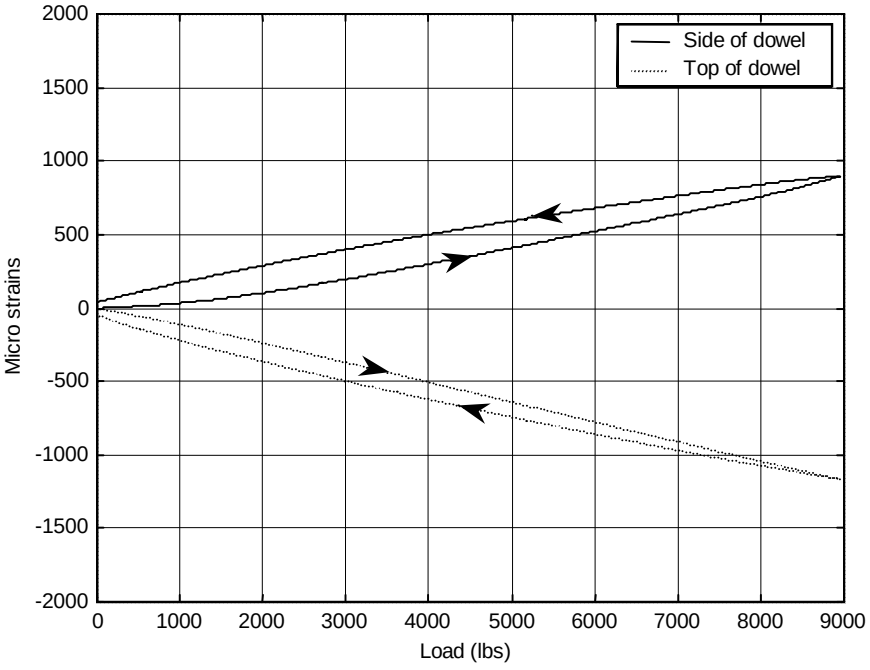

FIGURE 4.38 Load-strain relationship for specimen HJ38-2

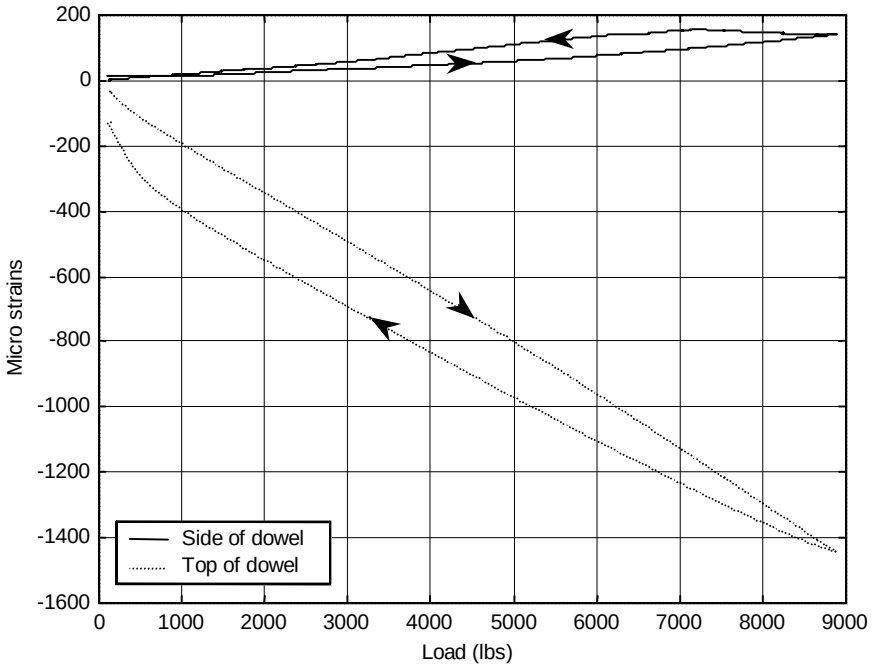

FIGURE 4.39 Load-strain relationship for specimen HJ38-3

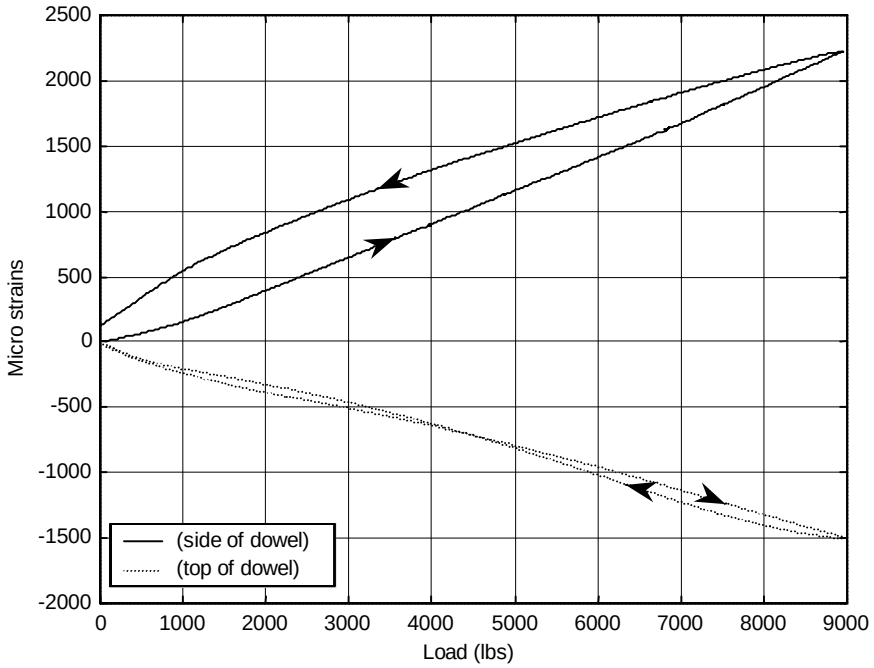

FIGURE 4.40 Load-strain relationship for specimen HJ31-6

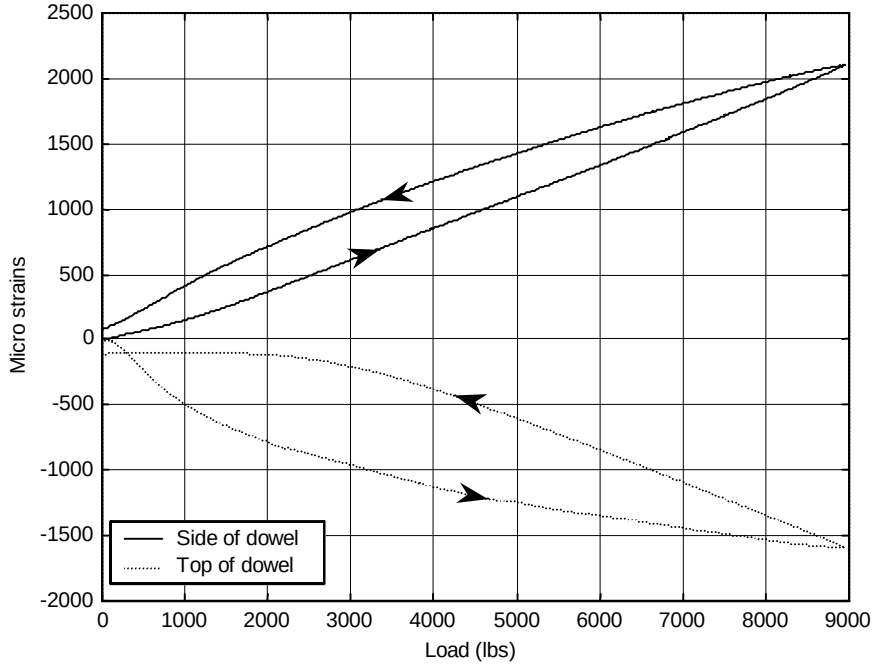

FIGURE 4.41 Load-strain relationship for specimen HJ31-7

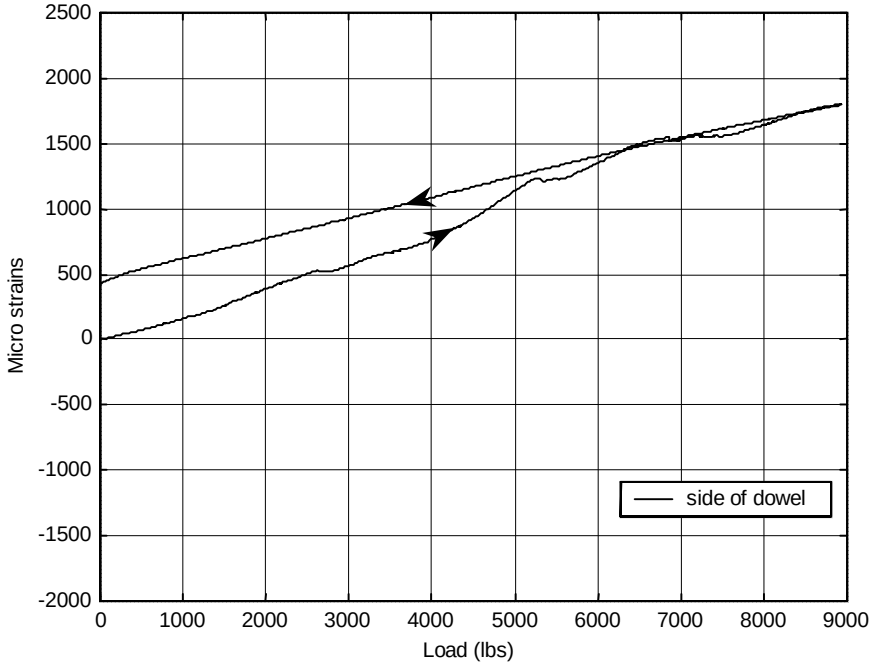

FIGURE 4.42 Load-strain relationship for specimen HJ31-8

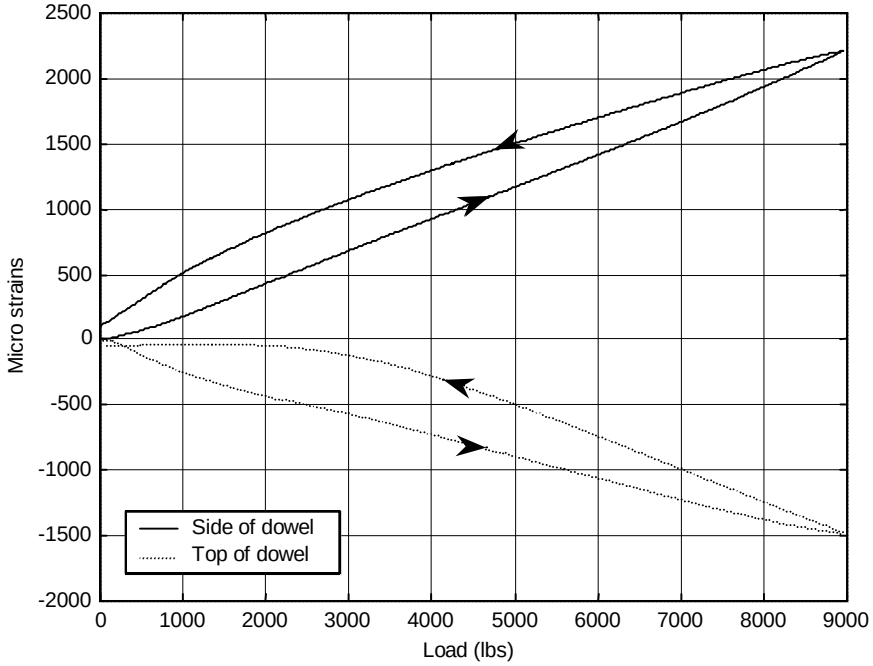

FIGURE 4.43 Load-strain relationship for specimen HJ31-9

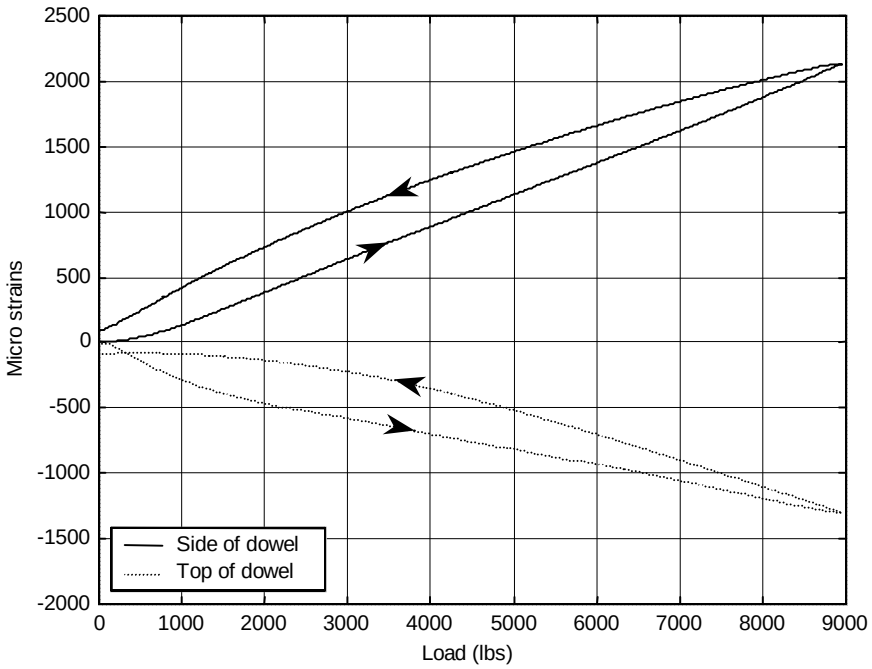

FIGURE 4.44 Load-strain relationship for specimen HJ31-10

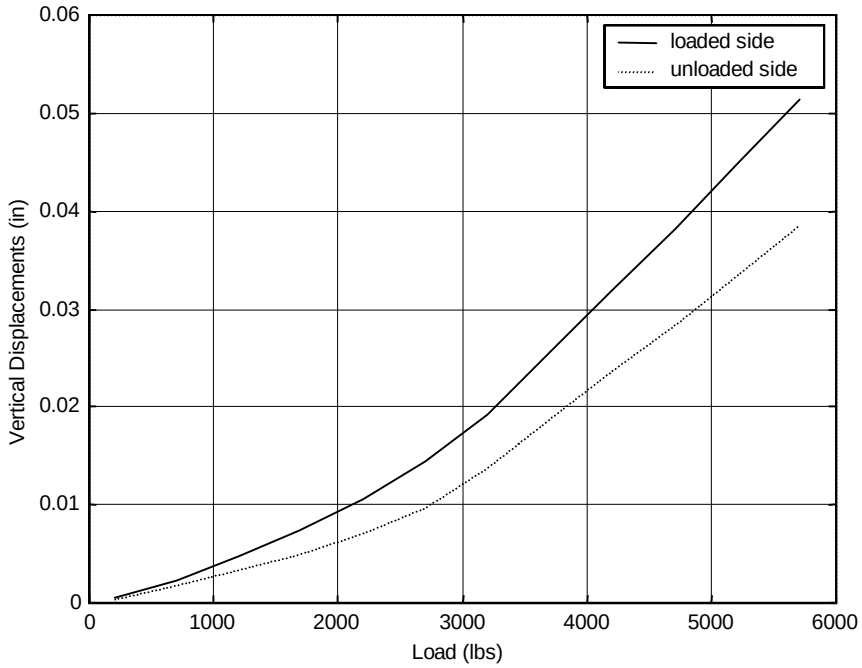

FIGURE 4.45 Load-displacement relationship for full joint specimen FJ-1

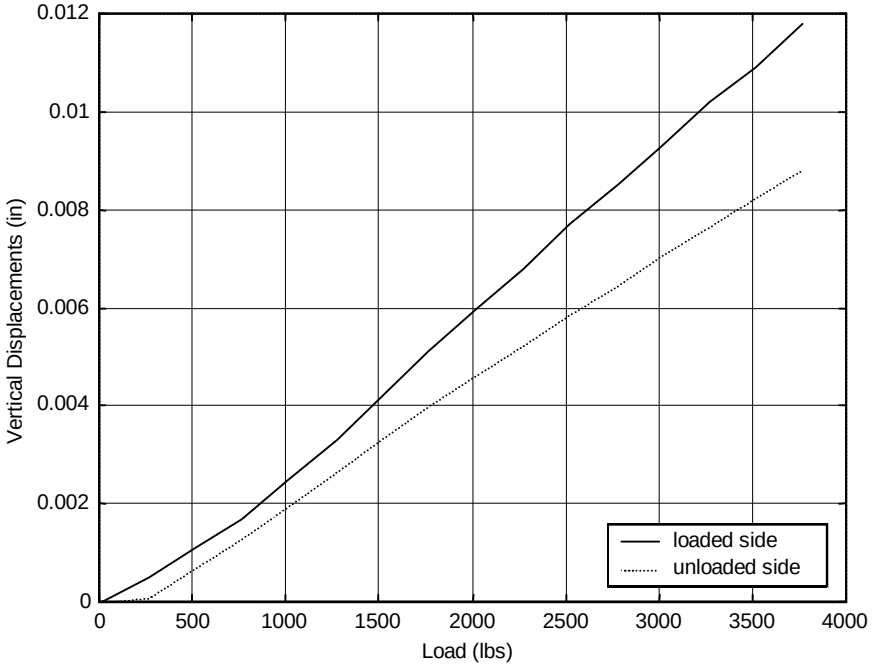

FIGURE 4.46 Load-displacement relationship for full joint specimen FJ-2

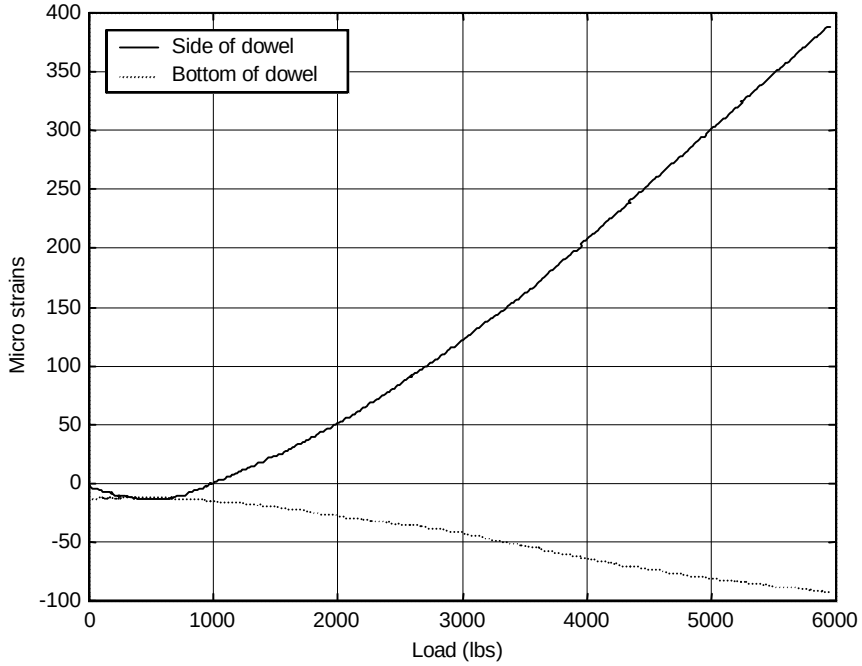

FIGURE 4.47 Load-strain relationship for full joint specimen FJ-1

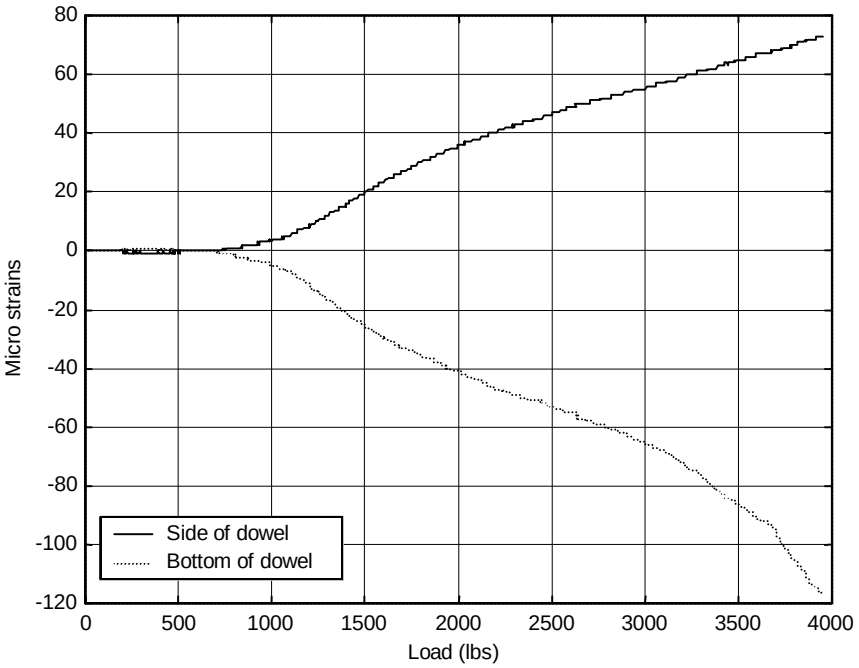

FIGURE 4.48 Load-strain relationship for full joint specimen FJ-2

CHAPTER FIVE

FINITE ELEMENT MODEL VERIFICATION

5.1. INTRODUCTION

The experimental results obtained in Chapter four offer an insight of the reasons for the development of distress modes in doweled transverse joints. However, it does not offer a solution to reduce or eliminate such distresses. It has been shown in Chapter three that the finite element modeling approach is capable of predicting the failure mechanism that was experimentally observed in chapter four. On the other hand, because of experimental limitations, it is not possible to provide a comprehensive quantitative validation for the 3DFEM results in chapter three. In this chapter 3DFE modeling will be used to simulate the behavior of the simulated joint specimens presented in chapter four. Since the 3DFEM assumptions and equation solver are the same as those in chapter three; a quantitative agreement with the experimental results would provide a validation of the full model of Chapter three. Additionally, the 3DFEM developed in this chapter will be used (after validation) to examine the effectiveness of an alternative dowel design. The alternative design will be shown to eliminate the high tensile and compressive stresses around the traditional steel dowels.

5.2. DESCRIPTION OF THE 3D FINITE ELEMENT MODEL

The 3DFEM dimensions are the same as those of the test specimens described in Chapter four. Both concrete specimens and dowel bars were simulated using the same finite element mesh employed in chapter three. Figure 5.1 and Figure 5.2 illustrate the 3DFE mesh and boundary conditions that simulate half and full joints respectively. Two models were developed for the half joints specimens, comprising dowel bars of diameter 1.25 in and 1.5 in. Figure 5.3 illustrates the embedded dowel bar within the full joint FEM.

5.3. MATERIAL PARAMETERS

The concrete material parameters in chapter three were adjusted to characterize those of the test specimens. Table 5.1 contains a listing of both the concrete and steel material constants used in the present analysis. The modulus of elasticity of the concrete material was calculated by the empirical formula found in the ACI Code:

$$E_c = \left(40{,}000\sqrt{f_c'} + 1{,}000{,}000\right)\left(\frac{w_c}{145}\right)^{1.5} \qquad (49), \text{ and } (50)$$

Where: E_c is the modulus of elasticity of the concrete (psi)

f_c' is the compressive strength of the concrete after 28 days (psi)

w_c is the unit weight of hardened concrete

The modulus of rupture of the concrete material was estimated to be from $6\sqrt{f_c'}$ to $12\sqrt{f_c'}$ and was taken: $f_r = 8.5\sqrt{f_c'}$

Table 5.1 Material parameters

Item	Material model	parameter	Half joint	Full joint
Concrete	Anisotropic brittle damage	Young's Modulus *(psi)*	3.96E+6	3.53E+6
		Poisson's ratio	0.18	0.18
		Density *(lb/in3)*	2.24e-4	2.24e-4
		Tension limit *(psi)*	630	537
		Shear limit *(psi)*	2750	2000
		Fracture toughness *(lbs/in)*	0.8	0.8
		Shear retention factor	0.03	0.03
		Viscosity *(psi/sec)*	104	104
Dowels	Linear elastic	Young's Modulus *(psi)*	29.00e+06	
		Poisson's ratio	0.30	
		Density *(lb/in3)*	7.324e-4	

5.4. LOADING CONDITIONS

The loading applied to the finite element modeling, was that used in the laboratory experiments. The load was applied on the model through a steel plate (20cmx13.8cm)(7.89inx5.43 in), equivalent to that used in the experimental study. A quasi-static load was applied on the loading plate starting from zero to 40.03 KN (9000lbs).

5.5. MODEL RESULTS

Figure 5.4 and Figure 5.5 illustrate the deformed half and full joint models respectively after the application of the load. Figure 5.6 shows the fringes of vertical strain around the dowel socket for the half joint model mounted with 1.25” dowel bar. The fringes show the formation of compressive and tensile strains in a similar fashion to what was observed in the pavement model in chapter 3. Figure 5.7 illustrates the fringes of vertical strains around the dowel socket in the unloaded side of the full joint model. In this case the compressive zone is located under the dowel bar.

5.5.1. Vertical strains

Strain data collected from the experimental tests were plotted against the strain results obtained from the finite element modeling of the experimental specimens. Figure 5.8 to Figure 5.15 illustrate the relationship between induced vertical strains at the concrete face, at the specified strain gage locations, and the applied load, for the half joint specimens. Figure 5.8 to Figure 5.10 show the results of the specimens fitted with 38.1 mm (1.5 in) dowel bar. In Figure 5.10, the tensile strains were collected at a distance of 0.5 inches from the edge of the dowel bar (the concrete material surrounding the dowel bar was found in a bad condition after taking off the forms). Results from specimen HJ38-4 were not available for the same reason. In all figures, the positive strain magnitudes are attributed to the tension zone at the sides of the dowel bar, and the negative strain magnitudes are attributed to the compression zone at the top of the dowel bar. The compressive strains for specimen HJ31-8 were not available due to the bad surface finish of the concrete material. As shown in the presented plot, a fairly good

agreement is obtained between the experimental data and the finite element results. The good agreement between the finite element results and the measured experimental data indicates the validity of the FE program results.

Figure 5.16 and Figure 5.17 show the data collected from the experiment test and the finite element model for the full joint specimens. In Figure 5.16, a fairly good agreement is observed for the compression strains. On the other hand a discrepancy is observed between those collected from the tensile zone. It is believed that the variation between the results comes from the existence of cracks in the concrete face in this particular zone. Figure 5.17 shows a good agreement between the finite element model and the measured strains from the test.

5.5.2. Comparison between FEM and measured vertical displacements

Comparing the collected deflections at the specimens face from the finite element models, and those measured from the experimental tests show a large discrepancy between the two. The maximum measured displacements were found to be 7.5 times larger than what the FEM provide. This discrepancy is attributed to several reasons. The first reason is that the rigid body motion is firmly restricted in the FE models by the applied boundary conditions, which totally constraints the vertical displacements at the supports. This condition is unlikely to occur in the experimental test were crushing of minute concrete fragments at the supports is inevitable. The second reason comes from the nature of the material model, which initiates concrete failure at the elements where stresses exceed a given threshold value. Therefore, stresses in those elements decay gradually, and stresses are redistributed at this location, but the failed elements don't actually disappear or vanish. On the other side in the experimental tests, once compression failure occurs, concrete particles are crushed, and when tension failure occurs, a crack is initiated, giving high displacement magnitudes.

Although the overall displacements are different, the relative displacements within each case are close. Thus, the deformation of the elements relative to each other is kept the same, which clarifies the good matching obtained in strains, and consequently

the induced stresses. To prove this concept, relative displacements of the loaded dowel bar in the FE joint model were used to calculate the force on the dowel. This force was compared with analytically calculated one for the same case of loading.

The loaded dowel bar incased in the FE joint model is considered as a beam with two end fixed supports, therefore will be subjected to the end moments, and shearing forces as shown in Figure 5.18. The reactions of this system is given by (51):

$$\begin{bmatrix} 12 & 6L & -12 & 6L \\ & 4L^2 & -6L & 2L^2 \\ & & 12 & -6L \\ \text{symm} & & & 4L^2 \end{bmatrix} \begin{bmatrix} w_1 \\ \theta_1 \\ w_2 \\ \theta_2 \end{bmatrix} = \begin{bmatrix} V_1 \\ M_1 \\ V_2 \\ M_2 \end{bmatrix} \frac{L^3}{EI}$$

where: L = length between two nodes on the dowel bar (1.0 in)

w_1 = vertical displacement at node one (-0.0045 in)

θ_1 = rotation angle at node one (0.0003 deg.)

w_2 = vertical displacement at node two (-0.0039 in)

θ_2 = rotation angle at node two (-0.0005 deg.)

$V_1 = V_2$ = Shear force on dowel bar

M_1 = Moment at node one

M_2 = Moment at node two

E = Modulus of elasticity of dowel (29E+06 psi)

I = Dowel moment of inertia (0.11984 in^4)

Substituting in the above equation, the resulting shearing force is calculated to be 5432.4 lb. The structural system of the joint specimen is illustrated in Figure 5.19. For the case of symmetric hinge location, the reaction at the hinge connection is calculated from the equation:

$$R = P\left[\frac{a^2}{4b^3}(3b - a)\right]$$

where P = applied load (9000 lbs)

a = distance from the applied load to the end support (26 in)

b = distance from hinge to the end support (30 in)

The reaction calculated is found to be 5530.27 lbs. The difference between the force magnitude calculated analytically, and that from the FE model are only 1.8 %, which indicate that the dowel bar within the model carries the same load exerted on the dowel bar in the experiment, thus producing the same stresses.

5.6. SPECIMEN VERSUS FULL PAVEMENT MODELS

In order to identify the accuracy with which the test specimens and loading conditions used in chapter 4 simulate the behavior in full pavement structure, the results from the finite element models of each structure will be compared. This comparison offers an insight of the stresses developed around the dowel bars according to the specimen arrangements, in comparison to those occurring in real pavement structures. Figure 5.20 to Figure 5.22 illustrate such a comparison for the vertical stresses, maximum principal stresses, and shear stresses respectively induced in the half joint specimen, and the pavement model. The stresses developed in the full pavement model are due to the application of 10,497 lbs FWD load, while the half joint specimen stresses correspond to an applied load amounting 1450 lbs. Figure 5.23 illustrate the distribution of vertical stresses along the loaded dowel bar for both FE models. The similarity between the induced stresses around the dowel bar in the simulated half joint specimen, and that in the full pavement structure show that at a load level of 1450 lbs, the half joint specimen is able to produce stresses around the dowel bar that are very close to what could occur in real pavement due to 10,497 lbs FWD load. Figure 5.24 to Figure 5.26 show plots of vertical stresses, shear stresses, and maximum principal stresses respectively around the dowel bar for the case of full joint specimen, and pavement structure. The stresses developed in the full joint specimen correspond to a load amounting 4090 lbs. Figure 5.27 illustrate the vertical stresses along the dowel bar for both the full joint specimen at a load of 4090 lbs, and the pavement structure. The stress plots indicate that the full joint

specimen can be utilized at a load of 4090 lbs, to induce stresses around the embedded dowel bar that are very close to those developed in rigid pavements. Figure 5.28 illustrates a comparison between the relative vertical displacement of the dowel bar for the full joint specimen at a load of 4090 lbs, and the pavement structure. The dowel deformation on the loaded side are similar for each case.

5.7. MODIFIED DOWEL DESIGN

The state of stresses around dowel bars should be relieved in order to extend the service life of transverse joints. This can be achieved by eliminating direct contact between the dowel and the surrounding concrete, especially at the region where high stresses occur. The modified dowel design should possess the following features:

1. Reduction of the high intensity stresses induced around the dowel bars.
2. Ability to absorb dynamic shocks due to traffic crossings of the joints.
3. Maintain the load transfer efficiency by eliminating cracks and concrete wear.
4. Cost effective design.
5. Simple installation.

The above feature can be achieved by providing a protective sleeve around the dowel that bonds permanently to the surrounding concrete, while allowing the dowel to slide freely it. This design modification was implemented in a finite element model as shown in Figure 5.29. The experimental measurements illustrated in Figure 5.30 indicate at least 50 % reduction in both compressive and tensile stresses around dowels. Figure 5.31 shows a comparison between the induced maximum principal stress around the dowel bar in rigid pavement structure and that around both the dowel bar, as well as the new dowel design, in the simulated half joint specimen subjected to a load of 1450 lbs. Figure 5.32 illustrates a plot of the vertical stresses induced around the dowel bar in pavement structure in comparison with those developed around the dowel bar and the new devise in the half joint specimen subjected to a load of 1450 lbs. From the two last plots, the better performance of the new design is well recognized. The plots indicate that

the new design is capable of reducing both tensile and compressive stresses around the concrete/device interface.

5.8. CONCLUSION

Both the experimentally measured strains and those collected from the finite element models were found to be in a fairly good agreement. This indicates that the techniques employed in developing the finite element models are capable of providing accurate responses. Therefore, it could be concluded that the use of the same techniques in simulation of pavement structures (as was presented in chapter three) would provide valid results. It was shown that similar stresses induced at the dowel-concrete interface in pavement structure could be obtained from applying a load of 1450 lbs on the half joint specimens, and 4090 lbs on the full joint specimen. In this chapter, a new alternative design of the regular dowel bar is proposed. The new design is shown to result in a remarkable reduction of the stresses induced in doweled transverse joints.

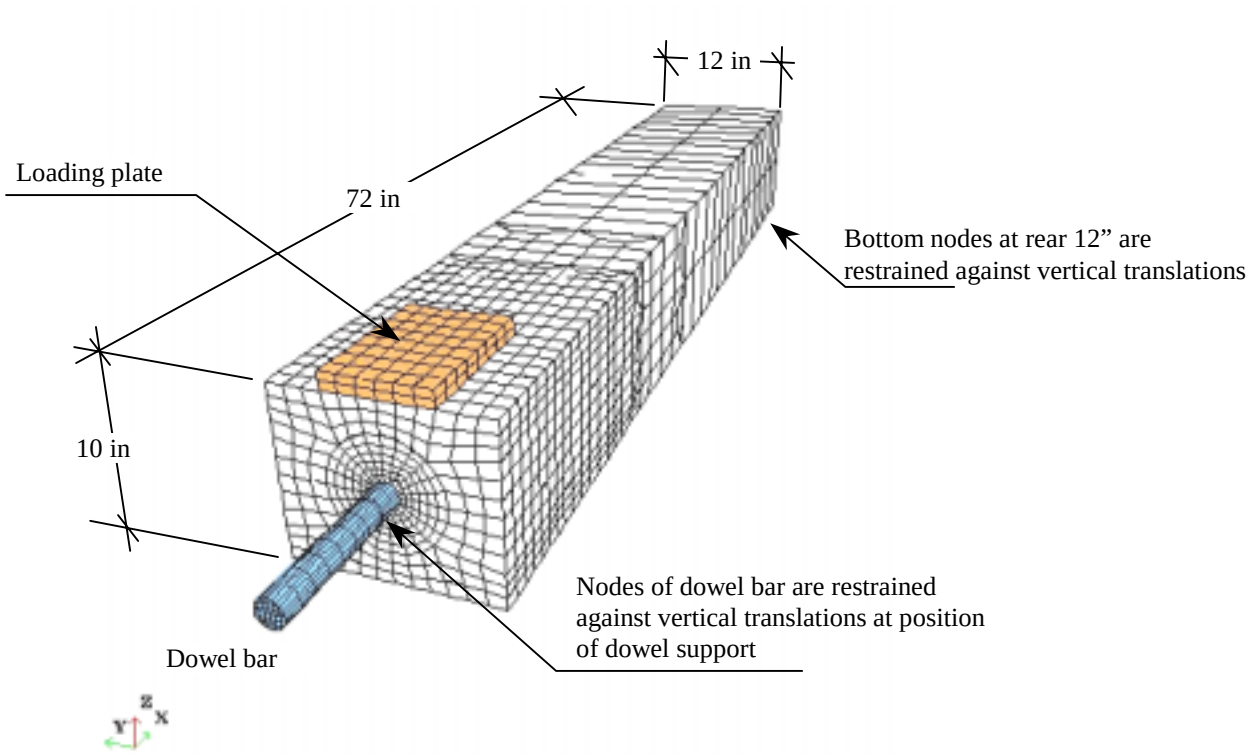

FIGURE 5.1 FEM of half joint specimen

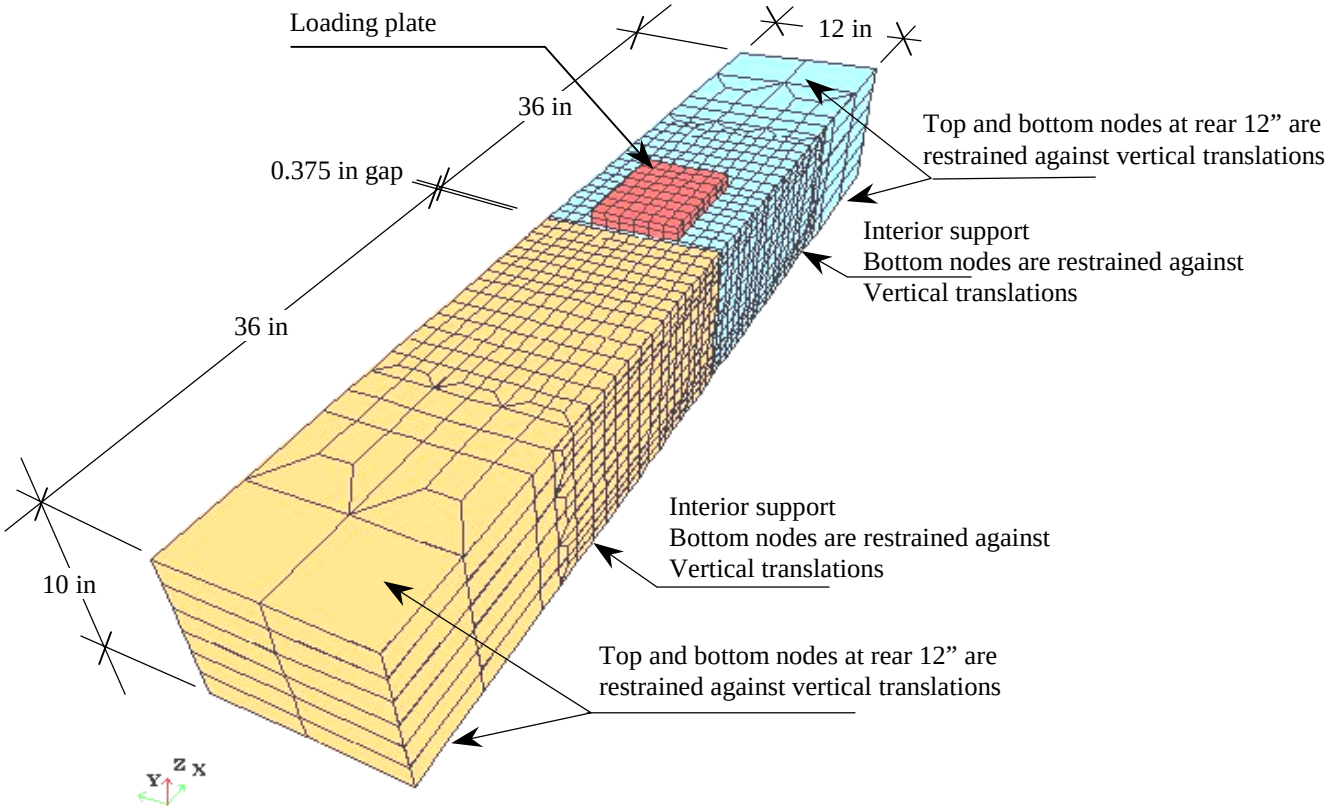

FIGURE 5.2 FEM of full joint specimen

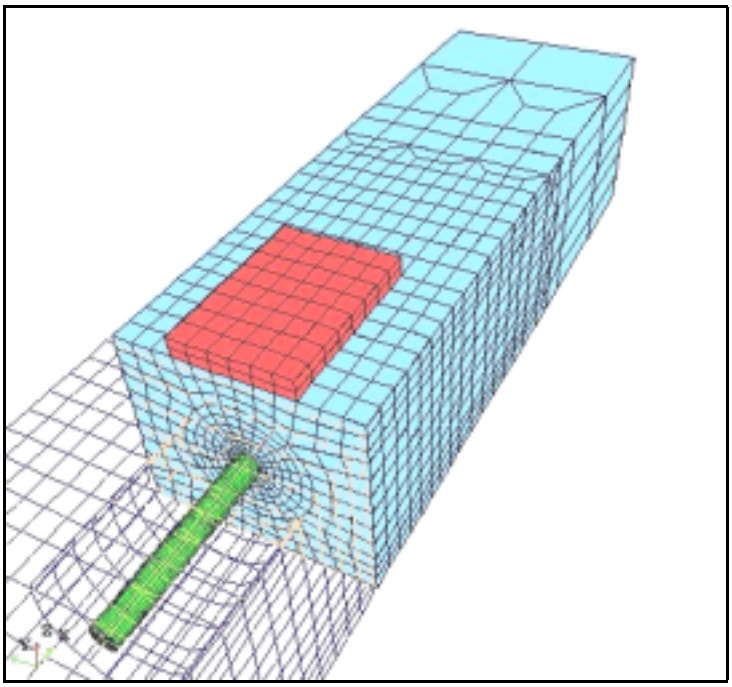

FIGURE 5.3 Full joint FEM showing embedded dowel bar

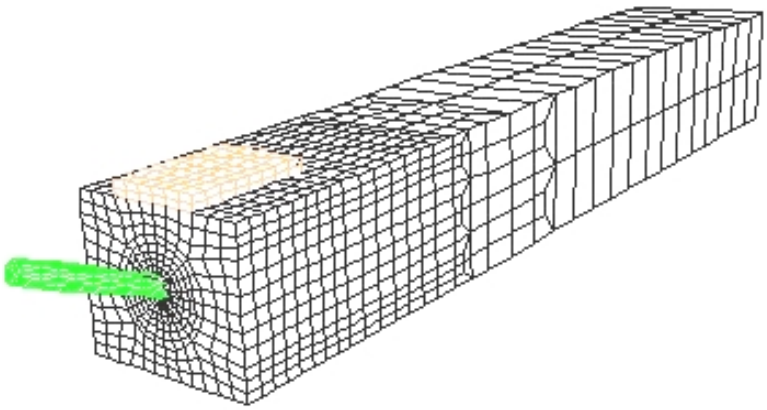

FIGURE 5.4 Deformation of half joint model

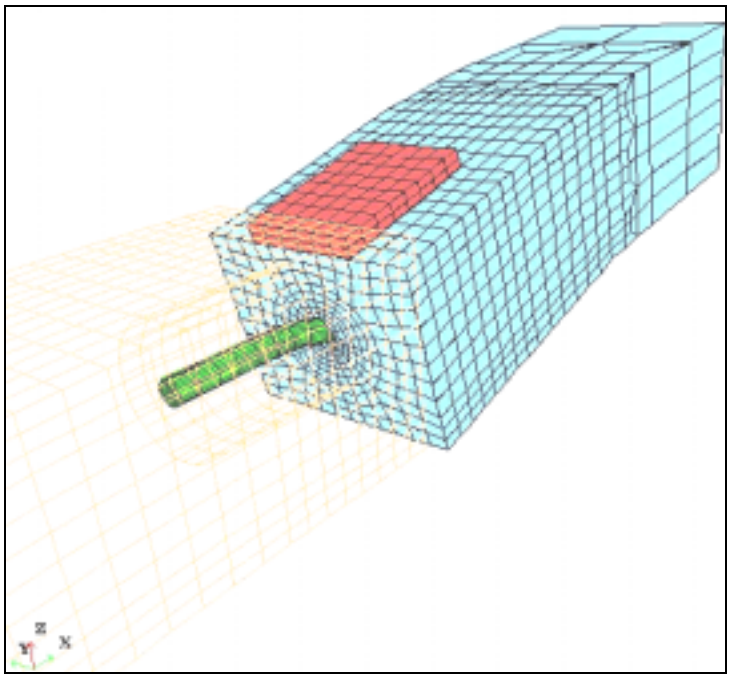

FIGURE 5.5 Deformation of full joint model

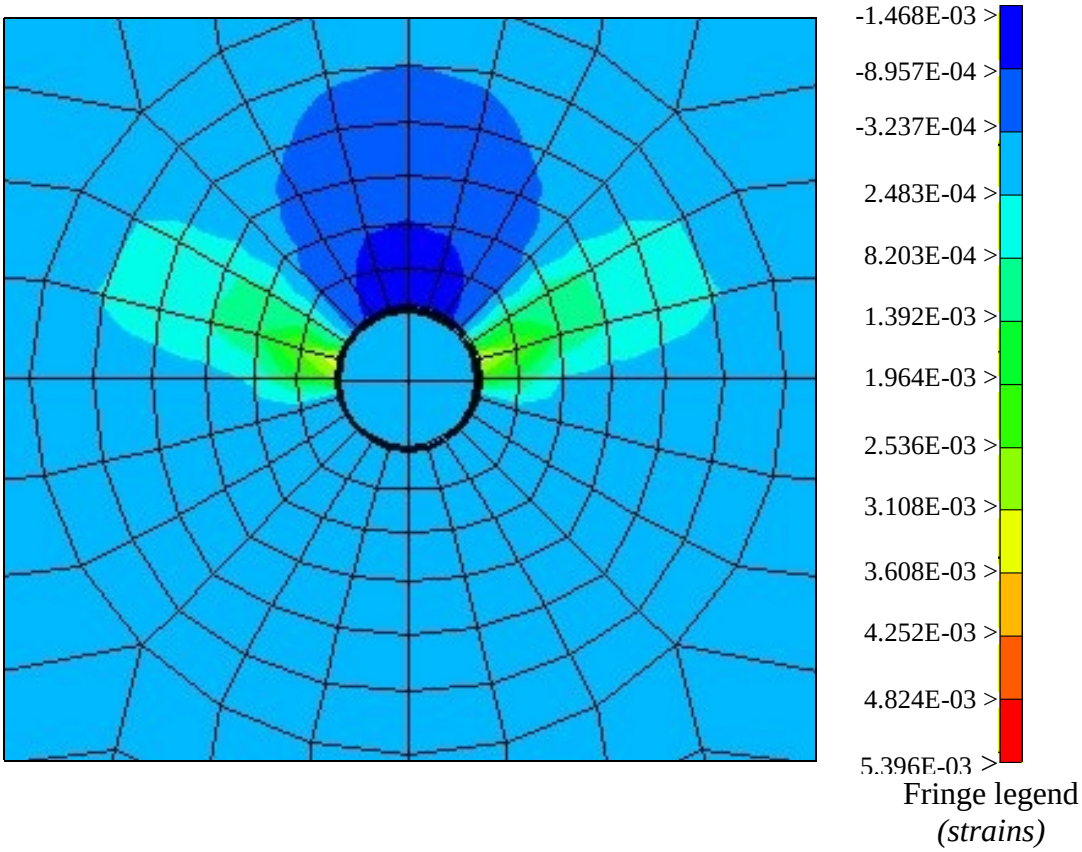

FIGURE 5.6 Fringes of vertical strains around 1.25” dowel socket In half joint model

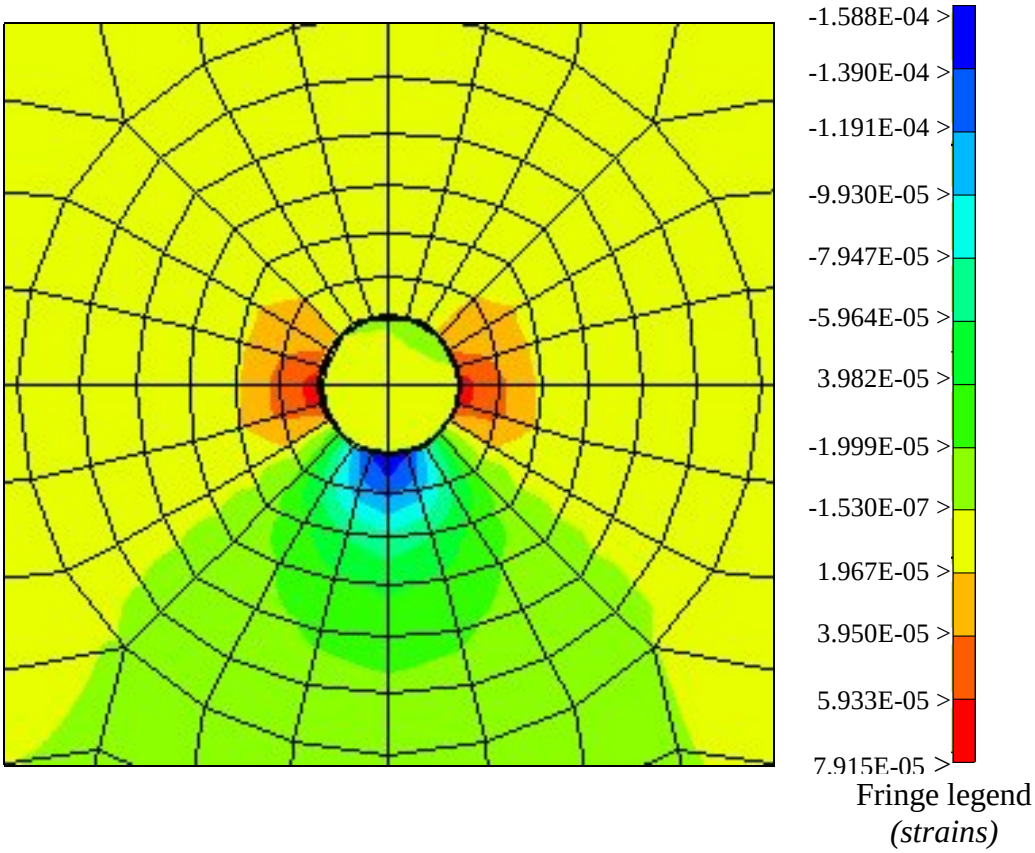

FIGURE 5.7 Fringes of vertical strains around unloaded side of Full model

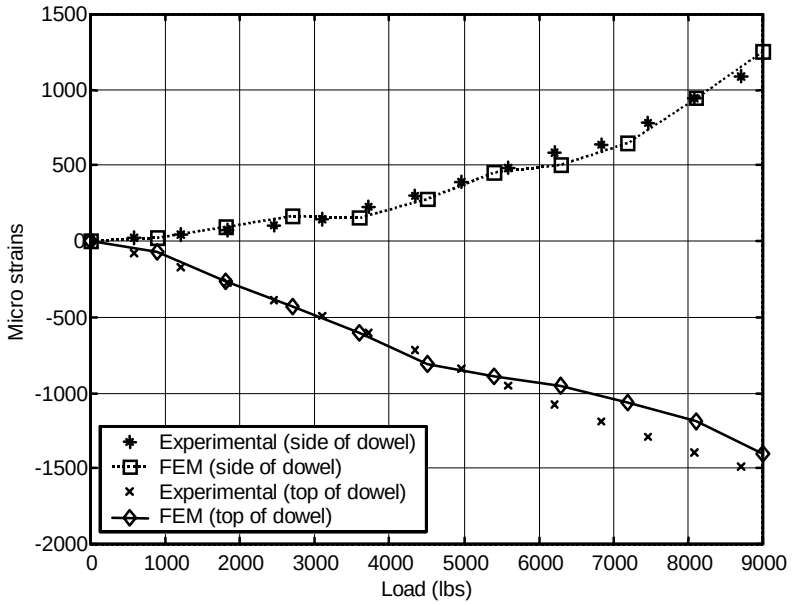

FIGURE 5.8 specimen HJ38-1

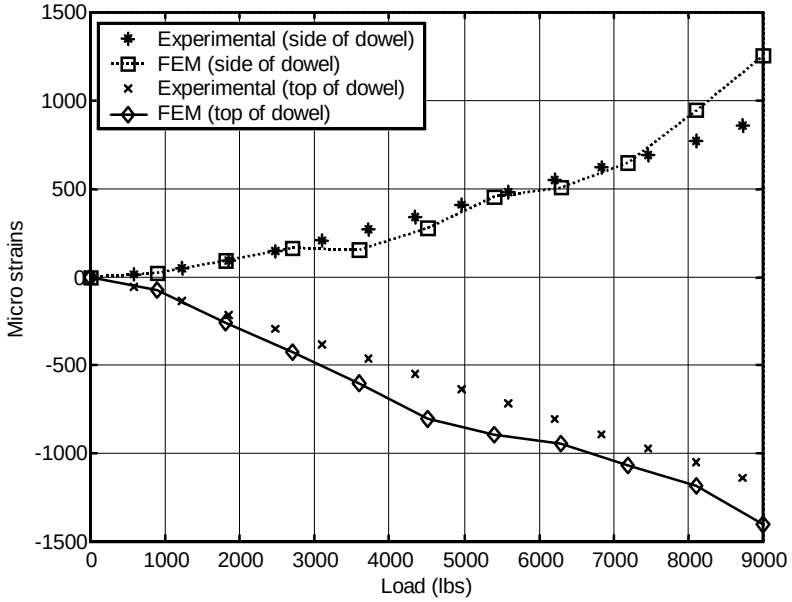

FIGURE 5.9 Specimen HJ38-2
(Dowel bar 1.5")

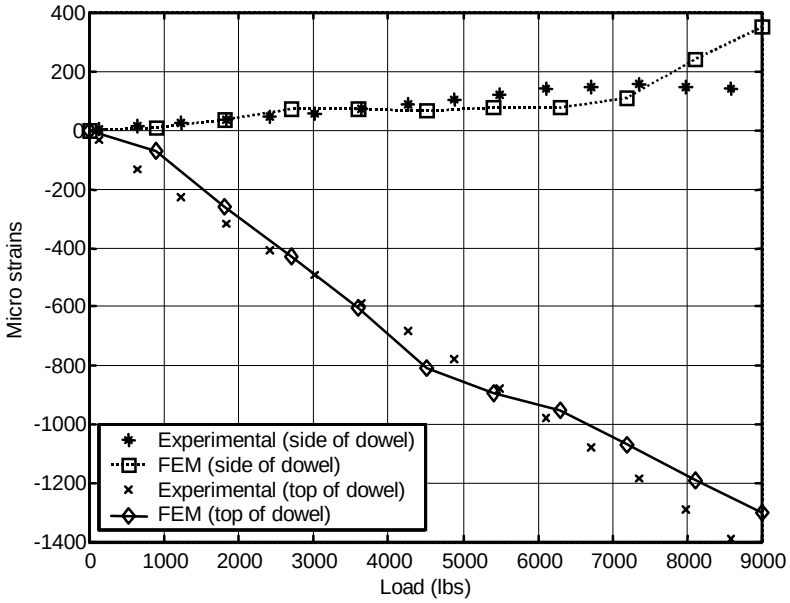

FIGURE 5.10 Specimen HJ38-3

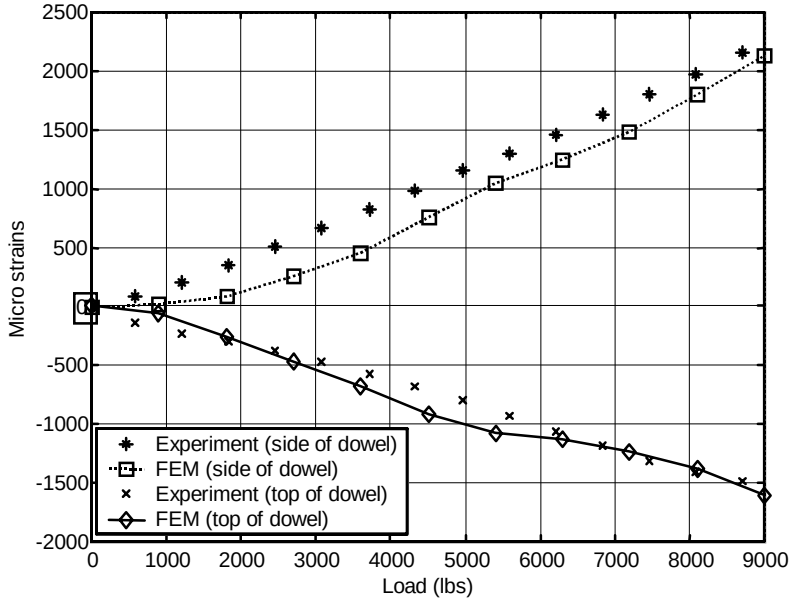

FIGURE 5.11 Specimen HJ31-6

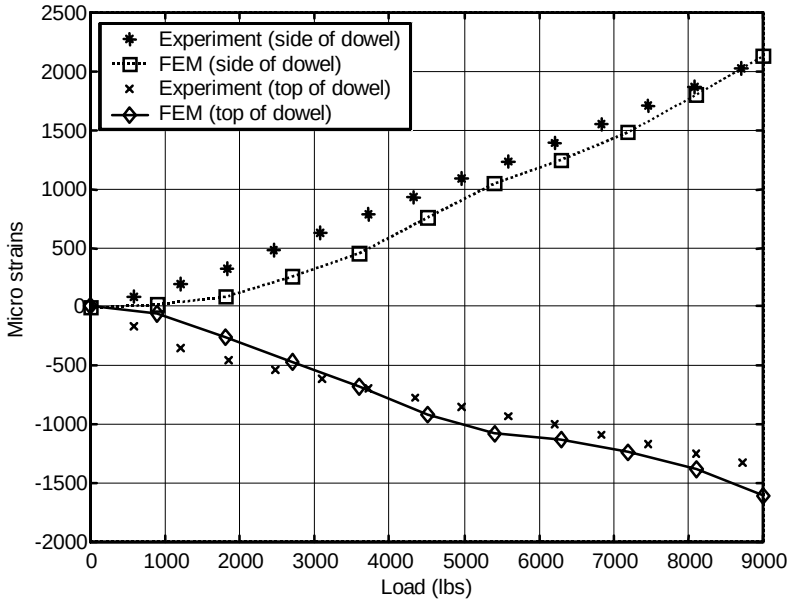

FIGURE 5.12 Specimen HJ31-7

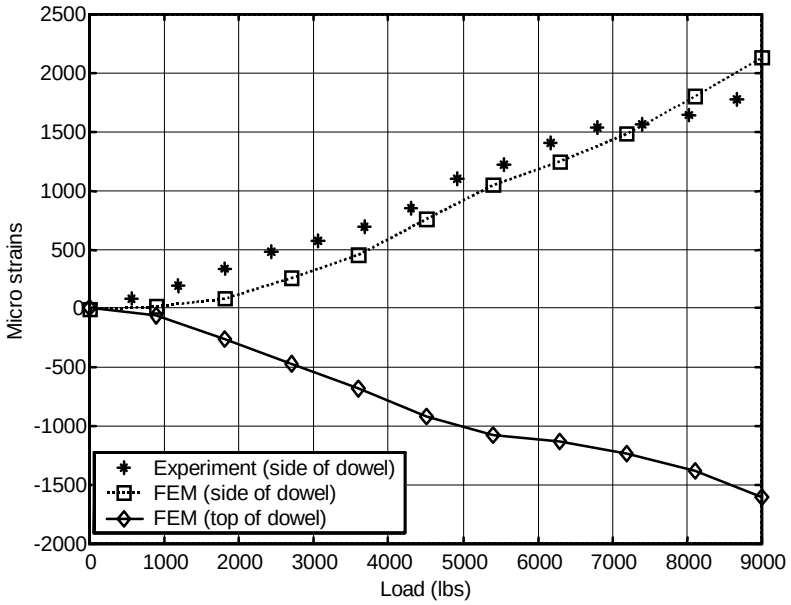

FIGURE 5.13 Specimen HJ31-8

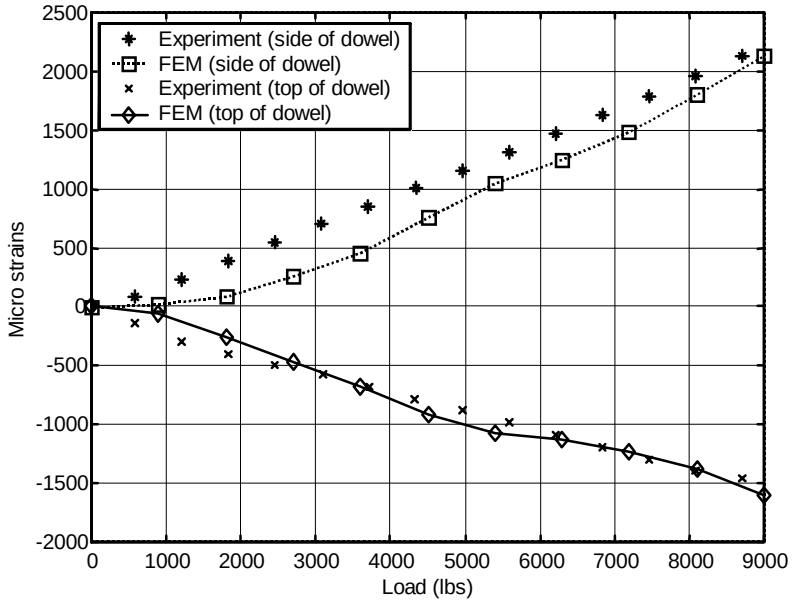

FIGURE 5.14 Specimen HJ31-9

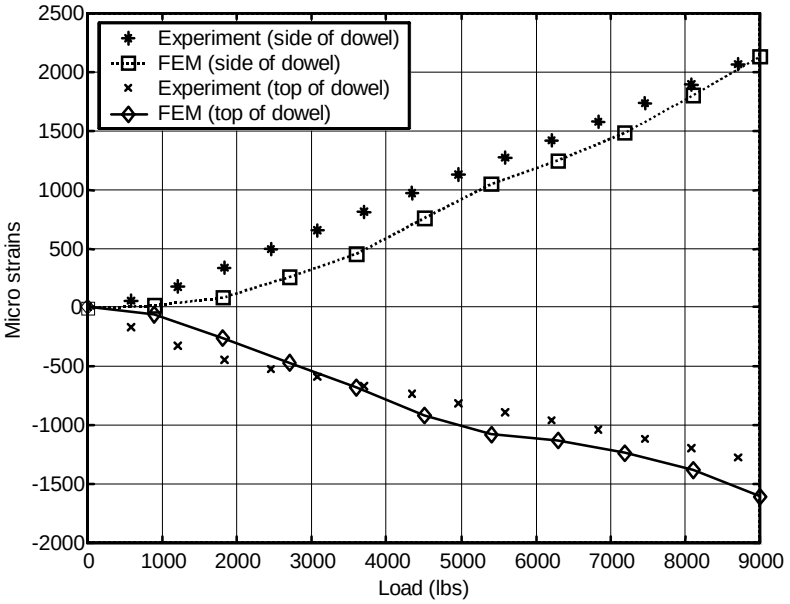

FIGURE 5.15 Specimen HJ31-10

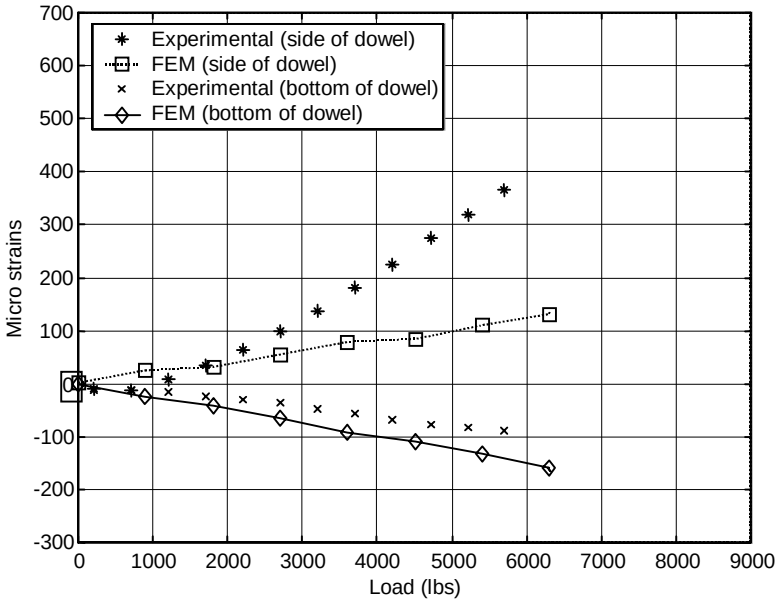

FIGURE 5.16 Specimen FJ-1

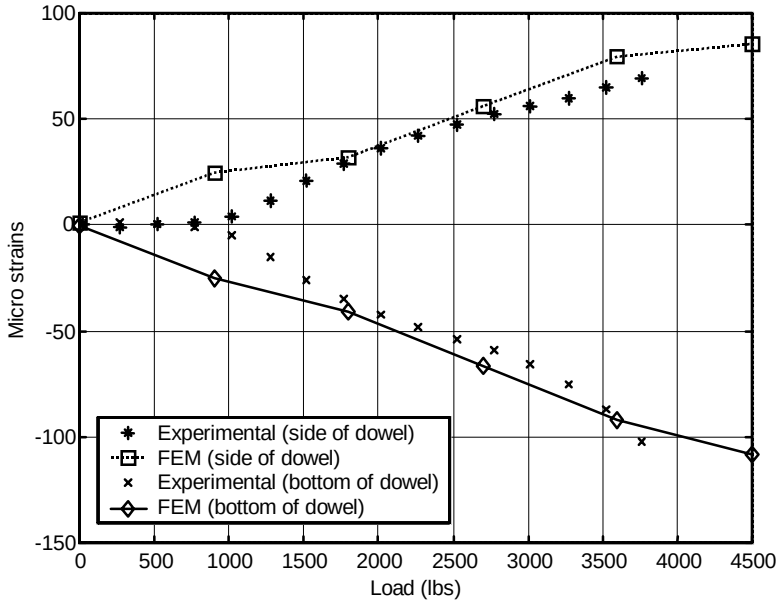

FIGURE 5.17 Specimen FJ-2

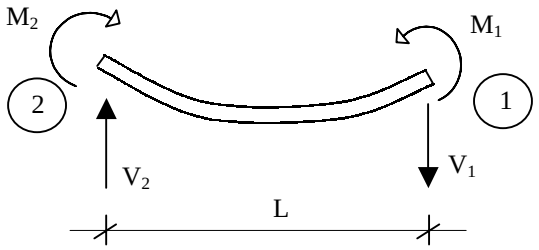

FIGURE 5.18 deformation and reactions on loaded dowel bar

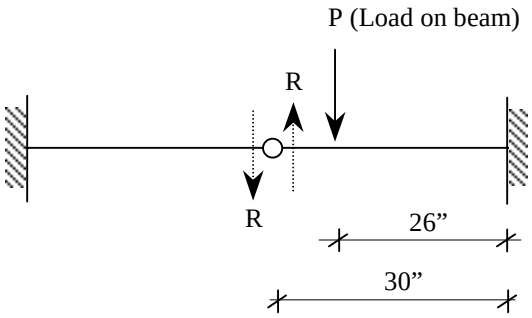

FIGURE 5.19 Structural system of joint specimen

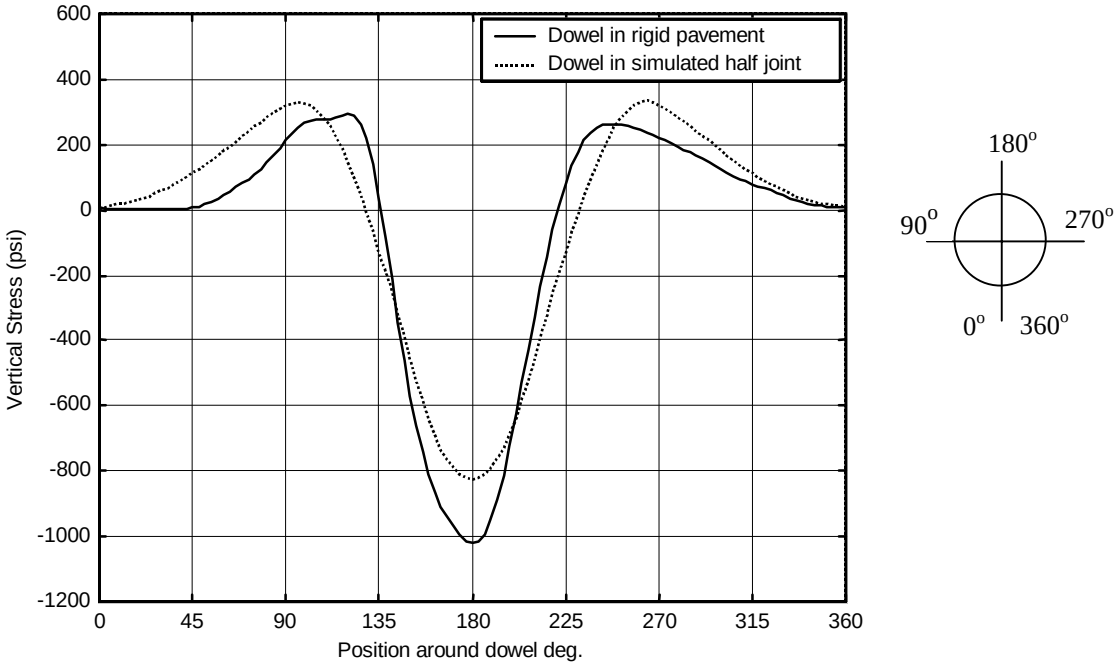

FIGURE 5.20 Vertical stresses around dowel bar in simulated half joint specimen, and rigid pavement

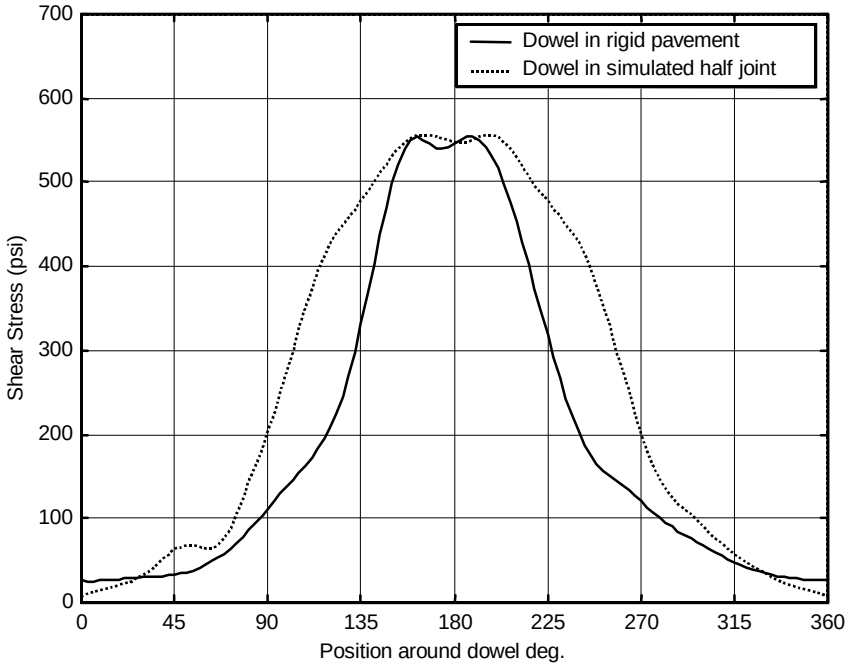

FIGURE 5.21 Shear stresses around dowel bar in simulated half joint specimen and rigid pavement

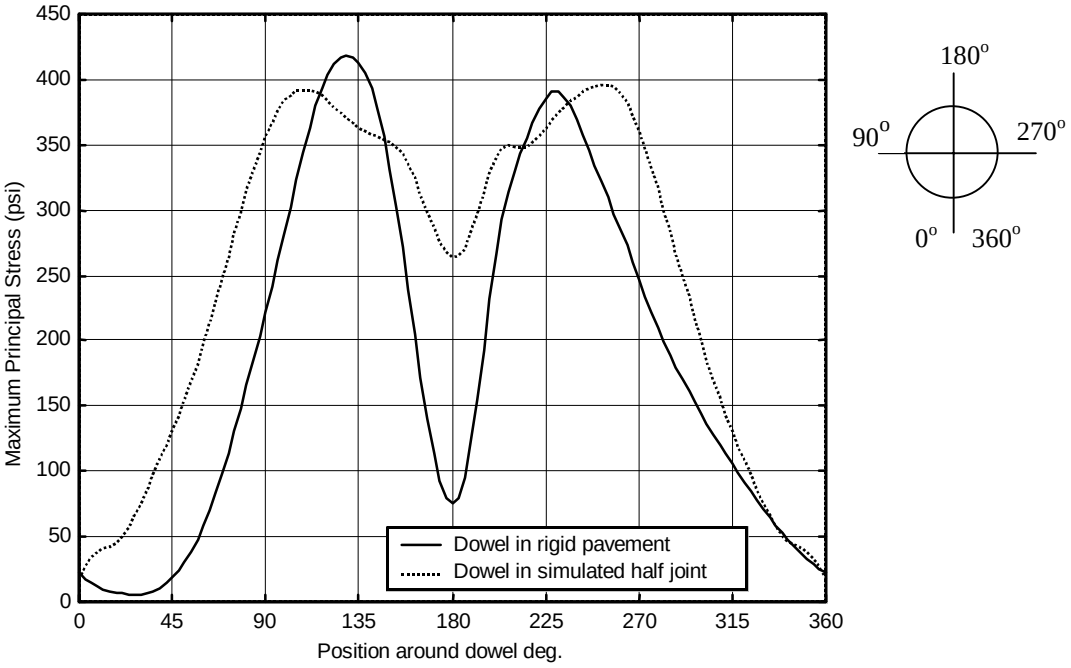

FIGURE 5.22 MPS around dowel bar at simulated half joint specimen, and pavement structure

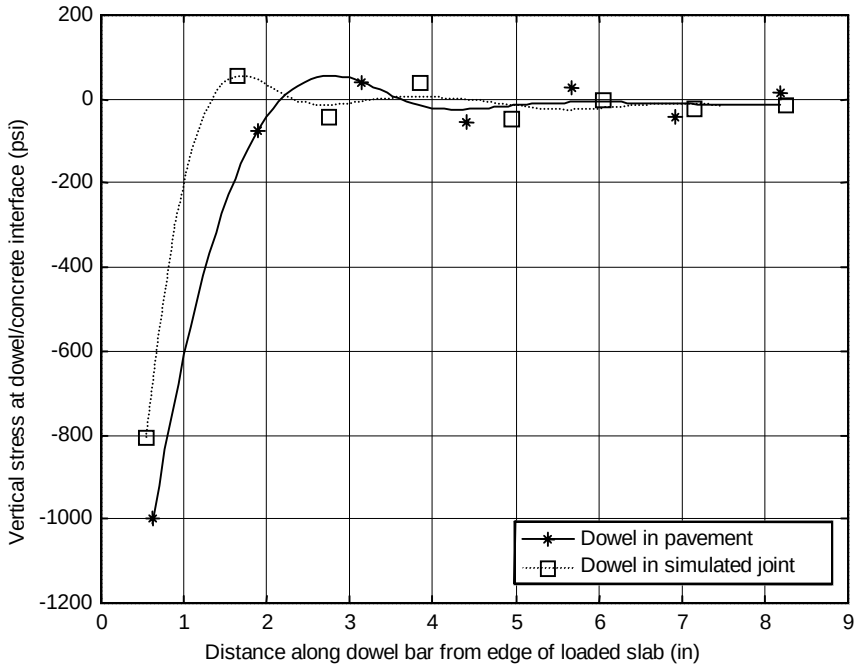

FIGURE 5.23 Vertical stress along dowel in simulated half joint, and rigid pavement

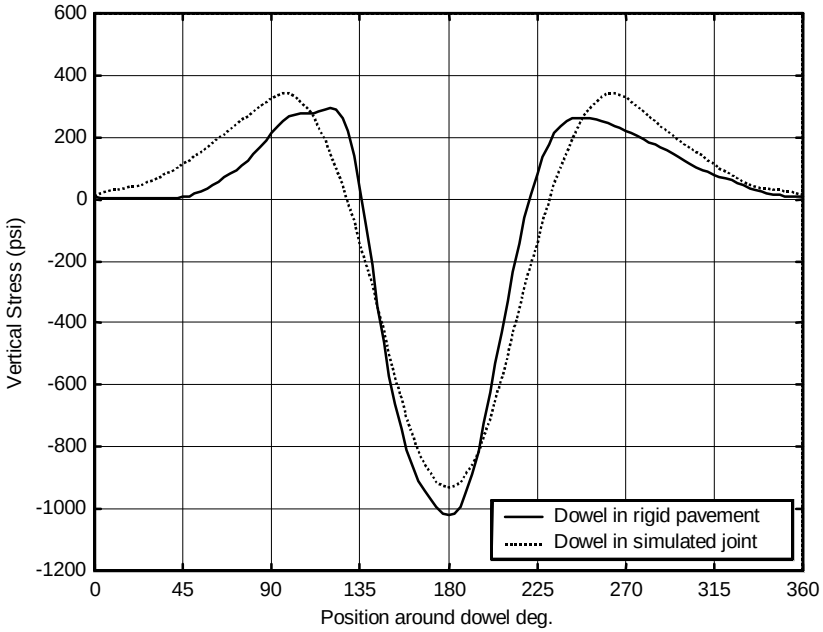

FIGURE 5.24 Vertical stresses around dowel bar in full joint specimen and pavement structure

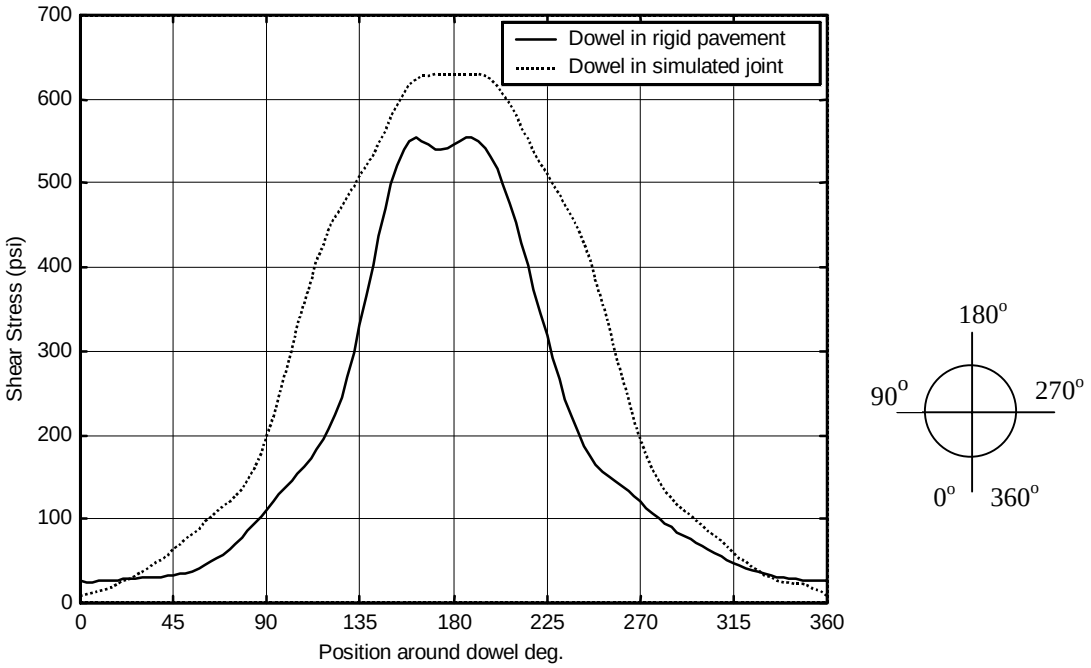

FIGURE 5.25 Shear stresses aroud dowel bar in full joint specimen and pavement structure

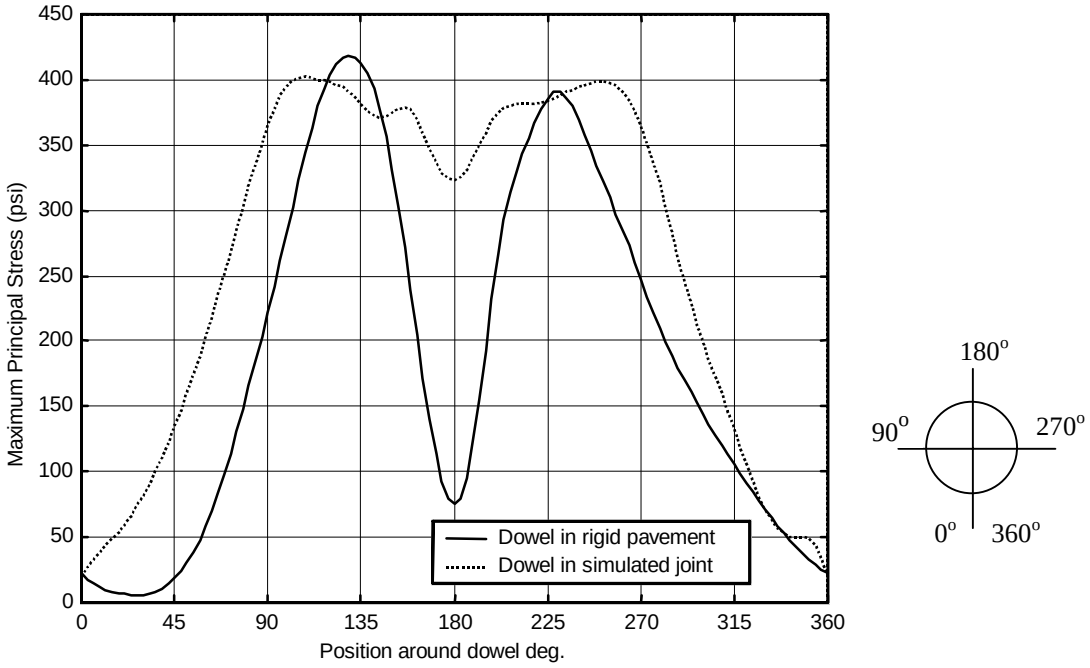

FIGURE 5.26 MPS around dowel bar in full joint specimen and rigid pavement

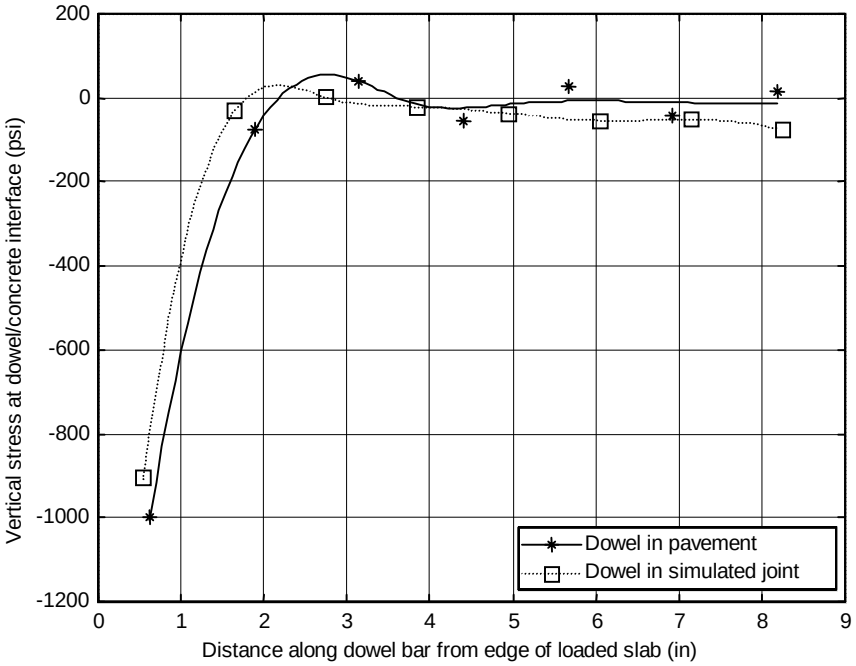

FIGURE 5.27 Vertical stress along dowel bar in full joint specimen and rigid pavement

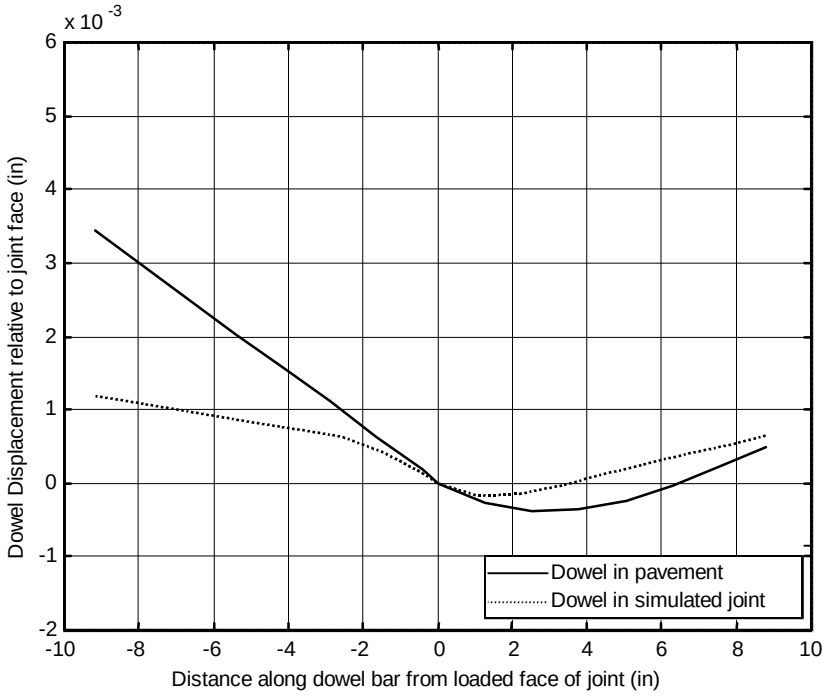

FIGURE 5.28 Deformation of dowel bar in full joint specimen and pavement structure

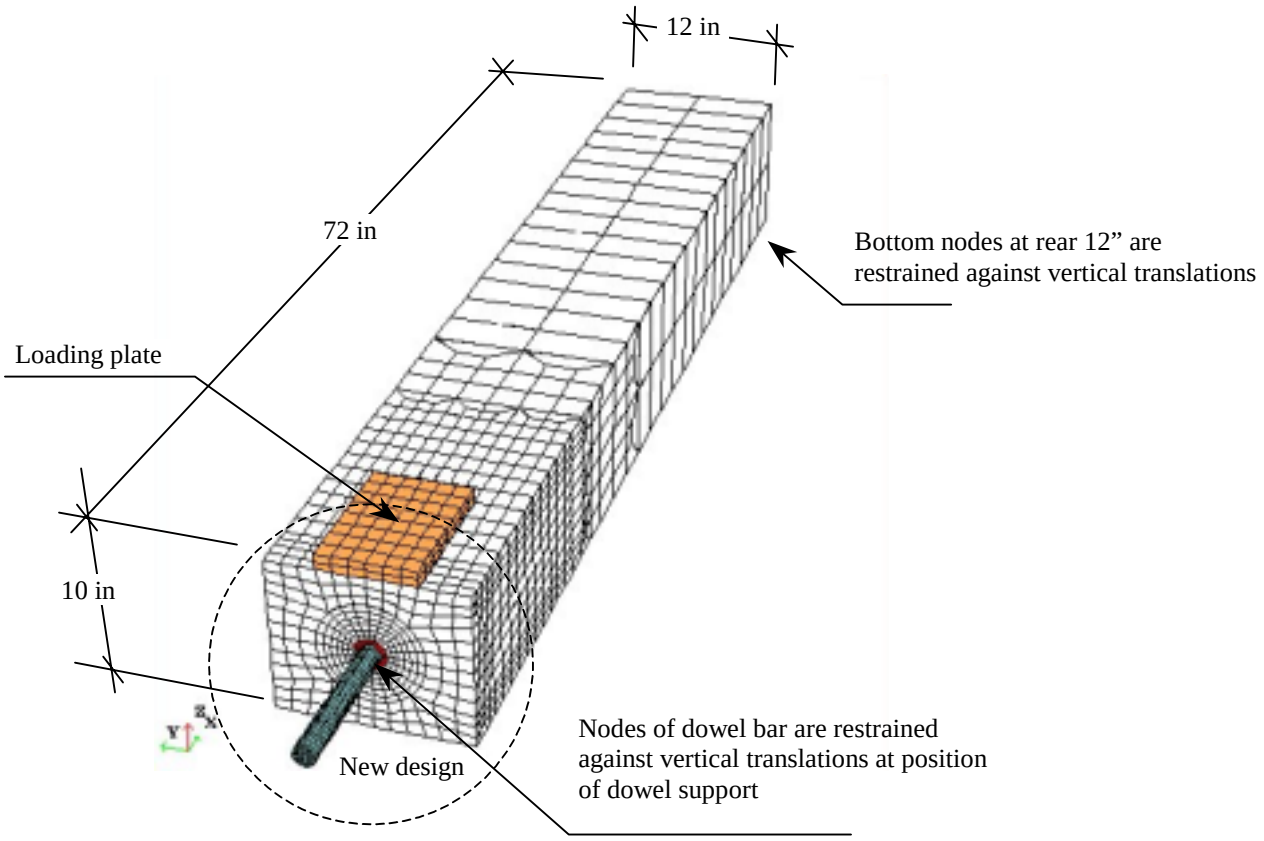

FIGURE 5.29 FEM for evaluation of new device

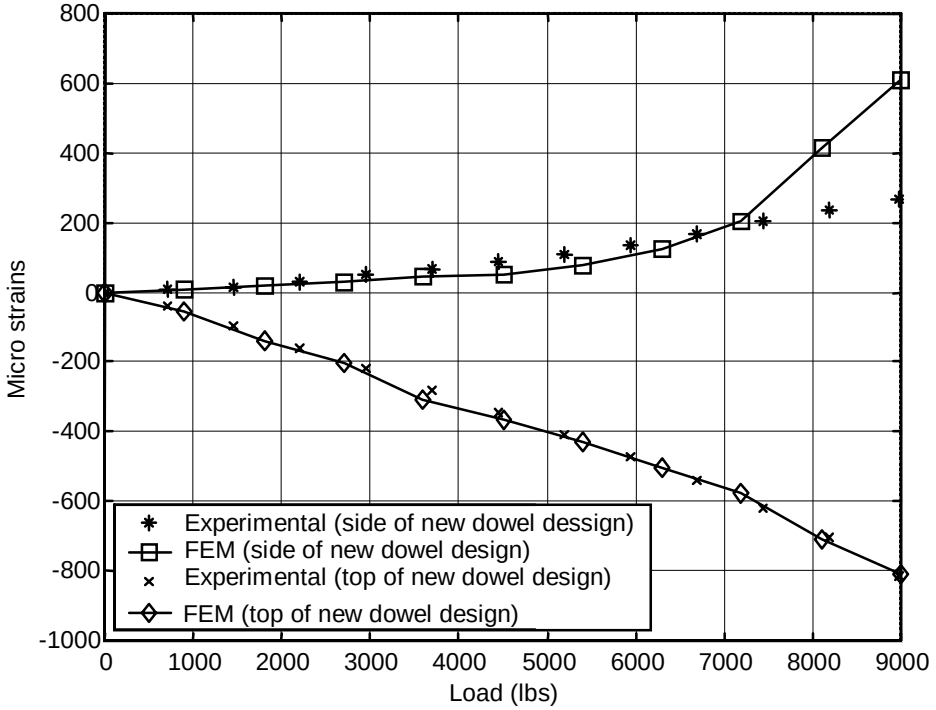

FIGURE 5.30 vertical strains in FEM containing new dowel design

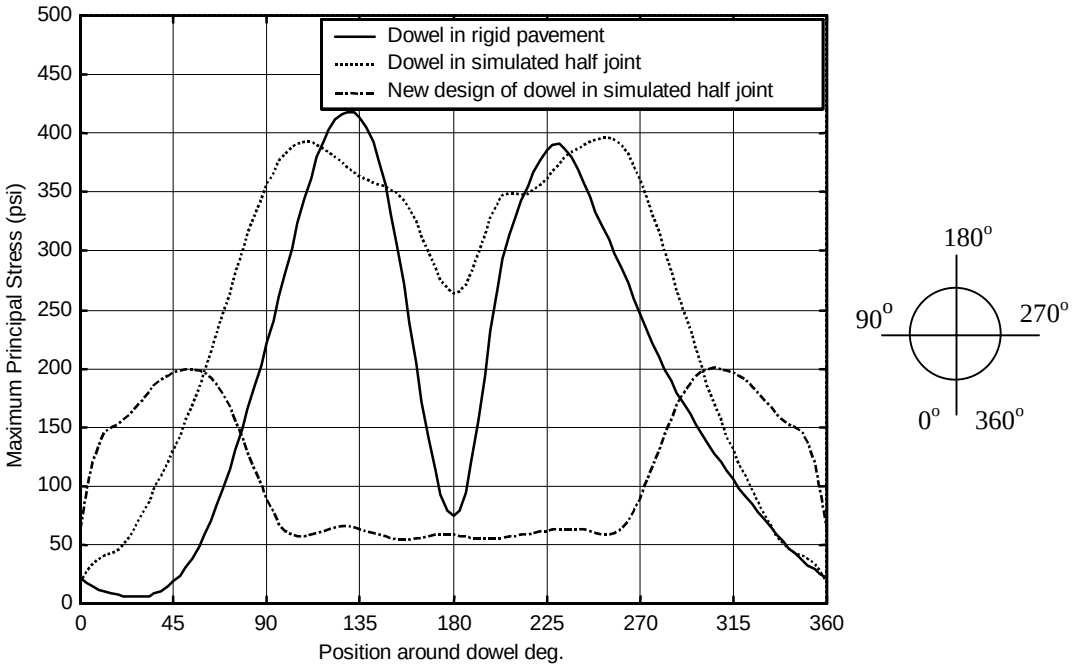

FIGURE 5.31 MPS around dowel bar in both rigid pavement, and half joint specimen in comparison with the new dowel design

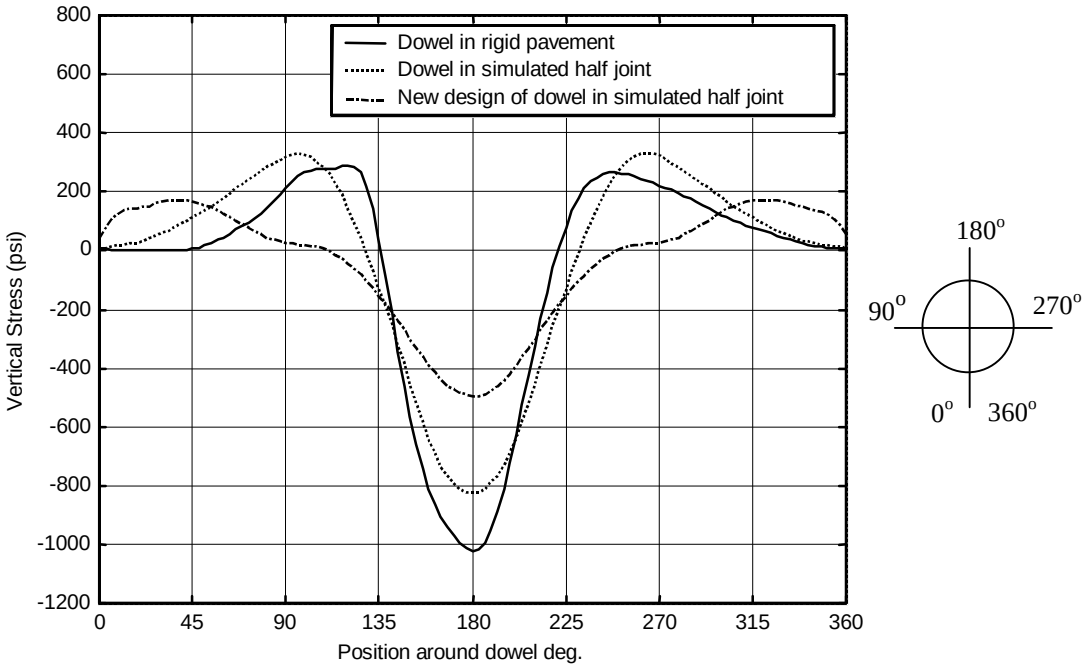

FIGURE 5.32 Vertical stresses around dowel bar in pavement structure, and simulated half joint, in comparison with the new dowel design

CHAPTER SIX

CONCLUSIONS AND PROPOSED FUTURE RESEARCH

6.1. CONCLUSIONS

This study focuses on the nature and magnitude of the stresses at the dowel-concrete interface in rigid pavement joints. The state of maximum stresses induced around the dowel bars were closely examined using 3DFEM. The results from an experimental study on simulated joints verified the FE models, and offered an insight into the behavior of regular coated dowel bars. Based on the results obtained from the developed FEM and the experimental study, the following conclusions can be withdrawn:

1. The results obtained from the FE simulation of pavement structures indicate that the current design of the regular coated dowel bar (18” long, and 1.25” diameter) satisfies the allowable compressive bearing stresses of concrete, due to the travel of the design axle load across the joint. These compressive stresses will eventually grow due to the application of several thousands of axle loads during the service life of the pavement structure.

2. Both FEM and experimental results indicate the existence of two types of stresses at the concrete-dowel interface. The first is the development of compressive stresses at the top and bottom of the dowel, and the second is the formation of tensile stresses at both sides of the dowel bar.

3. The tensile stresses are found to be more critical, as they exceed the allowable tensile strength of the concrete material, which initiate a tensile crack in the concrete socket on the sides of the dowel bar.

4. The distribution of stresses along the dowel bar shows that the concentration of both tensile and compressive stresses take place along the first 1.5 in from the face of the joint, and diminishes shortly inside the slab beyond that point.

5. The maximum induced stresses around the dowel bar in straight joints in comparison with those in skewed joints were found to be quite similar. It is concluded that skewing the joint did not enhance the performance of the dowel bar, and is considered to be an expensive ineffective refinement of the joint.

6. The test rig built for the purpose of testing simulated joint specimens proved to be a reliable facility for monitoring the joints characteristics such as displacements, and strains in the concrete material incasing the dowel bar.

7. Induced stresses around dowel bars in pavement structures can be simulated in the laboratory using simulated full joint specimens subjected to a static load amounting 4090 lbs, and 1450 lbs for the cases of simulated full and half joints respectively.

8. A new design for the dowel bar is proposed to relief both tensile and compressive stresses developed around regular dowel bars

9. The new design of the dowel bar is capable of reducing the maximum tensile and compressive stresses around regular dowels to at least 50% of their normal magnitude.

6.2. SUGGESTED FUTURE RESEARCH

The current study identifies the state of stresses developed around the dowel-concrete interfaces. It was shown that excessive tensile stresses occur at the first application of the load, which initiates tensile cracks in the concrete socket. Fatigue loading on pavement structure along the course of the pavement service life will eventually propagate the initiated cracks and increases the compressive bearing stresses in the dowel-concrete interface leading to crushing of concrete particles. The following research needs are proposed aiming to enhance the performance of the dowel bars.

1. Further studies are needed for the development of the alternative dowel design, aiming to come up with optimized dimensions for the new device.

2. The current study focused on the stresses around the dowel bars due to the application of axle loads. Further studies are needed to explore the effect of temperature variations through the slab depth on the induced stresses.

3. During the course of this research, it was found that no value of the coefficient of friction between regular dowels and concrete is available in the literature. Identification of this parameter is needed.

4. More research is needed to identify the effect of concrete curing at early stages of pavement constructions on the joints characteristics. This study would provide useful information on the residual stresses developed around the dowel bars due to shrinkage of concrete as well as the variation of moisture content and temperature in the slab at early stages.

REFERENCES

1. Sargand S., "Performance of Dowel Bars and Rigid Pavement", Draft Final Report, Federal Highway Administration, Open House and Workshop, Ohio University, Athens, Ohio, July 2000.

2. Buch Neeraj J., "Development of Empirical-Mechanistic Based Faulting Models in the Design of Plain Jointed Concrete Pavements", Ph.D. Thesis, Texas A&M University, August 1995.

3. Titus-Glover L., E.B.Owusu-Antwi, T.Hoener, and M.I.Darter, "Design and Construction of PCC Pavements", Volume II: Design Features and Practices That Influence Performance of Pavements. Publication No. FHWA-RD-98-127, October 1998.

4. Senadheera S.P., "Spalling in Concrete Pavements: It's Relationship to Coarse Aggregate in Concrete and a Framework for Design". Ph.D. Thesis, Texas A&M University, College Station, Texas, May 1995.

5. SHRP, "Distress Identification Manual for the Long-Term Pavement Performance Project", Strategic Highway Research Program, National Research Council, SHRP-P-338, Washington DC, 1993.

6. Ozbeki M. A., W.P. Kilareski, and D.A. Anderson, "Evaluation for Jointed Concrete Pavements", Transportation Research Record 1043, 1985.

7. Colley B.E., S. D. Tayabji, "Improved Rigid Pavement Joints", Transportation Research Record 930, TRB, National Research Council, Washington D.C., 1983.

8. Tabatabaie A.M., E.J. Barenberg, and R.E. Smith, "Longitudinal Joint Systems in Slip-Formed Rigid Pavements: Analysis of Load Transfer Systems for Concrete Pavements". Volume II, Publication No. FAA-RD-79-4, FAA, U.S. Department of Transportation, Washington D.C., November 1979.

9. Huang Yang H., "Pavement Analysis and Design", 1993, ISBN 0-13-655275-7.

10. Bradbury R.D., "Design of joints in concrete pavements", Proceedings No 12, Highway Research Board, 1932.

11. Timoshenko S., and J.M. Ledels, "Applied Elasticity", Westinghouse Technical Night School Press, Pittsburgh, PA, 1925.

12. Friberg B.F., “Design of Dowels in Transverse Joints of Concrete Pavements”. Transactions of the ASCE, Vol. 105,pp 1076-1095,1940.

13. Tabatabaie A.M., “Structural Analysis of Concrete Pavements Joints”, PhD Dissertation, Urbana, IL: University of Illinois, 1978.

14. Ioannides A.M., Y.H. Lee, and M.I. Darter, “Control of Faulting Through Joint Load Transfer Design”, Transportation Research Record No. 1286, Washington D.C., 1990,pp. 49-56.

15. Davids W.G., “Modeling of Rigid Pavements: Joint Shear Transfer Mechanisms and Finite Element Solution Strategies”, Ph.D. Dissertation, University of Washington, 1998.

16. Tabatabaie A.M., and E.J. Barenberg, “Finite Element Analysis of Jointed or Cracked Concrete Pavements”, Transportation Research Board No 671, 1978.

17. U.S. Army Engineer Ohio River Division Laboratories, “Field Tests of Doweled-joint Performance”, Cincinnati, OH, Final Report, November 1959.

18. U.S. Army Engineer Ohio River Division Laboratories, “Small-Scale Model Study of Doweled joints in Rigid Pavement for Military Airfields”, Cincinnati, OH, Unpublished Report, 1959.

19. Tayabji S.D., and B.E. Colley, “Improved Rigid Joints”, Transportation Research Record 930, 1983.

20. Tayabji S.D. and B.E. Colley, “Analysis of Jointed Concrete Pavements”, U.S. Department of Transportation, Federal Highway Administration, Publication No. FHWA/RD-86/041, February 1986.

21. Guo H., and M. Dong, “An Analytical Model for Evaluating Computer Programs for Structural Analysis of Jointed Concrete Pavements”, Workshop on Load Equivalency, Mathematical Modeling of PCC Pavements, Washington D.C., 1992.

22. Guo H., J. A. Sherwood, and M. B. Snyder, “Component Dowel Bar model for Load Transfer Systems in PCC Pavements”, Journal of Transportation Engineering, May/June 1995, pp. 289-297.

23. Chatti K., J. Lysmer, and C.L. Monismith, “Dynamic Finite Element Analysis of jointed concrete pavements”, Transportation Research Record 1449, 1994, pp. 79-90.

24. Zaghloul S.M., T.D. White, and T. Kuczeck, “Evaluation of Heavy Load Damage effect on Concrete Using Tree-Dimensional, Nonlinear Dynamic Analysis”. Transportation Research Record 1449, pp. 123-133,Washington D.C., 1994.

25. Uddin W., R.M. Hackett, A. Joseph, Z. Pan, and A.B. Crowly, “Three Dimensional Finite Element Analysis of Jointed Concrete Pavement Having Discontinuities”, Transportation Research Record 1482, pp. 26-32, Washington D.C., 1996.

26. Channakechava C., F. Barzegar, and G. Voyiadjis, “Nonlinear Finite Element Analysis of Plain Concrete Pavement With Doweled Joints”. Journal of Transportation Engineering, 199(5), pp. 763-781, 1993.

27. Shoukry S.N., and G. William, “3D FEM Analysis of Load Transfer Efficiency”, proceeding, First National Symposium on 3D Finite Element Modeling for Pavement Analysis & Design, pp. 40-50, Charleston, WV, 1998.

28. Friberg B., “Load and Deflection Characteristics of Dowels in Transverse Joints of Concrete Pavements”, Highway Research Board No. 18, Proceedings of the Annual Meeting, Washington D.C., 1938.

29. University of Illinois, “Engineering experiment Station, Experience in Illinois with Joints in Concrete Pavements”, Bulletin series No. 365, 1947.

30. Keeton J.R., “Investigation of Load Transfer Characteristics of Dowels”, Highway Research Board Proceedings, 1956.

31. Teller L.W., and H.D. Cashell, “Performance of Doweled Joints Under Repetitive Loading”, Public Roads, Vol. 30 No. 1, April 1958.

32. Ciolko A.T., P.J. Nussbaum, and B.E. Colley, “Load Transfer of Dowel Bars and Star Lugs”, Final Report, Construction Technology Laboratories, Skokie, IL, 1979.

33. Sargand S., and G. Hazen, “Evaluation of Pavement Joint Performance, Federal Highway Administration”, Report No. 14474(0), 1994.

34. Hammons M., “Development of an Analysis System for Discontinuities in Rigid Airfield Pavements”, US Corps of Engineers, Waterways Experiment Station, Technical Report; GL-97-3, 1997.

35. McGhee K.H., “NCHRP Synthesis of Highway Practice 211: Design, Construction, and Maintenance of PCC Pavement Joints”, National Cooperative of Highway Research Program, Washington, D.C.1995.

36. Kelleher K., and R.M. Larson, “The Design of Plain Doweled Jointed Concrete Pavements”, Fourth International Conference on Concrete Pavement Design and rehabilitation, Purdue University, pp. 279-292,1989.

37. Vyce J.M., “A Summary of Experimental Concrete Pavement in New York”, Research Report 141, Engineering Research and Development Bureau, New York State Department of Transportation, 1988.

38. NCHRP, “NCHRP Synthesis of Highway practice 19: Design, construction, and Maintenance of PCC Pavement joints”, Transportation Research Board, National Research Council, Washington, D.C., 1973.

39. Bischoff D.L., “Random Skewed Joints with and without Dowels”, Wisconsin Department of Transportation, Division of Transportation Infrastructure Development, Bureau of Highway Construction, Federal Experimental Project No. WI 85-01, Final Report WI/FEP-07-96., 1996.

40. McKenzie L.J., “Behavior of Plain PCC Pavement with Skewed joints randomly spaced”, Illinois Department of Transportation, Bureau of Material and Physical Research, Final Report No. FHWA-IL-PR-79., 1979

41. FHA, Application Notes, “LTPP Findings Pay Off for Pennsylvania”, FHWA-RD-00-064, Feb. 2000.

42. Shoukry S. N. and G.W. William, “Performance Evaluation of Backcalculation Algorithms Through Three-Dimensional Finite-Element Modeling of Pavement Structures”, Transportation Research Record, Journal of the Transportation Research Board No 1655, 1999.

43. Supplement to the AASHTO Guide for Design of Pavement Sructures, Part II, “Rigid Pavement Design & Rigid Pavement Joint Design”, American Association of State Highway and Transportation Officials, 1998.

44. Govindjee S., G.J. Kay, and J.S. Simo, “Anisotropic Modeling and Numerical Simulation of Brittle Damage in Concrete”, International Journal for Numerical methods in Engineering, Vol. 38, pp. 3611-3633, 1995.

45. William G.W., “Backcalculation of Pavement Layers Moduli Using 3D Nonlinear Explicit Finite Element Analysis”, M.Sc Thesis, West Virginia University, April 1999.

46. Sargand S.M., and D.I, Beegle, “Three Dimensional Finite Element Software Development and Verification Case Study”, Proceeding of the First National Symposium on 3D Finite Element Modeling for Pavement Analysis and Design, Charleston, West Virginia, 1998.

47. Brown S.F., “Determining of Young's Modulus for Bituminous Materials in Pavement Design”, Highway research Record No 431, HRB, National research Council, Washington, D.C., pp. 38-49, 1973.

48. Carrasquillo R.L., A.H. Nilson, and F.O. Slate, “Properties of High Strength Concrete Subject to Short Term Loads”, J. ACI, Vol 78, No 3, May-June 1981, pp. 171-178.

49. Martinez S., A.H. Nilson, and F.O. Slate, “Short Term Mechanical Properties of High Strength Lightweight Concrete”, Research Report No. 82-9, Dept. of Structural Engineering, Cornell University, August 1982.

50. Building Code Requirements for Structural Concrete, ACI 318-95, and Commentary, ACI 318R-95, American Concrete Institute, Farmington Hills, MI, 1995.

51. Bickford William B., “A first course in the finite element method”, 1994, ISBN 0-256-14472-9

APPENDIX I

CONCEPT OF FINITE ELEMENT MODELING

The finite element method is a numerical procedure to solve many types of structural analysis problems, in which the entire body is represented as an assembly of discrete elements and nodes. The solution is approximated for the discrete elements, and then combined to obtain the solution for the whole system. In its simplest forms, the outline of the finite element model solution is to compute the displacements at the nodes by solving the equation:

$$\{K\}[\Delta] = \{Q\}$$

Where: $\{K\}$= the Stiffness matrix of the element,

$[\Delta]$ = the displacement vector, and

$\{Q\}$= the discrete load vector.

The global response of the system is obtained through an interpolation function that transforms the displacements from the local coordinates of the element to the global coordinates of the system. Once the displacements at the nodes are computed, the compatibility between strains and displacements is used to obtain the strains at the element such as:

$$\varepsilon_x = \frac{\partial u}{\partial x}$$

where: u = the node displacement in the x Cartesian coordinate.

Using the appropriate constitutive law, stresses could be computed from strains that were obtained from the previous step. The implementation of the finite element method could be carried out by solving the problem by hand, which is a quite prohibitive task, or by using an existing code, or by generating a code to solve a class of problems. When solving dynamic problems with the finite element method, the solution is carried out by dividing the total response time of the system into much smaller time intervals called

time steps, or time increments. The equilibrium equations governing the dynamic response of the system are:

$$[M]\{\ddot{u}\}+[C]\{\dot{u}\}+[K]\{u\}=\{R^{ext}(t)\}$$

where [M] is the mass matrix,

[C] is the damping matrix,

[K] is the stiffness matrix,

$\{\ddot{u}\}$, $\{\dot{u}\}$, and $\{u\}$ are the nodal accelerations, velocities, and displacements vectors respectively, and $\{R^{ext}(t)\}$ is the external forces vector. This equation represents a system of nonlinear second order differential equations, are solved with explicit or implicit finite element codes using direct time integration techniques. That means that the values of the unknowns are determined at time $(t + \Delta t)$ based on knowledge of their values at time (t).

The implicit integration operator definition is completed by the Newmark formulae for displacement and velocity integration, which is:

$$u\big|_{t+\Delta t} = u\big|_t + \Delta t\dot{u}\big|_t + \Delta t^2\left[(1/2-\beta)\ddot{u}\big|_t + \beta\ddot{u}\big|_{t+\Delta t}\right]$$

$$\dot{u}\big|_{t+\Delta t} = \dot{u}\big|_t + \Delta t\left[(1-\gamma)\ddot{u}\big|_t + \gamma\ddot{u}\big|_{t+\Delta t}\right]$$

where β and γ are parameters of the system. Substituting into the equation of motion, the solution is obtained at time $(t + \Delta t)$.

The explicit dynamic analysis is based on integrating the equations of motion for the system using the explicit central difference formula, which is:

$$\ddot{u}\big|_t = \frac{1}{\Delta t^2}\left(u\big|_{t-\Delta t} - 2u\big|_t + u\big|_{t+\Delta t}\right)$$

$$\dot{u}\big|_t = \frac{1}{2\Delta t}\left(u\big|_{t+\Delta t} - u\big|_{t-\Delta t}\right)$$

Substituting into the equation of motion, the solution is obtained at time (t).

In this study, the explicit operation is used for many reasons. In the explicit method, the effective mass matrix is diagonal, and the solution is achieved automatically without having to solve the system of equations. The CPU cost per increment is directly proportional to the number of degrees of freedom in the model. On the other hand, in the implicit analysis, each increment consists of at least one iteration and usually more than one. Each iteration requires the solution of a set of simultaneous equations. The CPU cost per iteration is roughly proportional to the number of degrees of freedom in the model

squared. In this study, the explicit finite element code LS-DYNA was used to explore the stresses induced in the dowel bar/concrete interface by generating a three dimensional finite element model of a jointed rigid pavement.

LS-DYNA3D SOFTWARE

LS-DYNA3D is a general-purpose finite element code developed and marketed by Livermore Software Technology Corporation. Its origins dates back in the mid-seventies when DYNA3D was developed by J. Hallquist. Since then, adding new capabilities evolved the software considerably, and its new features expanded its range of applications. The software consists of one source that compiles under FORTRAN compilers on UNIX workstations and supercomputers. The code enables spacial discretization by use of four-node tetrahedron and eight node solid elements, two node beam elements, three and four node shell elements, eight node solid shell elements, truss elements, membrane elements, discrete elements, and rigid bodies. The software currently contains approximately one hundred constitutive models to cover a wide range of material behavior. One of its features is the use of a contact-impact algorithm, which allows difficult contact problems to be treated easily, and with a relatively low cost. The contact-impact algorithm permits gaps and sliding along material interfaces with friction.

RoCJte 13, Box 82-B
Morgantown, WV 26505
(304) 598-0267

APPENDIX II

CONCRETE MIX PROPERTIES

165 Rolling Meadows Road
Waynesburg, PA 15370
(412) 852-1112

HOY
REDI-MIX CO.

Client:	Roy Redi-Mix Co.	Mix ID:	**#12564 CementMid-Ran! 4000**
, **Project:**	General Mix Designs	Target	**PSI** AlE **Poly 997 Morgantown**
Location:	Morgantown, WV	**Plant** Loc.	
Date:	9/7/99		

Cementitious Materials: ASTM C **150** & C **618 Type** 1	**Supplier** Armstrong Cement	**SSD Wt.** 5641b	**Abs.** V **01.** 2.87 cu.ft.
Aggregates: ASTM C 33 & ASTM C 330 Greer			
57 Limestone	**Greer**	950 Ib	5.64 cu.ft.
Stocker Sand	**Stocker Sand** & **Gravel Greer**	1147 lb	6.99 cu.ft.
Greer 67 Limestone		950 Ib	5.64 cu.ft.
Percent Air:		6.0%	1.62 cu.ft.
Water:	31.81 Gal. of Water, lbs=	2651b	4.25 cu.ft.
	Total:	3876 **Ib**	27 cu.ft.
Air- Entraining Agent: ASTM C **260** MB AE90	Master Builders		2.82 ***ozlyd***
Other Admixes: ASTM C **494** Polyheed 997	Master Builders		39.48 oziyd

Test Data:	Slump Range:	7 **in. 6.5%**	4 in.
	Air Content Range:		4.5%
	Unit Weight: Water/Cement		143 Ibs/cu.ft.
	Ratio: Average Field Test		0.47
	Data:		7 Day 5226 PSI
			28 Day 6154 PSI

We guarantee that the strengths produced by this mix design will meet the acceptance criteria ~ of ACI 318, "Building code Requirements for Reinforced Concrete" or ACI 301, "Specification for Specification for Structural Concrete for Buildings" when sampling and specimen preparation are performed by personal certified as technicians by the American Concrete Institute in full accord with applicable ASTM standards, and test specimens are handled, cured and tested in accordance with applicable ASTM standards. ASTM C-94 requireds that the ready-mix producer be given copies of test reports and we request that we receive these reports to properly monitor your project.

1.25 in STEEL DOWEL PROPERTIES

CERTIFIED MILL TEST REPOR

The First Two Digits Of The Heat Number Denote Plant of Origin:
55 - Kankakee, Illinois Steel Division
59 - Birmingham, Alabama Steel Division
70 - Seattle, Washington Steel Division
31 - Jackson, Mississippi Steel Division

BIRTHINGHAM STEEL CORP
KANKAKEE, IL STEEL DIVISION
972 EAST 4500 N ROAD
BOURBONNAIS, IL 60914-4127
(815)937-3131

5412702O
04/06/00
DATE:
55-I29437
B.L. NO.:
5500004073
LOAD NO.:

SOLD TO
• AMERICAN HWY TECHNOLOGY
• 2150 B SOUTH RT 45-52
• KANKAKEE, IL 60901
•
•

SHIP TO
• AMERICAN HWY TECHNOLOGY
• RT 45
• 1 BLOCK NO OF SOUTHTEC DRI
• KANKAKEE, IL

HEAT NO.*	DESCRIPTION	PHYSICAL TESTS					CHEMICAL TESTS									
		YIELD P.S.I.	TENSILE P.S.I.	ELONG % IN 8"	Bend	WT% DEF	C	Ni	Mn	Cr	P	Mo	S	V	Si	Cb	Cu	C.E
O#: 159692 500I4986	KANKAKEE, IL STEEL DIVISION 1-1/4" Rd 45'2"(Gr60/A706) ASTM A706-95b	63,400 437MPa	98,000 676MPa	14.0%	OK	~.7%	.26 .21	1.26 .15	.010 .06	.044 .038	.19 .001	.49						

BY CERTIFY THAT THE ABOVE FIGURES ARE CORRECT AS CONTAINED IN THE RECORDS OF THE CORPORATION.
MANUFACTURING PROCESSES OF THE STEEL MATERIALS IN THIS PRODUCT, INCLUDING
ING, HAVE OCCURRED WITHIN THE UNITED STATES IN COMPLIANCE WITH THE "BUY
AN" PROVISION OF THE SURFACE TRANSPORTATION ASSISTANCE ACT OF 1982.

RAY SPRINGER

1.50 in STEEL DOWEL PROPEERTIES

CERTIFIED MILL TEST REPORT

The First Two Digits Of The Heat Number Denote Plant of Origin:
03 - Kankakee, Illinois Steel Division
88 - Birmingham, Alabama Steel Division
79 - Seattle, Washington Steel Division
81 - Jackson, Mississippi Steel Division

DATE: 03/23/00

SOLD TO
• AMERICAN HWY TECHNOLOGY
• 2150 S SOUTH RT 45-52
• KANKAKEE, IL 60901

BIRMINGHAM STEEL CORP
KANKAKEE, IL STEEL DIVISION
972 EAST 4500 N ROAD
BOURBONNAIS, IL 60914-4127
(815)937-3131

B/L NO.: 55-I28564

LOAD NO.: 5500004012

SHIP TO
• AMERICAN HWY TECHNOLOGY
• RT 45
• 1 BLOCK NO OF SOUTHTEC DRI
KANKAKEE, IL

HEAT NO.*	DESCRIPTION	PHYSICAL TESTS				CHEMICAL TESTS										
		YIELD P.S.I.	TENSILE P.S.I.	ELONG % IN 8"	Bend	RWT & DEF	C	Ni	Mn Cr	P	Mo	S	V	Si	Cb	Cu	C.E
JOB: 157710																	
500I4171	KANKAKEE, IL STEEL DIVISION 1-1/2" Rd 45'2"(Gr420/A706) ASTM A706-95b ASTM A615/A615M-96a, GR 60	80,800 557MPa	115,800 798MPa	12.0%	OK	-.5%	.27 .11	1.47 .13		.012 .05	.036 .043			.26 .001		.33	
500I4172	KANKAKEE, IL STEEL DIVISION 1-1/2" Rd 45'2"(Gr420/A706) ASTM A706-95b ASTM A615/A615M-96a, GR 60	79,100 545MPa	111,900 772MPa	13.0%	OK	-.6%	.27 .10	1.46 .16		.010 .05	.042 .043			.27 .001		.32	

WE CERTIFY THAT THE ABOVE FIGURES ARE CORRECT AS CONTAINED IN THE RECORDS OF THE CORPORATION.

RAY SPRINGER

APPENDIX III

CALIBRATION OF MTS ACTUATOR

MTS

MTS Systems Corporation
14000 Technology Drive
Eden Prairie, MN 55344-2290

Calibration Report

Page: 1 of 2
Report Number: 2683-229
Site: 508288
Country Code: USA

Customer
Name: West Virginia University
System: 20Kip Structural
System ID: 20Kip
Location: Structural Lab

Equipment
Device Type: Force Transducer Model: BLH_U3g2 Serial No.: 07772
Calibration Data File Name: N/A
Controller/Conditioner Model: 407.12 Serial No.: 1038509E
Readout Device Model: 407 Serial No.: 1046895 Channel: Load
As Found System Condition: Good

Procedure
MTS Procedure: 1234 Rev. B
Calibration has been performed in accordance with: ASTM E4-99 Tolerance: +/- 1.0% of Force Applied
Method of Verification: Set-the-Force Method using Elastic Calibration Devices

Calibration Equipment Asset No.
Dead Weight Set: N/A HighLevel Board: N/A LowLevel Board: N/A DVM: 14019
DW Compensation: N/A
Temperature Readout: 12993 Additional Equip: N/A Standardizer: 11509 DJ320: 11510

Conditions
Ambient Temperature: 75 F Polarity(+): Retraction Bidirectional: No

Range: 1 Compression
Full Scale: 20Kip
As Found [ ] As Adjusted [X]
Excitation: 10.002 Shunt Cal.: Positive: 14640lbs Negative: N/A
Standard Asset No.: 12357 Delta K: 1
Lower Limit: 179.33lbs Upper Limit: 22000lbs
Zero Offset: -0.0037 Cal Fac: gain336.64

Report Units: Volts

Applied Force Percent	Series 1 Indicated Reading Ascending	Series 1 Indicated Reading Descending	Series 1 Errors Units Error Asc	Series 1 Errors Percent Error Asc	Series 1 Errors Units Error Desc	Series 1 Errors Percent Error Desc	Series 2 Indicated Reading Ascending	Series 2 Indicated Reading Descending	Series 2 Errors Units Error Asc	Series 2 Errors Percent Error Asc	Series 2 Errors Units Error Desc	Series 2 Errors Percent Error Desc	Repeatability Percent Error Asc	Repeatability Percent Error Desc
0	0.000		0.00	0.00			0.000		0.00	0.00			0.00	
-20	-1.999		0.00	-0.05			-2.003		0.00	0.15			0.20	
-40	-3.999		0.00	-0.02			-4.002		0.00	0.05			0.07	
-60	-6.002		0.00	0.03			-6.001		0.00	0.02			0.02	
-80	-8.000						-8.004		0.00	0.05			0.05	
-100	-10.002			0.02			-9.999		0.00	-0.01			0.03	

Errors at Zero Force are computed in % of Range.
The resolution of this Data Set is reflected in the least significant digit reported.
Total measurement uncertainty of the data supplied is equal to or less than +/-0.25% of reading.

Range: 1 Tension

Report Units: Volts

Applied Force Percent	Series 1 Indicated Reading Ascending	Series 1 Indicated Reading Descending	Series 1 Errors Units Error Asc	Series 1 Errors Percent Error Asc	Series 1 Errors Units Error Desc	Series 1 Errors Percent Error Desc	Series 2 Indicated Reading Ascending	Series 2 Indicated Reading Descending	Series 2 Errors Units Error Asc	Series 2 Errors Percent Error Asc	Series 2 Errors Units Error Desc	Series 2 Errors Percent Error Desc	Repeatability Percent Error Asc	Repeatability Percent Error Desc
0	0.000		0.00	0.00			0.000		0.00	0.00			0.00	
20	1.999		0.00	-0.05			2.000		0.00	0.00			0.05	
40	3.999		0.00	-0.02			4.001		0.00	0.03			0.05	
60	6.000		0.00	0.00			6.004		0.00	0.07			0.07	
80	8.002		0.00	0.03			8.004		0.00	0.05			0.02	
100	10.000		0.00	0.00			10.007		0.01	0.07			0.07	

Errors at Zero Force are computed in % of Range.
The resolution of this Data Set is reflected in the least significant digit reported.
Total measurement uncertainty of the data supplied is equal to or less than +/-0.25% of reading.

System was found to be: In Tolerance [X] Out of Tolerance [ ]

MTS Systems Corporation Measurement Standards are Traceable to the National Institute of Standards and Technology

Notes: Intial calibration after controller upgrade.

Performed By: Joseph Thieret Date: 8-Feb-00

Signature:

Next Recommended Calibration Due Date: 8-Feb-01 fcal9903PC

APPENDIX IV

CALIBRATION CERTIFICATES OF LVDTs

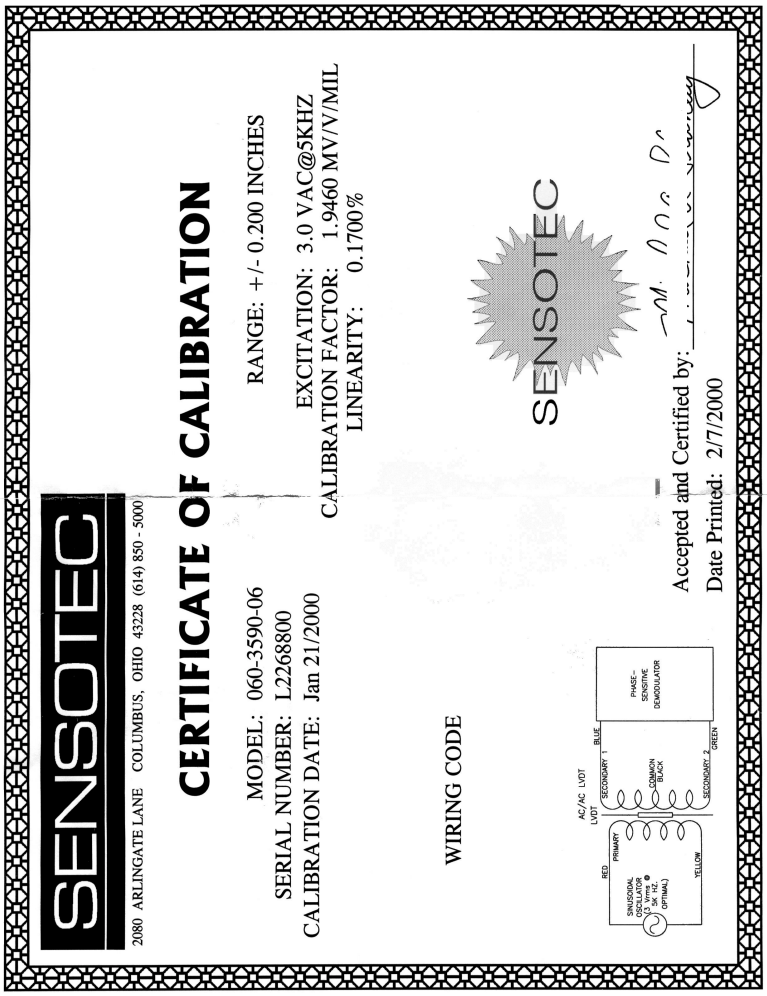

SENSOTEC

2080 ARLINGATE LANE COLUMBUS, OHIO 43228 (614) 850 - 5000

CERTIFICATE OF CALIBRATION

MODEL: 060-3590-06
SERIAL NUMBER: L2268800
CALIBRATION DATE: Jan 21/2000

RANGE: +/- 0.200 INCHES

EXCITATION: 3.0 VAC@5KHZ
CALIBRATION FACTOR: 1.9460 MV/V/MIL
LINEARITY: 0.1700%

WIRING CODE

SENSOTEC

Accepted and Certified by:

Date Printed: 2/7/2000

SENSOTEC

2080 ARLINGATE LANE COLUMBUS, OHIO 43228 (614) 850 - 5000

CERTIFICATE OF CALIBRATION

MODEL: 060-A797-05
SERIAL NUMBER: L0081300
CALIBRATION DATE: 04/08/1999

RANGE: +/- 0.500 INCH
EXCITATION: 3.0 VAC@5KHZ
CALIBRATION FACTOR: 1.5970 MV/V/MIL
LINEARITY: 0.1200%

WIRING CODE

AC/AC LVDT (other types, cable fitted)

WIRE	DESIGNATION
RED and YELLOW	Supply
GREEN and BLUE	Output
BLACK	Secondary Center
SHIELD	Shield (ground at instrument end)

* These devices are designed to give best results under the specified conditions, but some will operate over a wide range of voltage and frequency.
* See Data Sheets for details.
* The voltage between the primary and secondary must not exceed 100 volts.

SENSOTEC

Accepted and Certified by: Michael A Stanley
Date Printed: 4/8/1999